Arctic Biology Field Course

Qeqertarsuaq 2025

UNIVERSITY OF COPENHAGEN
FACULTY OF SCIENCE

ARKTISK STATION

Arctic Biology Field Course

Qeqertarsuaq 2025

Publication information and how to cite this report

Title: Arctic Biology Field Course, Qeqertarsuaq 2025

Published by: Arctic Station
University of Copenhagen
3953 Qeqertarsuaq
Greenland

Marine Biological Section
Department of Biology
University of Copenhagen
Universitetsparken 4
2100 Copenhagen Ø
Denmark

Publishing year: 2025

Edited by: Niels Daugbjerg and Per Juel Hansen, Department of Biology, University of Copenhagen, Denmark

ISBN: 978-87-89143-31-6

Cover page photo: Niels Daugbjerg

Citation: The report can be cited in full:
Arctic Biology Field Course, Qeqertarsuaq 2025. Daugbjerg, N. and Hansen, P.J. (Eds.). Arctic Station, University of Copenhagen, p. 1-163.

or in part:

Author(s), 2025. Title of paper. In: Arctic Biology Field Course,Qeqertarsuaq 2025. Daugbjerg, N. and Hansen P.J. (Eds.). Arctic Station, University of Copenhagen, p. x-x (add page numbers).

For information about the Arctic Station visit: www.arktiskstation.ku.

Table of Contents

Preface

Admission to the *Arctic Biology Field Course* (7.5 ECTS) is granted through a competitive application process that emphasizes individual motivation and quality of proposed fieldwork based projects. For this year's course, which focused on the marine ecosystem, we received 34 applications. Following a rigorous evaluation, 14 participants were selected.

After an initial meeting for all participants four project groups were established. In the months leading up to our departure, each group engaged with the supervisors in a series of online and physical meetings to ensure optimal preparation. These sessions were dedicated to further developing the hypothesis-driven projects, finalizsing equipment and packing lists, and writing initial drafts of the project introductions.

Hence, we all came well prepared when meeting up at the Copenhagen airport and ready to conduct field work in Arctic marine waters. But a combination of aircraft mechanical failaure and bad weather (strong winds) prevented us from leaving Nuuk for 5 days. We were therefore stuck in the capical of Greenland being accomodated at two different hotels and when we finally arrived at the Arctic Station we were left with only 5 days to conduct the projects. Thus, when stranded in Greenland's capital, we turned this setback into an opportunity, using the time to develop a robust contingency plan (Plan B) for the projects. This involved refining hypotheses and adapting protocols for water sampling and experimental setup. Upon finally reaching the Arctic Station, we were confronted with a compressed five-day timeline. Further persistent strong winds prevented sampling in Disko Bay, ultimately reducing dedicated experimental time for the two glacier rock flour groups to just three days, while the macroalgal-pH group had five days. Consequently, these projects were severely impacted. Only the project on macroalgal diversity and biomass was spared the direct effects of the weather at Qeqertarsuaq, though it too had to be completed in half the allotted time.

We were profoundly impressed by your incredible adaptability and your flexibility when entering "change-of-plan-mode" for navigating the numerous challenges and delays. Your tireless energy, fantastic teamwork, and admirable social skills were all crucial in making the most of a difficult situation. Although "The Delay" came to define this field course, we are delighted that all studies included in this report ultimately yielded impressive results. This year, we suspended the otherwise valuable tradition of maintaining a shared course diary. Due to the significant delays, we simply prioritized our limited time on the essential field and laboratory work.

All participants of the Arctic Biology Field Course wish to express our profound appreciation for the financial support from the Board of the Arctic Station and the Department of Biology at University of Copenhagen. Our thanks also go to the Porsild crew for their help in the field and to the Arctic Station staff for their logistical support. The course instructors would like to personally thank Kirsten S. Christoffersen and Kisser Thorsøe for their swift communication in the planning stages.

Niels Daugbjerg and Per Juel Hansen, 20 August 2025

Course participants

In the back, from left to right: Jens Hvid Lund, Per Juel Hansen (teacher), Luka Alexander Civa, Niels Daugbjerg (teacher), Marie Neel Jørgensen, Emma Nitschky Juvik.

Middle row: Marie Neel Jørgensen, Ane Stendal Svendsen, Emma Cecilie Østergaard Buch, Signe Korte Petersen, Nanna Meilholm Christiansen.

Front row: Emily Aileen Faye, Julie Elisabeth Brantley Boesen, Mia Madsen, Ida Valbjørn Christensen, Amalie Kargaard Jensen.

Report 1

Jens Hvid Lund, Luka Alexander Civa & Mia Valentin Madsen (2025). Short-term effects of macronutrients, trace metals and varying doses of glacial rock flour on arctic phytoplankton communities - a study from Disko Island, west Greenland.

Short-Term Effects of Macronutrients, Trace Metals and Varying doses of Glacial Rock Flour on Arctic Phytoplankton Communities - A Study from Disko Island, west Greenland

Jens Hvid Lund, Luka Alexander Civa & Mia Valentin Madsen

Department of Biology, Marine Biological Section, University of Copenhagen

Abstract

The Arctic Ocean experiences strong seasonal variation in light, ice cover, and nutrient availability. Following the spring bloom, macronutrients such as nitrate, phosphate, and silicate are rapidly depleted, often resulting in nutrient limitation during summer. Climate change is expected to intensify these constraints through altered stratification and freshwater input, while also increasing the delivery of glacial rock flour (GRF), which can influence both nutrient availability and light conditions. This study investigated the short-term effects of macronutrients, trace metals, and varying doses of GRF on Arctic phytoplankton communities at two sites near Disko Island, West Greenland: Røde Elv and Fast Station, sampled at both the surface layer (SL) and deep chlorophyll maximum (DCM). Experimental incubations over two days were assessed using changes in chlorophyll a (Δchl *a*) and maximum quantum yield of photosystem II ($\Delta F_v/F_m$) as proxies for biomass accumulation and photochemical efficiency, respectively. Macronutrient addition (NPS) consistently increased both Δchl *a* and $\Delta F_v/F_m$ at SL, indicating relief from nitrogen and/or phosphorus limitation. Macronutrients combined with trace metals caused an even greater response, suggesting a co-limitation of trace metals and macronutrients. GRF combined with NPS showed no detectable positive or negative effect on phytoplankton cells. This suggests that nutrients bound within GRF were not yet fully mobilized within the experimental timeframe. A longer incubation period would likely be required to determine whether GRF could influence phytoplankton growth and if a dose-response was observable. Between locations and depths no difference in suspended particulate matter was found due to the Røde Elv sampling site being too far away from the river outlet. These likely caused similar experimental conditions and possibly explains the lack of consistent significant results or clear trends between locations and depths.

Keywords: Glacial Rock Flour (GRF) – Nutrient Limitations – Arctic Marine Environment – Phytoplankton – Short Term Dose Response Experiment

1. Introduction

The Arctic Ocean is characterized by strong seasonality in light availability, ice cover, and nutrient availability. During the spring bloom, macronutrients such as nitrate (NO_3^-), phosphate (PO_4^{3-}), and silicate ($Si(OH)_4$) are rapidly consumed by phytoplankton, often leading to nutrient depletion in surface waters during summer (Frey et al., 2022). Especially nitrate has been found to be a limiting factor in many marine ecosystems including in the Arctic (Bristow et al., 2017).
As the water column in Arctic waters becomes stratified due to ice melt and freshwater input, vertical mixing is reduced, limiting nutrient resupply from deeper layers. This seasonal depletion can constrain phytoplankton growth despite adequate light conditions, ultimately influencing primary productivity, food web dynamics, and carbon sequestration in the Arctic marine ecosystem (Randelhoff et al., 2020). Phytoplankton account for approx. half of the annual fixed carbon on the planet and stand as the main driver of the biological pump in the world's oceans (Falkowski et al., 1998; Field et al., 1998). This makes these organisms not only the foundation of marine food webs but also a major component in the global climate system. Understanding their seasonal variation and limiting factors are thus of great importance, especially in the Arctic Ocean where climate change is expected to influence nutrient input and availability (Garcia et al., 2024).

In addition to macronutrients, trace metals such as iron (Fe) are essential for key physiological processes, including photosynthesis, nitrogen assimilation, and enzyme activity. Even at low concentrations, trace metal availability can regulate phytoplankton growth and species composition (Bristow et al., 2017) and iron have been found to limit phytoplankton growth in around 20% of the world’s ocean (Boyd et al., 2007). A natural source of macronutrients, such as phosphorus and silicium as well as trace metals like iron, is glacial rock flour (GRF). GRF is a fine mineral sediment generated by glacial grinding of bedrock and delivered to coastal waters through meltwater runoff in large quantities (Bendtsen et al., 2024).

As climate change accelerates glacial melts, GRF input to coastal waters is expected to increase substantially. GRF can stimulate phytoplankton growth by supplying essential nutrients, but high particle loads may also reduce light penetration or alter particle dynamics in ways that inhibit photosynthesis or other physiological processes. This dual potential is reflected in previous experimental studies, which have reported both positive and negative effects depending on species composition, environmental conditions, and exposure time (Lund, 2025; Bendtsen et al., 2024; Maselli et al., 2023). However, studies on the effect of GRF on Arctic phytoplankton communities

remain limited underlining the need for further investigation into the effect of GRF on Arctic phytoplankton communities.

Therefore, this study investigated how Arctic phytoplankton communities respond to the addition of macronutrients and trace metals to determine to what extent they are limited by these nutrients but also tested varying doses of GRF in a short-term incubation experiment. Seawater samples were collected from two locations near Arctic Station, Disko Island, West Greenland: "Røde Elv," located close to shore near the outlet of a river rich in GRF, and "Fast Station," situated further offshore where GRF concentrations are expected to be lower. Samples were taken from both the surface layer (SL) and the deep chlorophyll maximum (DCM) and then incubated with either macronutrients (NPS), NPS + trace metals (NPST) or NPS with three different concentrations of GRF (GRF1, GRF2 & GRF3). The purpose of including variations in both location and depth was to capture differences in nutrient availability and natural exposure to GRF. This allows for assessing whether responses of phytoplankton communities to nutrients and GRF additions depend on their prior environmental conditions. Responses were quantified by measuring chlorophyll *a* (chl *a*) and F_v/F_m as a proxy for biomass and photosynthetic efficacy, respectively.

To improve our understanding of the impact of macronutrients, trace metals and GRF on phytoplankton communities in the arctic coastal waters, the experiments were designed to test the following hypotheses:

H1: Addition of macronutrients (*NPS*) will increase F_v/F_m and **chlorophyll *a*** compared to the control across locations and depths.

H2: Addition of trace metals together with macronutrients (*NPST*) will result in a **greater** increase in F_v/F_m and **chlorophyll a** than *NPS* alone.

H3: Treatments with **NPS + GRF** will yield **similar responses** to *NPST* as GRF is expected to supply Fe, Si, and other micronutrients.

H4: There will be a **positive dose-response** in F_v/F_m and **chlorophyll a** with increasing GRF concentration ($GRF_1 < GRF_2 < GRF_3$).

H5: Treatment effects will be **stronger at SL than at DCM**, and **stronger at Fast Station than at Røde Elv** due to lower natural content of micro- and macronutrients.

1.1 Aim of study

The initial aim of this study was to incubate seawater cultures with six different treatments over a period of approximately 7 days to assess the long-term response of Arctic phytoplankton communities to GRF compared to control treatments. However, due to travel delays, the available experimental period was reduced to three days which limited the ability to fully capture long-term dynamics. Consequently, the study objective was revised to focus on elucidating the short-term effects of GRF, macronutrients, and trace metals on phytoplankton photosynthetic efficiency and biomass.

2. Methods and materials

2.1. Field site and data collection

The fieldwork and data collection were conducted in the coastal waters of Arctic Station outside of Disko Island, west Greenland (69º15’12’’N, 53º31’03’’W). The site is located within Disko Bay, a seasonal Arctic marine environment influenced by both glacial meltwater from the Greenland ice sheet and seasonal sea ice cover. The seafloor topography near the field site ranges from 30 to 350 meters depth and is characterized by a stratified water column in the summer due to freshwater input from glacier runoff. Surface layers are typically fresher and more turbid during late summer, reflecting enhanced meltwater release, while deeper layers remain colder and more saline (Møller et al., 2023). The field sites comprised two different locations, “Fast Station” and “Røde Elv” as seen in Fig. 1. The sample location Røde Elv was close to shore near the outlet of the river of the same name “Røde Elv” (69.2445 N, 53.5022 W) located on Disco Island with a high content of GRF. Fast Station (69.1833 N, 53.5166 W) was located further out in the ocean where concentrations of GRF were expected to be much lower.

Fig. 1. Satellite overview from Google Earth of the two sample locations "Fast Station" (69.1833 N, -53.5166 W) and "Røde Elv" (69.2445 N, 53.5022 W). From these two locations, surface samples were measured at 2 meters and deep chlorophyll max was measured at 22.5 and 12 m for Fast Station and Røde Elv, respectively. Samples for marine phytoplankton were taken to a depth of 50 m.

Water samples were collected in 10 L Niskin bottles from the research vessel "Porsild" (IMO: 9088445) and included both surface samples and DCM samples:

1. The surface water near the outlet of Røde Elv (2m depth)
2. DCM depth at the outlet of Røde Elv (12m depth)
3. The surface water at Fast Station (2m depth)
4. DCM at Fast Station (22.5m depth)

The collected water was passed through a 200 µm mesh filter during transfer into 20 L carboys, ensuring the removal of zooplankton to prevent grazing on the phytoplankton present in the samples. Furthermore, netplankton tows for investigating the phytoplankton communities were also conducted at both stations down to a depth of 50 m.

2.1.1 CTD data and environmental setting

Vertical profiles of salinity, temperature, chl *a*, dissolved oxygen, photosynthetically active radiation (PAR) irradiance, and depth were recorded at Røde Elv and Fast Station on 13 and 15 July

2025 using an AML-6 CTD (Conductivity, Temperature, Depth) probe. Across the two sampling days, skies were mostly cloudy, and wind conditions ranged from calm to light breeze. The CTD descended at a velocity of ~0.3 m s^{-1} from approx. 1 m to either 60 m or 100 m depth, continuously measuring salinity, temperature (°C), chl *a* (µg L^{-1}), PAR irradiance (µmol photons m^{-2} s^{-1}), dissolved oxygen (mg L^{-1}), and depth (m). These measurements were conducted to characterize the abiotic conditions at the sampling sites in Disko Bay.

2.2. Preparations of treatments and experimental setup

For all 4 location samples, the following procedure was applied. The 20 L of seawater was distributed into six 2-liter blue-cap bottles and filled to 1.6 L. To five of the bottles, 1.6 mL of NaH_2PO_4 (Monosodium phosphate) (0.5 g/100 mL), $NaNO_3$ (Sodium nitrate) (7.5 g/100 mL) and Na_2SiO_3 (Sodium metasilicate) were added, abbreviated as NPS on the labels. In addition, 1 mL of L1 trace-metal solution was added to one bottle and called NPST. See Guillard and Hargraves (1993) for preparation of the L1 media. The following concentrations of dry GRF, originally collected from Ilulialik in Nuuk Fjord, were then added to three of the bottles containing NPS:

Table 1. Overview of treatments and the concentration of glacial rock flour added to 1 liter.

Treatments	Concentration of glacial rock flour (g L^{-1})
NPS+GRF_1	0.0506
NPS+GRF_2	0.3256
NPS+GRF_3	0.8253

One bottle received neither GRF nor trace metals: “NPS” and the last bottle only received 1.6 L of seawater to serve as control. In total 1.6 liters of six treatments were prepared and labeled for each location: Control, NPS, NPST, NPS+GRF_1, NPS+GRF_2 and NPS+GRF_3.

Each treatment was to be tested in triplicates, so the 1.6 L of each treatment were distributed into three 500 mL bottles and labelled as replicate 1, 2 and 3. All 500 mL bottles were placed in 5°C under around 100 µmol photons m^{-2} s^{-1} light intensity in a random order. Since GRF precipitate, the bottles were turned every second hour during the experimental period.

2.3. F_v/F_m

The ratio of variable to maximal fluorescence (F_v/F_m) is used to estimate the maximum quantum efficiency of Photosystem II (PSII) photochemistry in phytoplankton under dark-adapted conditions. It is calculated as: Fv/Fm = (Fm - Fo) / Fm

F_0 is the minimal fluorescence yield when all PSII reaction centers are open, and F_m is the maximal fluorescence yield after a saturating light pulse has closed all PSII centers (Kitajima & Butler, 1975). In nutrient-replete phytoplankton, F_v/F_m typically ranges from 0.65 to 0.75 (Kolber et al., 1994; Suggett et al., 2009), whereas lower values are indicative of physiological stress caused by factors such as nutrient limitation, temperature stress, or exposure to toxic material (Behrenfeld & Kolber, 1999).

On day 0, three samples of 20 mL from each location were stored in the dark at 4°C for 30 minutes to measure the initial stress level of the cells. F_v/F_m was measured for each replicate using a Chelsea Technology LabSTAF fluorometer. The temperature of the cooling water pumped into the LabSTAF was set to 3°C for the temperature in the LabSTAF to be around 4.5°C. The following parameters were noted: F_v, F_m, F_v/F_m, temperature and date.

On day 2 the procedure was repeated but with 20 mL from each of the 500 mL bottles. The standard deviation for all triplicates was calculated.

2.4. Chlorophyll *a*

Chl *a* was measured as a proxy for phytoplankton biomass. On day 0, 350 mL sample water was transferred from each 20 L bottle to a 500 ml blue cap bottles. From these bottles, 100 ml samples were turned gently 10 times prior to being transferred to a Sartorius Combisart 1-branch manifold for ethanol extraction at 15 kPa/150 mbar. Filters were then collected and added to 15 ml Falcon tubes along with 5 ml 96% ethanol and then incubated for 24h at 4°C. After 24h, all 9 Falcon tubes were turned gently 5 times and then 1.2 mL was transferred to 1.5 ml Screw Neck clear glass bottles after which fluorescence measurements were conducted in a Turner Design Trilogy fluorometer. This procedure was repeated for all treatments at every location on day 1 and 2.

2.5. Suspended particulate matter

A volume of 1.5 L was transferred to a 2 L blue cap bottle from each of the 20 L samples. The 1.5 L was then filtered through a 0.7 µm Advantec KMP-k3 manifold. The filters were weighed before filtration. After filtration they were kept in a tray and incubated for 4h at 65°C. After 4 hours, the filters were weighed to determine the amount of suspended particulate matter.

2.6. pH

On day 0 and 2 pH was measured using a WTW pH 3210 electrode. The electrode was calibrated using technical buffer solutions at pH = 7 and pH = 10.01 and used a 3 mol L^{-1} KCl reference electrolyte (KCl-250). Prior to sample measurements the pH electrode was conditioned in deionized water and gently dried. pH was measured twice to ensure that potential changes in pH did not influence treatment effects, as photosynthetic activity of microorganisms can increase pH during incubation (Maselli et al., 2023).

2.7. Diversity of net-phytoplankton

Samples of marine phytoplankton were collected twice (13 and 15 July) at the Fast station by lowering a plankton net with a pore size of 20 µm to a depth of 50 m. The samples therefore each represent an integrated sample of the phytoplankton community with a cell size > 20 µm. Upon return to the laboratory at the Arctic Station, the samples were analyzed using an upright Olympus microscope (BX51) equipped with Nomarski Interference contrast. Images were taken with a digital camera model DP10.

2.8. Statistical analyses

Statistical analyses and visualizations were conducted in R version 4.4.3. within the RStudio environment (version 2024.12.1+563) using a combination of packages such as ggplot2, Car, Emmeans, Tidyverse. Statistical analyses included one-way analyses of Variance (ANOVA) tests. One-way ANOVA analyses allowed for the examination of the individual effects of different independent variables on a dependent variable. The independent variables in these experiments were the 6 different treatment groups, and the dependent variables were chl *a*, F_v/F_m, suspended particulate matter and pH. In cases of significant treatment effects, Tukey's HSD post hoc tests were further conducted to test significant variance between all treatment groups. Model assumptions for one-way ANOVA included 1) Independence of observations, which was ensured by the experimental design with independent replicates. 2) Normality of residuals, which was

assessed by Shapiro-Wilk tests and inspection of Q-Q plots. 3) Homogeneity of variances, which was evaluated through visual inspection of residuals vs. fitted plots and scale-location plots. In one instance (chl *a* at Røde Elv SL) the Shapiro-Wilk test indicated a deviation from normality ($p < 0.05$), however visual inspection of the residual distribution did not reveal substantial departures from normality, the ANOVA analyses were carried out despite the significant Shapiro-Wilk test result. Tables of ANOVA-tests and model assumptions checks can be seen in the supplementary material as Figs. S1-S13. Statistical significance was set at $\alpha = 0.05$. Codes of significance were: * = $p < 0.05$; ** = $p < 0.01$; $p < 0.001$.

3. Results

3.1. CTD data domparisons between fast station and Røde Elv

Vertical profiles of salinity, temperature, chl *a*, dissolved oxygen, photosynthetically active radiation irradiance and depth were recorded at Røde Elv and Fast station on 13 and 15 July 2025 (Fig. 2 and 3). On 13 July, surface salinity was lower at Røde Elv compared to Fast Station, with both converging to ~32-33 below ~10 m. Temperature at the surface was ~5-6 °C and decreased to ~1-1.5 °C near 100 m at both locations. A clear stratification was observed at ~12 m at Røde Elv, coinciding with a DCM at ~10-15 m. At Fast Station, the DCM was broader, spanning ~10-27 m. Dissolved oxygen was highest in surface waters and declined with depth, while PAR decreased rapidly through the upper 20-30 m, reaching near-zero values below ~30 m.

By 15 July, stratification at Røde Elv had risen to ~9 m, and the DCM had deepened to ~15-20 m. At Fast Station the DCM extended to ~26 m. Surface salinity and temperature patterns remained similar between dates, though slight changes in chl *a* distribution and dissolved oxygen profiles reflected the vertical shifts in stratification. PAR attenuation patterns were comparable between dates, but the near-zero light zone was reached slightly deeper on 15 July. These temporal changes, particularly in stratification depth and DCM position, were observed at both sampling sites during the study period.

3.1.1. July 13, 2025

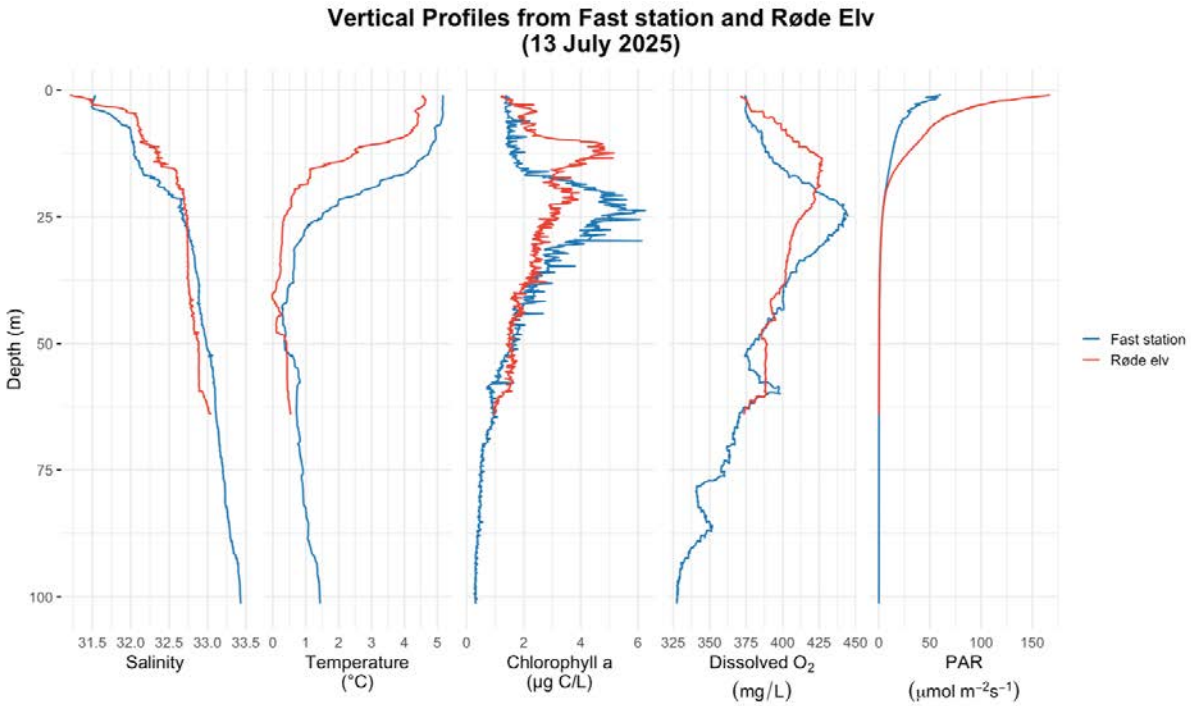

Fig. 2. Vertical profiles of salinity, temperature, chlorophyll a, dissolved oxygen, and PAR at Fast Station (blue) and Røde Elv (red) on 13 July 2025. Depth profiles show lower surface salinity at Røde Elv relative to Fast Station, converging below ~10 m. A pronounced DCM occurred at ~10-15 m at Røde Elv and over a broader depth range (~10-27 m) at Fast Station. Dissolved oxygen was highest in surface waters and declined with depth, while PAR decreased sharply in the upper 20-30 m, reaching near-zero below ~30 m.

3.1.2. July 15, 2025

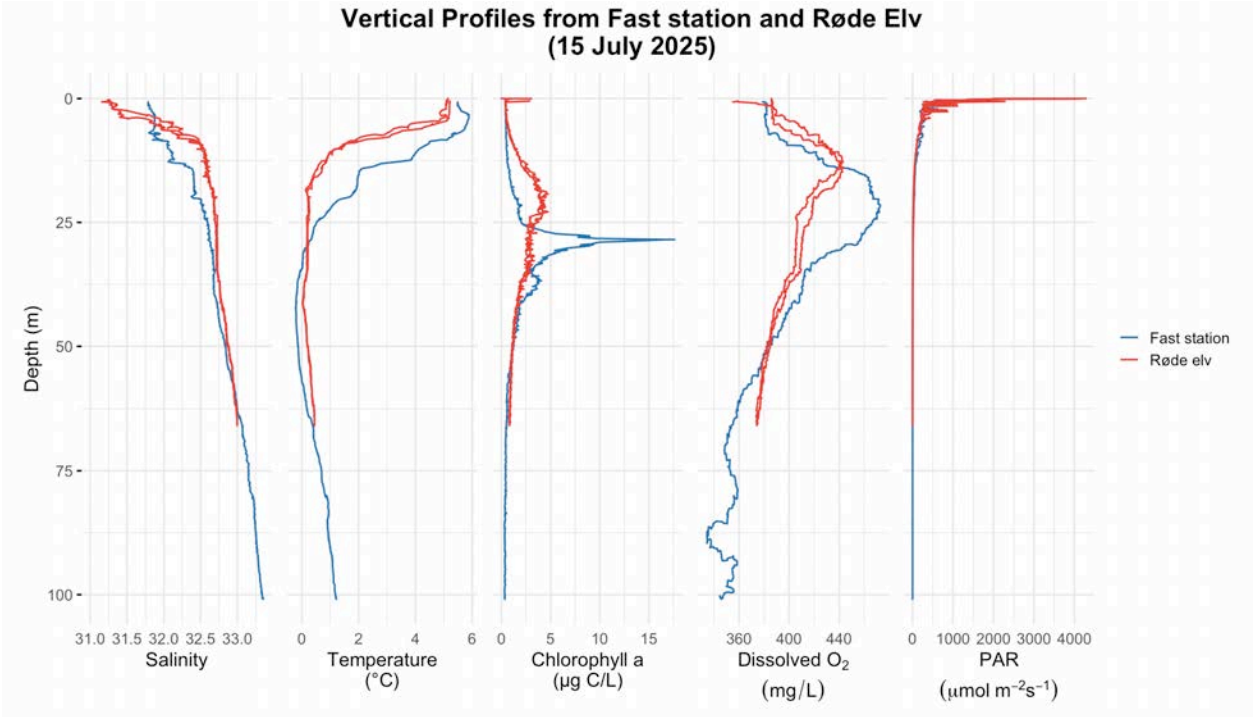

Fig. 3. Vertical profiles of salinity, temperature, chlorophyll a, dissolved oxygen, and PAR at Fast Station (blue) and Røde Elv (red) on 15 July 2025. Stratification at Røde Elv rose to ~9 m, and the DCM deepened to ~15-20 m. At Fast Station, the DCM extended to ~26 m. Salinity and temperature patterns remained similar between dates, while dissolved oxygen and Chla distributions reflected the shifts in stratification depth. PAR attenuation patterns were comparable, with near-zero light levels reached slightly deeper than on 13 July.

3.2. F_v/F_m

Fig. 4 shows F_v/F_m values at day 0 and day 2 for each treatment at Røde Elv SL, Fast Station SL, and Fast Station DCM. At Fast Station SL and Fast Station DCM, F_v/F_m generally increased from day 0 to day 2 across all treatments, whereas Røde Elv SL showed smaller and more variable changes.

At Fast Station DCM and Fast Station SL F_v/F_m had increased from day 0 to day 2 in all treatments, but not significantly (Fig. 5). At Fast Station SL, F_v/F_m increased with around 0.05-0.075 with all treatments, with NPS, NPST and GRF_1 increasing the most, and at Fast Station DCM F_v/F_m increased with around 0.075-0.125 with all treatments with NPST, GRF_1, -2 & -3 having increased the most. At Røde Elv SL all treatments resulted in only a small average increase in F_v/F_m, with

NPST increasing the most. However, replicates of every treatment showed both an increase and decrease of F_v/F_m causing large variation, making it hard to determine if the treatments had a positive or negative effect on the phytoplankton community from Røde Elv SL. When comparing each treatment between locations it was found for all treatments, F_v/F_m increased more at Fast Station SL compared to Røde Elv SL, but only with GRF_2 having yielded a significant result. When comparing between depths F_v/F_m at Fast Station DCM had increased more with every treatment compared to Fast Station SL once again with GRF_2 yielding the only significant response (Fig. 6). Røde Elv DCM was not measured due to logistical difficulties.

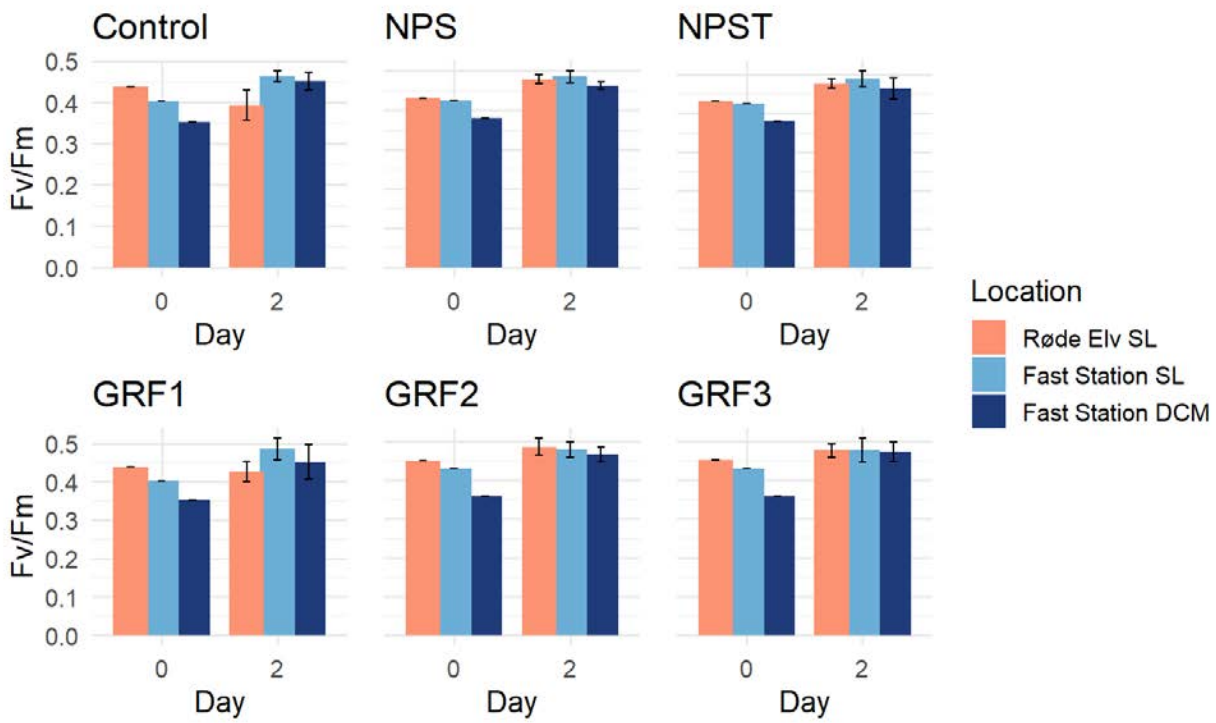

Fig. 4. F_v/F_m measurements at Day 0 and Day 2 for each treatment (Control, NPS, NPST, GRF_1, GRF_2, GRF_3) across sampling locations (Røde Elv SL, Fast Station SL, Fast Station DCM). At Fast Station SL and Fast Station DCM, F_v/F_m generally increased from day 0 to day 2 across all treatments, whereas Røde Elv SL showed more variable changes.

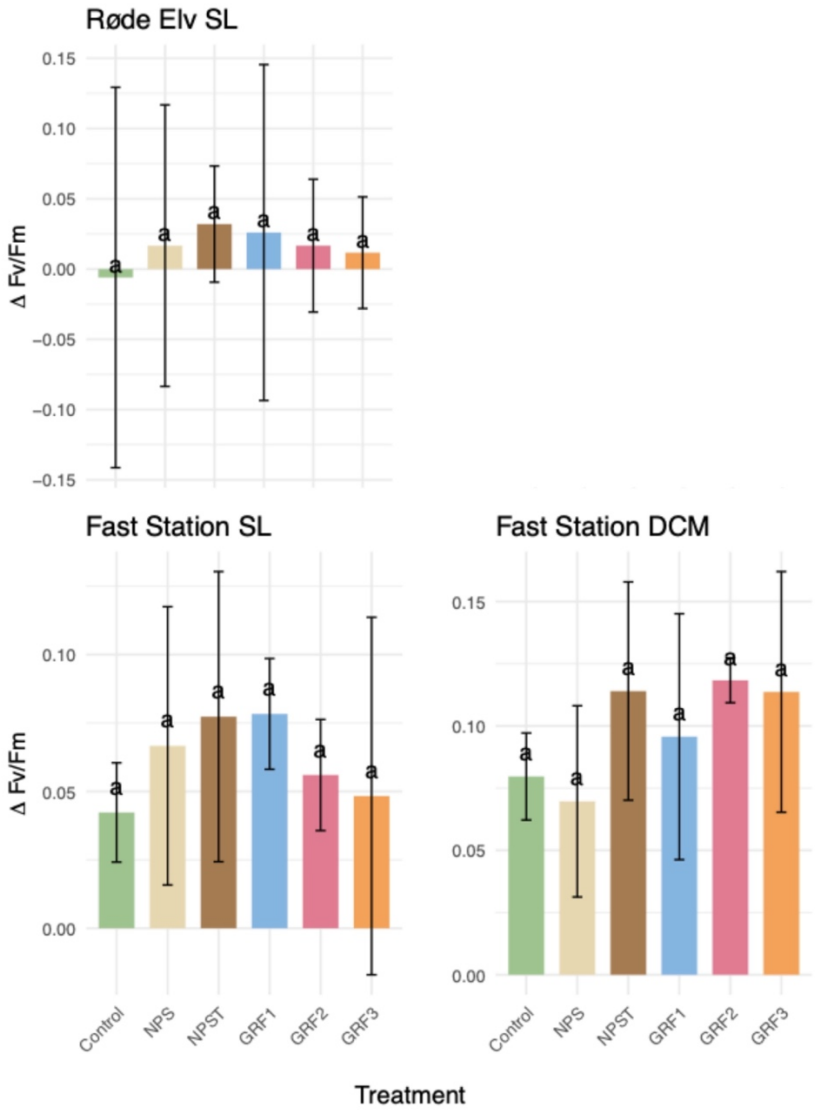

Fig. 5. Change in F_v/F_m ($\Delta F_v/F_m$) from day 0 to day 2 for each treatment at Røde Elv SL, Fast Station SL, and Fast Station DCM. No statistical significances were observed between treatments at any location as indicated by the similar letter a.

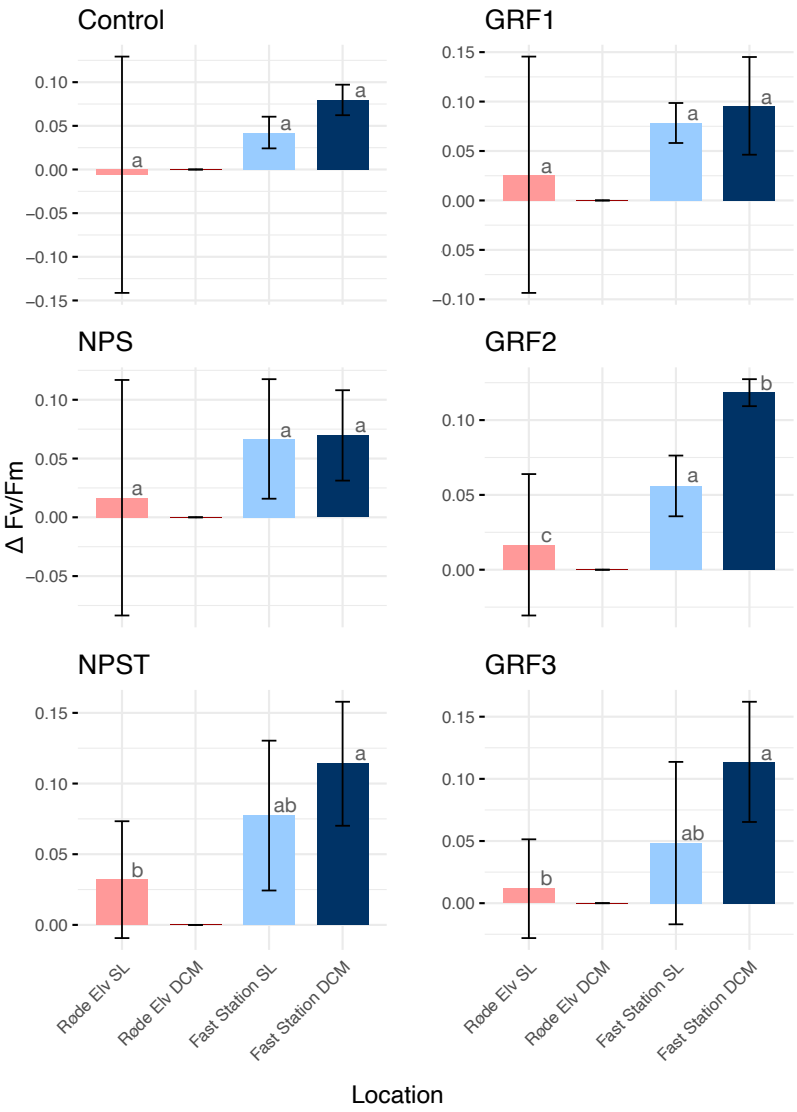

Fig. 6. Change in F_v/F_m ($\Delta F_v/F_m$) from day 0 to day 2 for each location and depth across all treatments: Control, NPS, NPST, and three GRF concentrations (GRF_1-GRF_3). Significant differences were only observed for GRF_2, which showed a greater increase at Fast Station SL compared to Røde Elv SL, and at Fast Station DCM compared to Fast Station. No other significant differences were detected.

3.3. Chlorophyll *a*

Absolute chl *a* concentrations increased from day 0 to day 2 across most treatments and locations, with the highest values generally observed at Fast Station DCM and the lowest at Røde Elv SL (Fig. 7). Water samples from Røde Elv SL, Fast Station SL and Fast Station DCM increased in chl *a* with every treatment between day 0 to day 2 with all treatments having increased more than the control

(Fig. 8). Only at Fast Station SL a significant increase was found compared to the control, which was for NPST, GRF2 and GRF3, with the rest of the treatments at the three locations yielding no significant results. At Røde Elv SL and Fast Station SL, NPST had increased more than NPS and at Fast Station DCM NPS and NPST increased the same amount.

At Røde Elv DCM the natural control had decreased in chl *a* after two days, with the rest of the treatments having replicates that had both increased and decreased in chl *a*, except for NPST where all replicates increased, making it difficult to determine whether a treatment had caused an increase or decrease in the rest of the treatments at Røde Elv DCM (Fig. 8).

When comparing the change of chl *a* between each location, chl *a* increased more at SL compared to DCM at both locations. At SL, no difference was found between Fast Station and Røde Elv, but at DCM Fast Station increased more in every treatment compared to Røde Elv (Fig. 9).

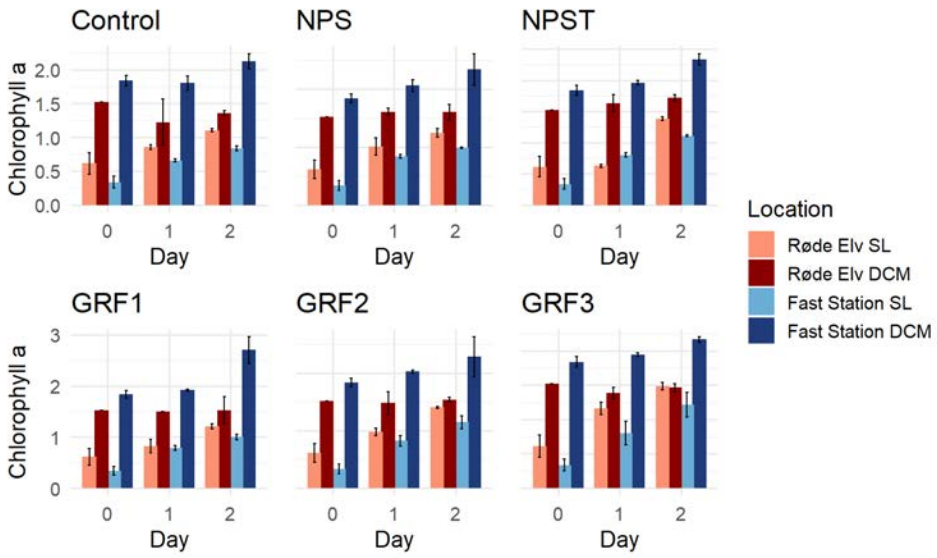

Fig.7. Chl a measurements at Day 0, Day 1 and Day 2 for each treatment (Control, NPS, NPST, GRF$_1$, GRF$_2$, GRF$_3$) across sampling locations (Røde Elv SL, Røde Elv DCM, Fast Station SL, Fast Station DCM). For all locations and treatments, chl a generally increased from Day 0 to Day 2, with the highest absolute concentrations consistently recorded at Fast Station DCM and the lowest at Røde Elv SL. Røde Elv DCM showed stable or slightly decreasing concentrations for some treatments, including the control, while Fast Station SL and DCM exhibited marked increases across most treatments.

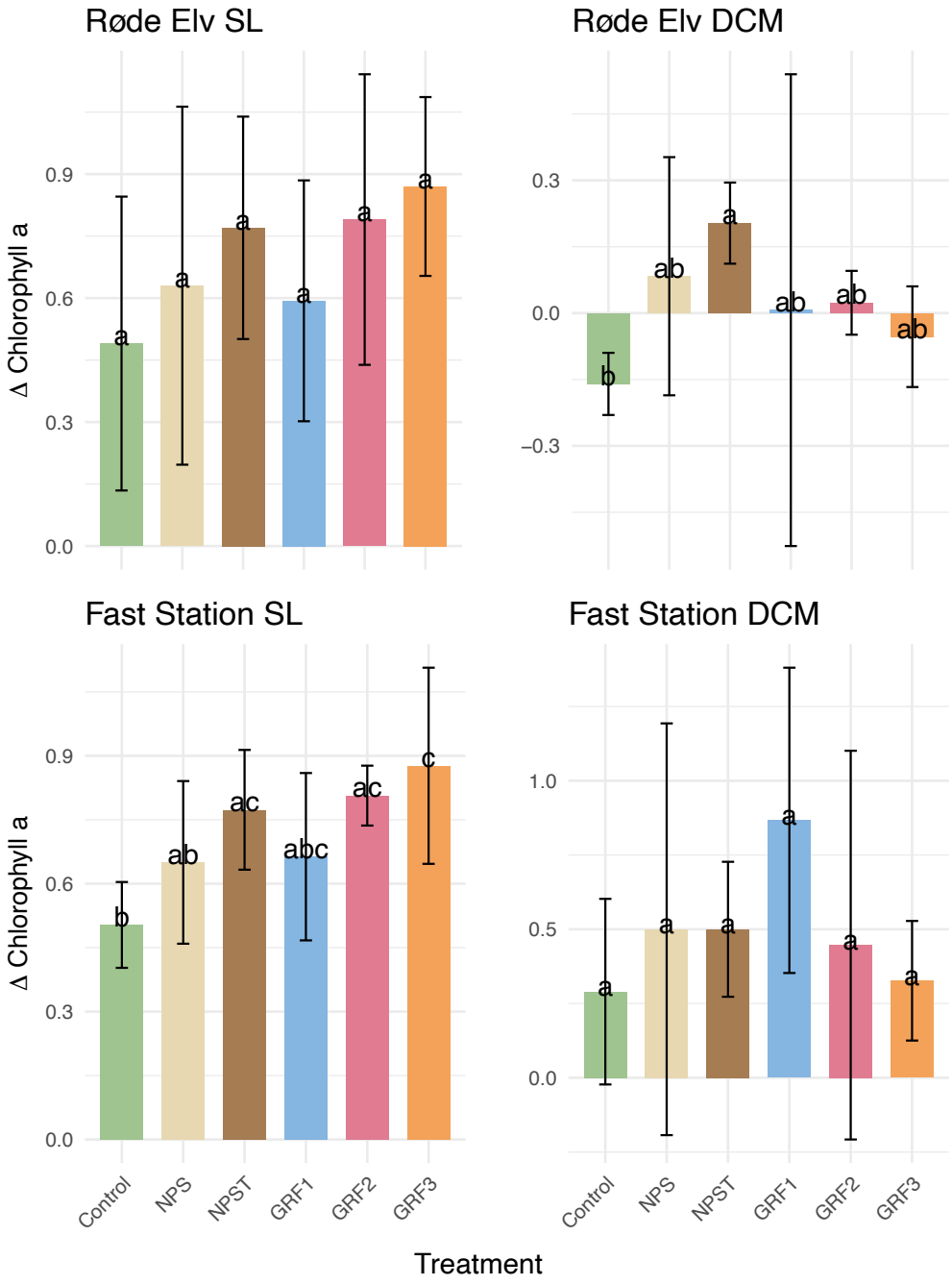

Fig. 8. Change in chl a (Δchl a) from day 0 to day 2 for each treatment at Røde Elv SL, Røde Elv DCM, Fast Station SL, and Fast Station DCM. Statistical differences were only observed at Fast Station SL with NPST, GRF_2 and GRF_3 having increased significantly more than the control treatment and at Røde Elv DCM where NPST had increased significantly more than the control treatment. At Røde Elv SL and Fast Station DCM no significant variation was found between treatments.

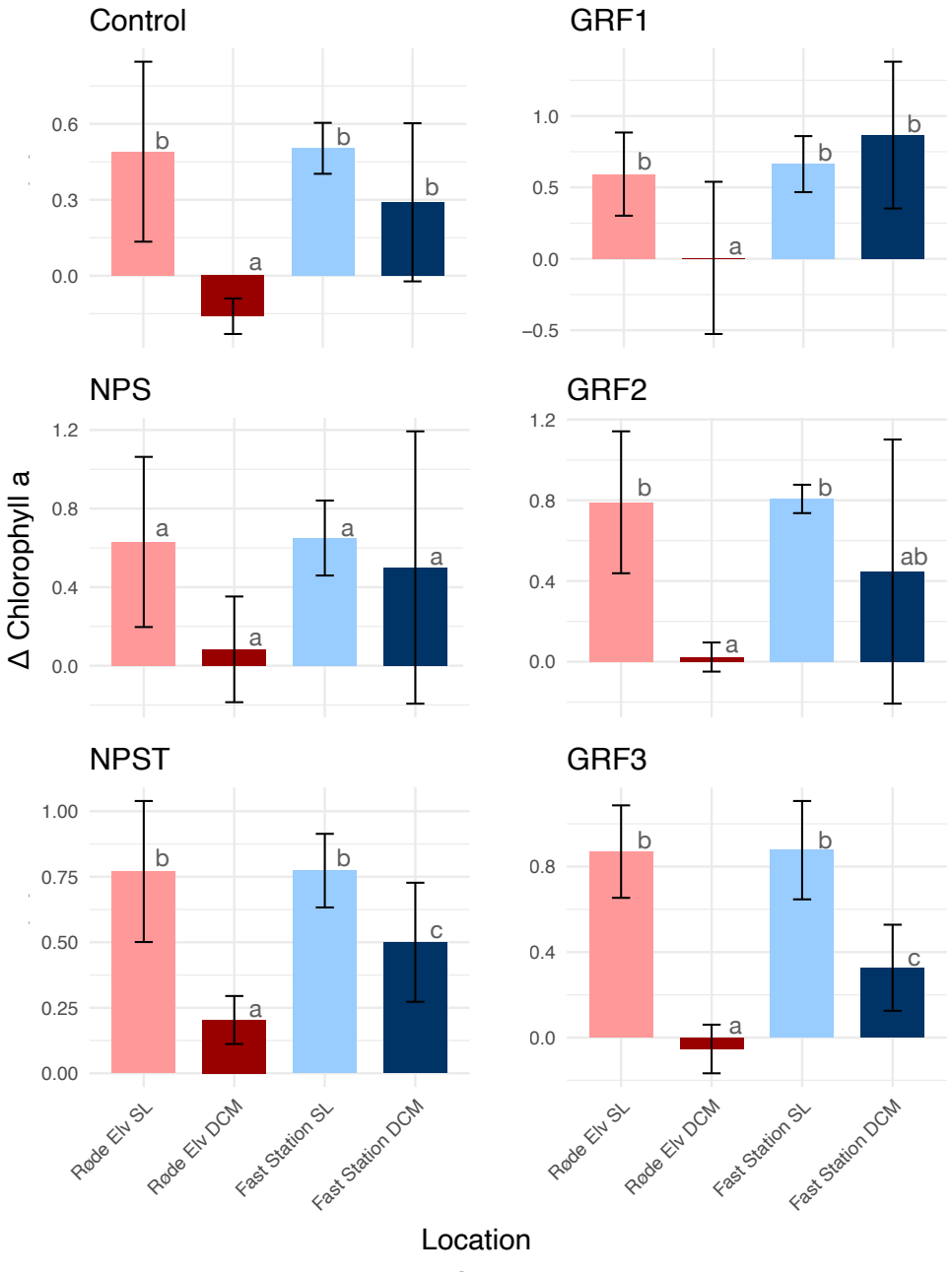

Fig. 9. Change in chl a (Δchl a) from day 0 to day 2 for each location and depth across all treatments: Control, NPS, NPST, and three GRF concentrations (GRF_1-GRF_3). Within Fast Station SL, NPST, GRF_2, and GRF_3 increased significantly more than the control treatment. Within Røde Elv DCM, NPST increased significantly more than the control. When comparing between locations, chl a increased more at Fast Station DCM than at Røde Elv DCM for all treatments. No other significant differences were detected.

3.4. Suspended particulate matter

No statistically significant difference of suspended particulate matter (g L^{-1}) was found between locations (Fig. 10). Between 0.0155 and 0.0165 g L^{-1} was measured for all nine replicates causing very little variation within each location and between locations.

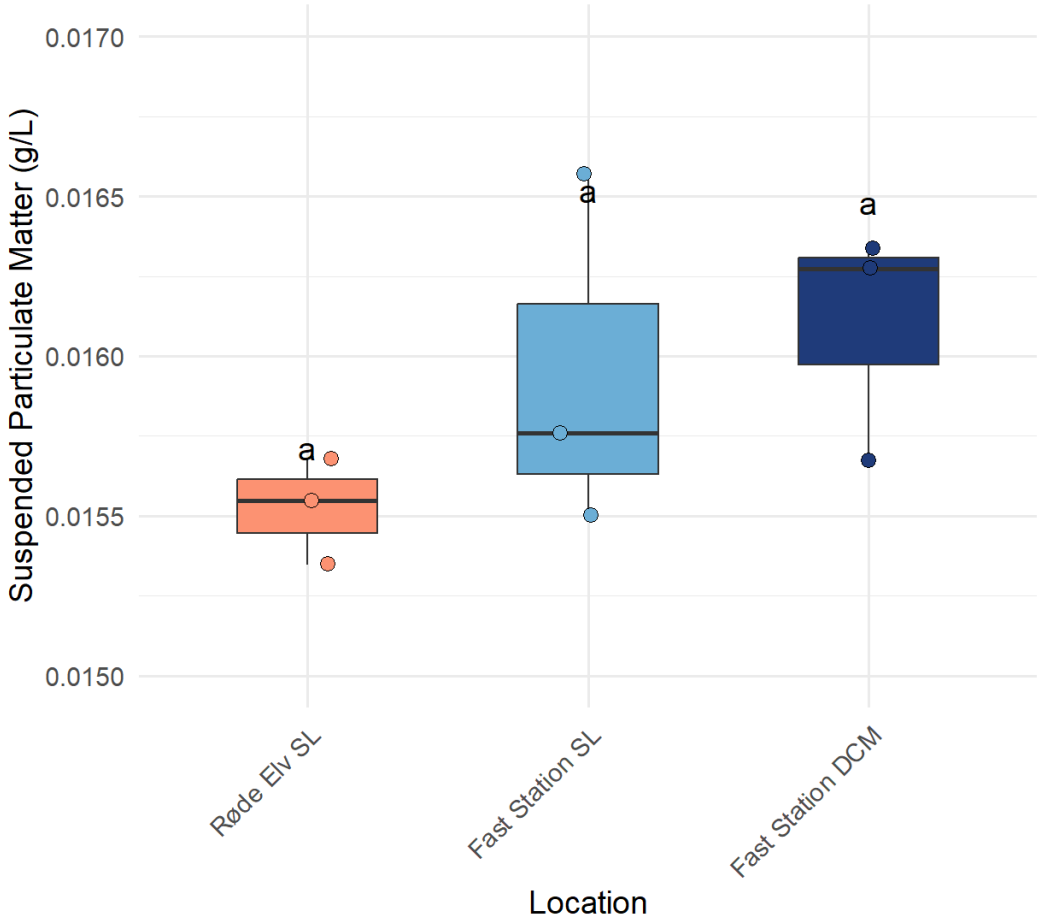

Fig. 10. Suspended particulate matter (g L^{-1}) measured at Røde Elv SL, Fast Station SL, and Fast Station DCM. No statistically significant differences were detected between locations with values ranging from approximately 0.0155 to 0.0165 g L^{-1} across all replicates.

3.5. pH

Initial pH values on day 0 ranged from 8.04 to 8.17 across locations and depths (Fig. 11). After two days of incubation, pH had generally increased by 0.2-0.5 units in all treatments except the controls, which showed only minor or negative changes. The most pronounced increases were observed at Fast Station SL, particularly for NPS, NPST, and the GRF treatments, where ΔpH approached +0.48 (Fig. 12). At Røde Elv SL, only NPS resulted in a significantly greater increase than the control,

while the GRF and NPST treatments showed intermediate, non-significant values. A similar pattern was observed at Fast Station SL, where NPS again produced the largest ΔpH and was significantly higher than both the control and NPST. In contrast, GRF treatments at this site did not differ significantly from NPS or from each other. At Fast Station DCM, NPS yielded the highest ΔpH, significantly exceeding NPST and the control, while GRF_1 and GRF_2 were also higher than the control but comparable to GRF_3. Across all locations, final pH values remained within 8.03-8.48.

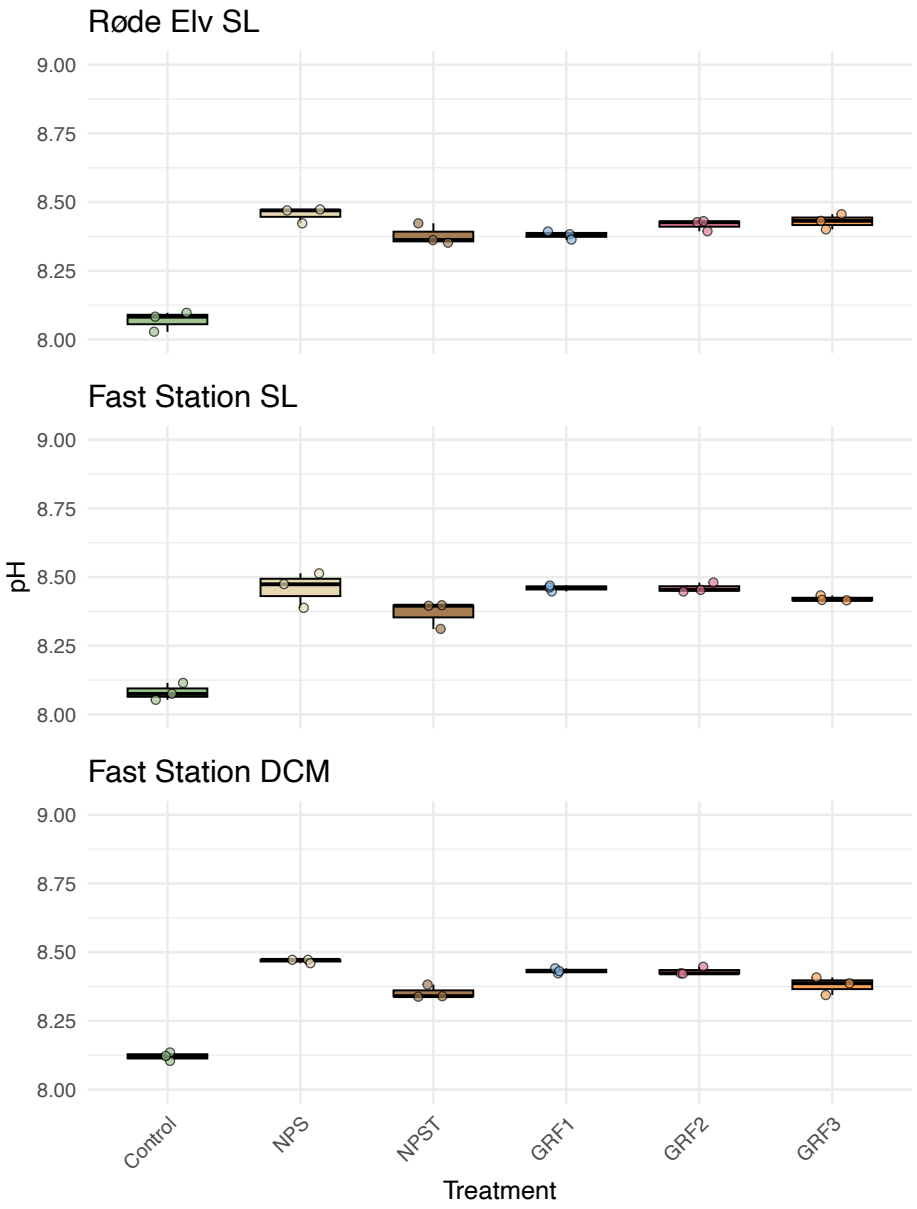

Fig. 11. Initial pH across treatments at each site and depth. Values ranged from 8.04 to 8.17, with no substantial differences between treatments at the start of the experiment.

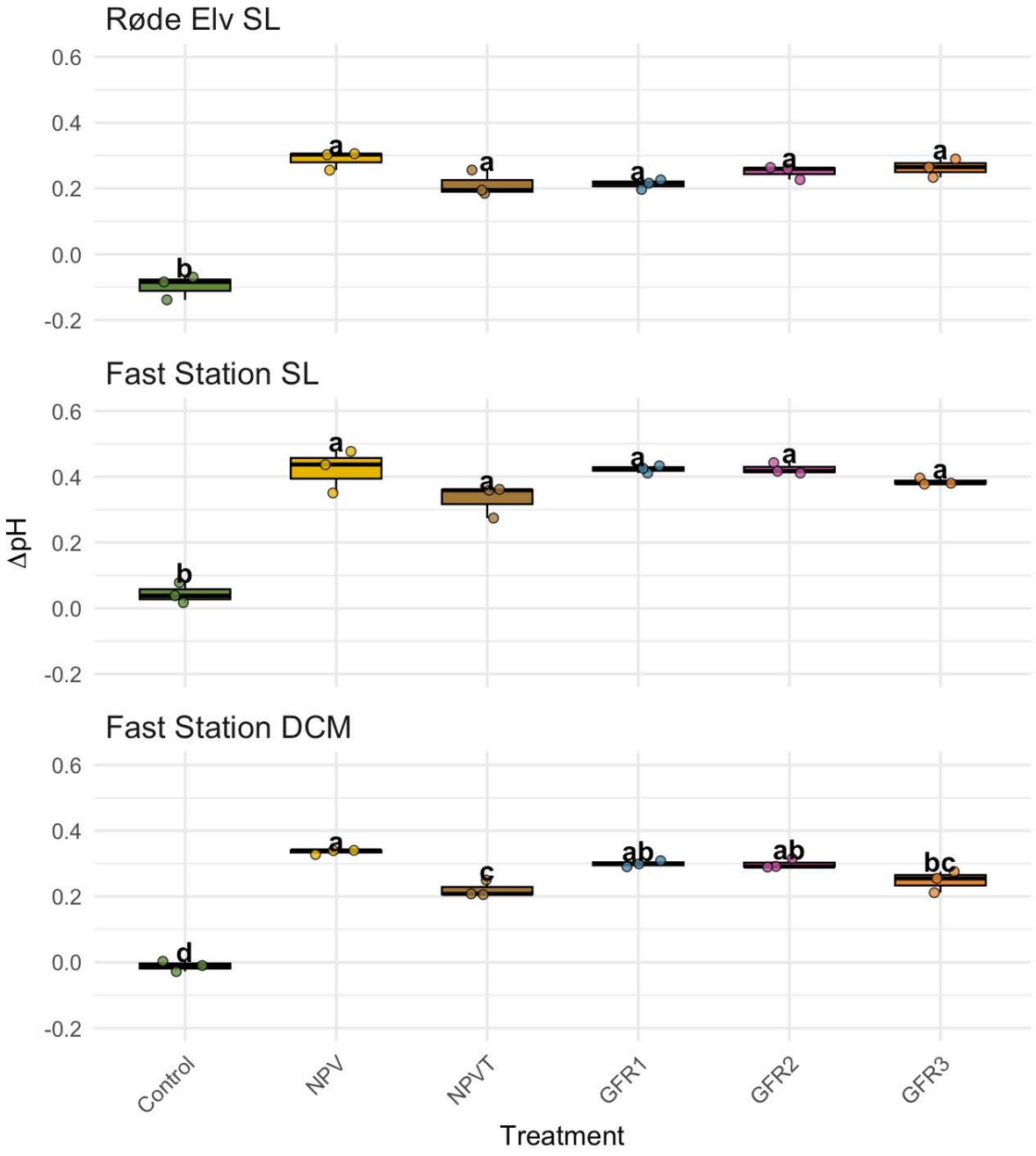

Fig. 12. Change in pH (ΔpH) across treatments at each site and depth. At Røde Elv SL, only NPS increased pH significantly compared to the control. At Fast Station SL, NPS produced the highest ΔpH, significantly exceeding the control and NPST, while GRF treatments were not significantly different from NPS or from each other. At Fast Station DCM, NPS yielded the highest ΔpH, significantly exceeding NPST and the control, while GRF_1 and GRF_2 were also higher than the control but comparable to GRF.

3.6. Observations of net-phytoplankton community

Based on light microscopy, the net phytoplankton community was very sparse despite having filtered approx. 25.1 m^3 (($p*(0.4m)^2$ x 50 m) = 25,100 L) of water and observing several drops (Fig. 13). Both samples had relatively low cell abundances of centric diatoms (*Chaetoceros* spp. *Rhizosolenia* sp., *Thalassiosira* sp.), the silicoflagellate *Dictyocha speculum*. Additionally, a few individuals of heterotrophic dinoflagellates were also observed (*Protoperidinium*, *Gyrodinium* and *Phalacroma*). Several small-sized but unidentified heterotrophic dinoflagellates were also seen. With respect to species of *Chaetoceros* and *Rhizosolenia*, they looked physiological unhealthy with degrading chloroplasts and broken valves. The net plankton sample from 15 July contained about 50 individuals of *Calanus hyperboreus* and a single sea angel (*Clione*).

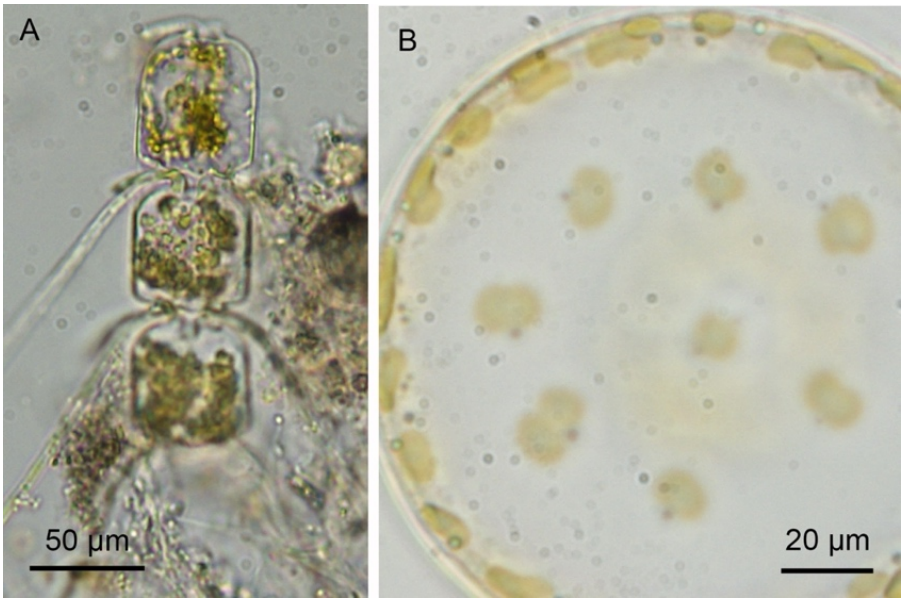

Fig. 13. Images of two of the very few net phytoplankton species observed in the plankton sample collected at the Fast station in July 2025. A: Chaetoceros sp. Notice the detritus surrounding the not very healthy-looking chain of this centric diatom. B: One of the very few healthy-looking centric diatoms, likely a species of Thalassiosira.

4. Discussion

4.1. Short-term response to macronutrients and trace metals yields increased Fv/Fm and chl *a* across locations and depths

The aim of this study was to investigate the short-term responses of Arctic phytoplankton communities to additions of macronutrients, trace metals, and dose-responses due to varying

concentrations of GRF. At the SL of both locations, F_v/F_m and chl *a* increased compared to the control, consistent with H1, when treated with NPS. This suggests that macronutrient addition (NPS) relieved nitrogen and/or phosphorus limitation, a common feature in Arctic surface waters during summer after the spring bloom (Arrigo et al., 2010; Moore et al., 2013). The increase of photosynthetic efficiency (F_v/F_m) alongside higher chl *a* indicates that the phytoplankton communities were able to both increase photosynthetic capacity and accumulate biomass when nutrients became available. At the SL at both locations, both F_v/F_m and chl *a* increased even more when trace metals were added (NPST), showing that trace metals also play a key role in limiting growth during the Arctic summer, which furthermore aligns with H2. This suggests a co-limitation between macronutrients and trace metals of phytoplankton communities near Disco Bay at the surface layer.

At Fast Station DCM, F_v/F_m decreased when treated with NPS and increased when treated with NPST. This suggest that at DCM, the phytoplankton are mainly limited by trace metals, most possibly iron, and are saturated with macronutrients. However, when looking at chl *a* levels, NPS and NPST at Fast Station DCM increased the same amount, suggesting that trace metals do not, in fact, have a limiting effect. These results would instead suggest that the limiting factor at DCM is macronutrients, contradicting the observation derived from F_v/F_m. However, due to the large variation in the data, it is difficult to determine exactly which of these observations are most reliable, but it at least suggest that at DCM the phytoplankton are still limited by some nutrients, be it macronutrients or trace metals.

It is also important to note that chl *a* is only a proxy for phytoplankton biomass, and an increase does not necessarily reflect cell proliferation. Microscopy revealed a sparse net-phytoplankton community, with many individuals appearing physiologically degraded, showing broken valves and deteriorating chloroplasts. With this poor condition it is possible that the biomass increase inferred from chl *a* may reflect pigment upregulation in stressed or senescent cells rather than active growth.

4.2. Inconsistent responses to varying doses of GRF

Due to the findings in previous studies on phytoplankton communities (Bendtsen et al., 2024) it was hypothesized, that the NPS+GRF treatments would yield the same response as the NPST treatment due to the natural content of trace metals in GRF. In this study, NPS + GRF treatments did not consistently match NPST between locations with examples of higher, lower

or no change in levels of F_v/F_m and chl *a* when comparing NPST treatments with NPS+GRF treatments after two days, thus H3 could not be fully supported. Previous incubation studies by Bendtsen et al. (2024) and Lund (2025) suggested that the minerals and nutrients in GRF would be mobilized and stimulate growth after around 2 days. Due to the inconsistency in results when comparing NPS+GRF with NPST in this short-term experiment, it is thus likely that the trace metals bound within GRF was not rapidly released/mobilized and that a longer time scale would be required to determine if the NPS+GRF treated natural communities would yield the same results as the NPST treated cultures.

Similarly, a longer experimental duration would also be necessary to assess if a positive dose-response relationships was observable between GRF concentrations. Due to the overall lack of significant results showing if GRF had a positive impact on the communities, a positive dose response cannot be tested, and thus H4 cannot be fully supported. However, a negative dose-dependent reaction could still be observable due to shading or toxicity. In a recent study by Maselli et al., (2023) they examined how meltwater runoffs from glaciers which carries GRF into marine ecosystems would impact protist microplankton in four Greenlandic fjords during summer. They found that autotrophic microplankton was negatively affected by GRF due to reduced light penetration. Even though this study cannot determine whether GRF would increase growth and the physiological conditions of the cells, the results show no negative effect of GRF after two days, which would be expected, if shading had a significant impact. In all samples treated with NPS+GRF, chl *a* and F_v/F_m levels where higher compared to the control and showed greater or almost no difference compared to NPS alone, showing that GRF did not negatively impact the cells. Between NPS+GRF concentrations, no negative dose-dependent effect due to shading or toxicity was observed either.

The pH data show a clear and significant increase after two days in the NPS, NPST, and NPS+GRF1–3 treatments compared with the controls across all locations and depths. This increase is likely driven by enhanced biological activity, whereby photosynthetic uptake of CO_2 raises pH (Flynn et al., 2015). While chl *a* and F_v/F_m showed few statistically significant responses with explanations mostly based on trends, the pH data provide clear evidence that the phytoplankton communities responded to nutrient enrichment in the coastal Arctic waters. The observed pH increases in NPS+GRF1–3 treatments is most likely attributable to the addition of dissolved macronutrients, as nutrients bound within the GRF were likely not yet mobilized, as discussed above.

4.3. Comparing locations and depths

When comparing results across locations and depths, few statistically significant effects were detected, and no consistent trends were observed. The two proxies often yielded contrasting patterns, making it difficult to determine the response between locations and depths. Considering chl *a* alone, significant differences were found between the SL and the DCM, with SL samples showing greater increases in chl *a*. This aligns with H5 as the nutrient-depleted surface layers would be more responsive to nutrient additions, whereas the DCM, with more favorable light and nutrient conditions, would be less likely to exhibit a pronounced response. However, the Røde Elv DCM data were derived from an irregular and highly variable dataset not collected by us, and F_v/F_m showed a greater increase at the DCM across all treatments compared to the SL, contradicting the observations derived from chl *a* levels, making it difficult to draw definitive conclusions from these results.

For most treatments, comparisons between Fast Station and Røde Elv showed no significant differences. This lack of clear patterns may be due to the Røde Elv sampling site being located too far from the river outlet causing the suspended particulate matter concentrations to be similar between locations and depths (Fig. 10). Sampling directly at the Røde Elv outlet would likely have resulted in substantially higher natural GRF and associated nutrient concentrations compared to Fast Station, potentially leading to more consistent and distinct phytoplankton responses between locations across treatments. As hypothesized in H5, samples collected from a location with high natural GRF concentrations were expected to exhibit a reduced response to nutrient addition since nutrients would be more abundant compared to Fast Station, where GRF concentrations were presumed to be lower. However, the observed similarity in suspended particulate matter between locations and depths prevents any clear conclusions regarding the role of GRF abundance in driving any observed responses.

5. Limitations and future studies

This study had some limitations that should be considered. The incubation time was relatively short which may not have been enough for phytoplankton communities to fully adjust to the treatments. Many species require several days to exit the lag phase and enter active growth,

meaning the responses we observed likely reflect short-term fluctuations rather than sustained growth.

This is particularly relevant for communities naturally exposed to lower GRF concentrations, as these may need more time to activate the physiological mechanisms required to utilize trace metals. A longer incubation would likely provide a clearer picture of treatment effects. Additionally, future sampling could benefit from including sites further upstream in Røde Elv, where GRF concentrations and sediment influence are expected to be higher, potentially revealing stronger responses.

To gain a more complete understanding, future studies could combine longer incubation periods with repeated measurements over time, sample sites with different GRF exposure histories, and include molecular or biochemical markers. Including a treatment with trace metals alone, without concurrent macronutrient additions, could have provided further insight into the specific role of trace metals in driving the observed responses, disentangled from potential interactive effects with macronutrients. These steps would help clarify the role of GRF in influencing phytoplankton productivity across different Arctic environments.

6. Conclusion

This study demonstrates that macronutrients, particularly nitrogen and phosphorus, limit phytoplankton growth in the surface layer at both Røde Elv and Fast Station in Disko Bay, as evidenced by increased chl *a* and F_v/F_m following NPS addition. The combined addition of macronutrients and trace metals elicited a stronger response, indicating potential co-limitation by both macronutrients and trace metals. In contrast, GRF combined with NPS showed no measurable effect over the short experimental period, suggesting that nutrients bound within GRF were not yet bioavailable. No negative response due to shading or other factors was observed. These findings imply that GRF could influence phytoplankton growth over longer timescales once nutrients from GRF became mobilized, while immediate productivity in Arctic summer waters is primarily controlled by the availability of macro- and trace nutrients. Across locations and depths, no consistent patterns or significant differences were observed, likely due to the similar concentrations of suspended particulate matter. This may be explained by the Røde Elv sampling site not being sufficiently close to the river outlet, where GRF concentrations are expected to be highest, causing similar nutritional conditions between

sampling sites. Future studies should conduct long-term incubations experiments on communities sampled at GRF rich environments to determine to what extent the natural occurrence of GRF has an impact on the ability of phytoplankton to utilize GRF.

Future studies should include longer incubation periods to capture potential delayed effects of GRF nutrient release and sample sites located further upstream in Røde Elv to ensure higher GRF exposure. Combining such sampling with repeated measurements over time and across varying GRF exposure histories would provide a more complete understanding of GRF's role in Arctic phytoplankton productivity.

7. Acknowledgments

We would like to thank the Board for the Arctic Station and Department of Biology for providing all the finances for this course. Furthermore, we would like to especially thank our professors Niels Daugbjerg and Per Juel Hansen for giving us the opportunity to attend this course and for their guidance and support throughout this study.

8. References

Arrigo, K. R., van Dijken, G. L., & Pabi, S. (2010). Impact of a shrinking Arctic ice cover on marine primary production. Geophysical Research Letters, 37(15), L15603. https://doi.org/10.1029/2010GL044263

Behrenfeld, M. J., & Kolber, Z. S. (1999). Widespread iron limitation of phytoplankton in the South Pacific Ocean. Science, 283(5403), 840–843. https://doi.org/10.1126/science.283.5403.840

Bendtsen, J., Daugbjerg, N., & Hansen, J. L. S. (2024). Glacial rock flour increases photosynthesis and biomass of natural phytoplankton communities in subtropical surface waters: A potential means of action for marine CO2 removal. Frontiers in Marine Science, 11. https://doi.org/10.3389/fmars.2024.1416421

Bendtsen, J., Daugbjerg, N., Vallentin Larsen, K., Dyrberg Dahms, R., Richardson, K., & Rosing, M. (2023). Impact from glacial rock flour on phytoplankton growth and the carbonate system. EGU General Assembly 2023, Vienna, Austria, 24–28 Apr 2023, EGU23-7285. https://doi.org/10.5194/egusphere-egu23-7285

Boyd, P. W., Jickells, T., Law, C. S., Blain, S., Boyle, E. A., Buesseler, K. O., Coale, K. H., Cullen, J. J., de Baar, H. J. W., Follows, M., Harvey, M., Lancelot, C., Levasseur, M., Owens, N. P. J., Pollard, R., Rivkin, R. B., Sarmiento, J., Schoemann, V., Smetacek, V., … Watson, A. J. (2007). Mesoscale iron enrichment experiments 1993–2005: Synthesis and future directions. Science, 315(5812), 612–617. https://doi.org/10.1126/science.1131669

Bristow, L. A., Mohr, W., Ahmerkamp, S., & Kuypers, M. M. M. (2017). Nutrients that limit growth in the ocean. Current Biology, 27(11), R474–R478. https://doi.org/10.1016/j.cub.2017.03.030

Falkowski, P. G., Barber, R. T., & Smetacek, V. (1998). Biogeochemical controls and feedbacks on ocean primary production. Science, 281(5374), 200–206. https://doi.org/10.1126/science.281.5374.200

Field, C. B., Behrenfeld, M. J., Randerson, J. T., & Falkowski, P. (1998). Primary production of the biosphere: Integrating terrestrial and oceanic components. Science, 281(5374), 237–240. https://doi.org/10.1126/science.281.5374.237

Flynn, K. J., Clark, D. R., Mitra, A., Fabian, H., Hansen, P. J., Glibert, P. M., Wheeler, G. L., Stoecker, D. K., Blackford, J. C., & Brownlee, C. (2015). Ocean acidification with (de)eutrophication will alter future phytoplankton growth and succession. Proceedings of the Royal Society B, 282(1804), 20142604. https://doi.org/10.1098/rspb.2014.2604

Frey, K. E., et al. (2022). Arctic Ocean primary productivity: The response of marine algae to climate warming and sea ice decline. https://doi.org/10.25923/0je1-te61

Guillard, R. R. L., & Hargraves, P. E. (1993). Stichochrysis immobilis is a diatom, not a chrysophyte. Phycologia, 32(3), 234–236. https://doi.org/10.2216/i0031-8884-32-3-234.1

Kolber, Z. S., Barber, R. T., Coale, K. H., Fitzwater, S. E., Greene, R. M., Johnson, K. S., Lindley, S., & Falkowski, P. G. (1994). Iron limitation of phytoplankton photosynthesis in the equatorial Pacific Ocean. Nature, 371(6493), 145–149. https://doi.org/10.1038/371145a0

Kitajima, M., & Butler, W. L. (1975). Quenching of chlorophyll fluorescence and primary photochemistry in chloroplasts by dibromothymoquinone. Biochimica et Biophysica Acta (BBA) - Bioenergetics, 376(1), 105–115. https://doi.org/10.1016/0005-2728(75)90209-1

Lund, J. H. (2025). Dual response of glacial rock flour on two species of dinoflagellates.
Maselli, M., Meire, L., Meire, P., & Hansen, P. J. (2023). Effects of glacial flour on marine micro-plankton: Evidences from natural communities of Greenlandic fjords and experimental studies. Protist, 174(1), 125928. https://doi.org/10.1016/j.protis.2022.125928

Moore, C. M., Mills, M. M., Langlois, R. J., Milne, A., Achterberg, E. P., LaRoche, J., & Geider, R. J. (2013). Processes and patterns of oceanic nutrient limitation. Nature Geoscience, 6(9), 701–710. https://doi.org/10.1038/ngeo1765

Møller, E. F., Christensen, A., Larsen, J., Mankoff, K. D., Ribergaard, M. H., Sejr, M., Wallhead, P., & Maar, M. (2023). The sensitivity of primary productivity in Disko Bay, a coastal Arctic ecosystem, to changes in freshwater discharge and sea ice cover. Ocean Science, 19, 403–420. https://doi.org/10.5194/os-19-403-2023

Negrete-García, G., Luo, J. Y., Petrik, C. M., Manizza, M., & Barton, A. D. (2024). Changes in Arctic Ocean plankton community structure and trophic dynamics on seasonal to interannual timescales. Biogeosciences, 21(22), 4951–4973. https://doi.org/10.5194/bg-21-4951-2024

Oschlies, A., Bach, L. T., Fennel, K., Gattuso, J.-P., & Mengis, N. (2025). Perspectives and challenges of marine carbon dioxide removal. Frontiers in Climate, 6, 1506181. https://doi.org/10.3389/fclim.2024.1506181

Randelhoff, A. M., Randelhoff, V. M., & Rysgaard, S. (2020). Pan-Arctic Ocean primary production constrained by turbulent nitrate fluxes. Frontiers in Marine Science, 7, 150. https://doi.org/10.3389/fmars.2020.00150

Suggett, D. J., Moore, C. M., Hickman, A. E., & Geider, R. J. (2009). Interpretation of fast repetition rate (FRR) fluorescence: Signatures of phytoplankton community structure versus physiological state. Marine Ecology Progress Series, 376, 1–19. https://doi.org/10.3354/meps07830

Appendix A – Supplementary Data

Model Assumptions for Chlorophyll a

1.1. Model Assumptions for Chlorophyll a at Røde Elv Surface Layer

```
---- Røde Elv SL ----

        Shapiro-Wilk normality test

data:  residuals(model)
W = 0.88084, p-value = 0.02697
```

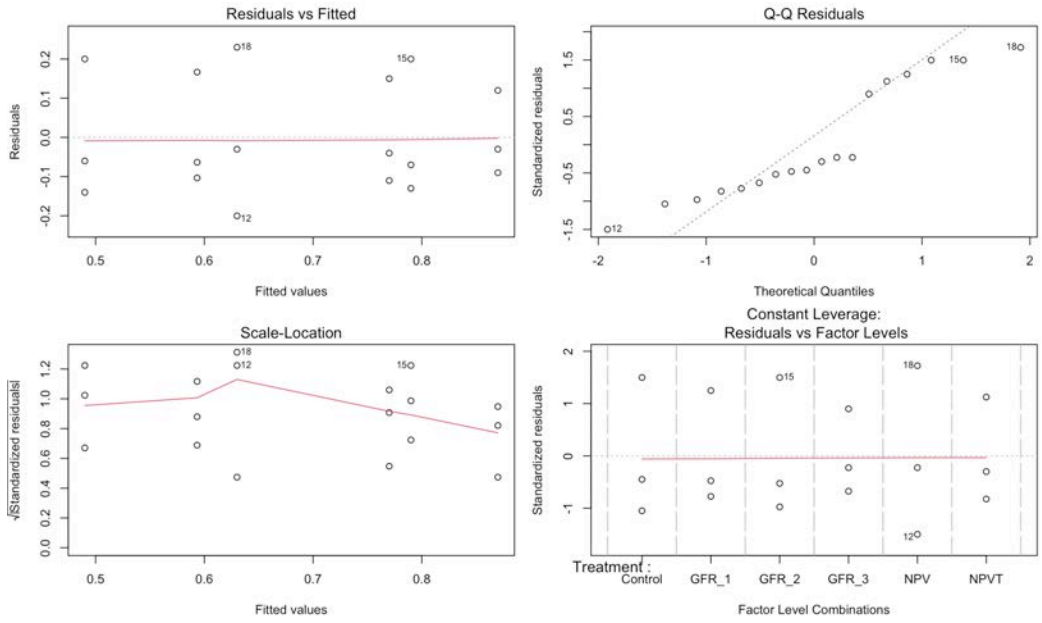

Fig. S1. Diagnostic Plots and Shapiro-Wilk Normality Test Results for Chlorophyll a at Røde Elv SL. Diagnostic plots include Residuals vs Fitted, Q-Q plot of residuals, Scale-Location plot, and Residuals vs Factor Levels. Visual inspection of plots indicated no substantial deviations from model assumptions. Shapiro-Wilk test for normality showed significance at p = 0.03.

Model Assumptions for Chlorophyll a at Røde Elv Deep Chlorophyll Max

```
---- Røde Elv DCM ----

        Shapiro-Wilk normality test

data:  residuals(model)
W = 0.91052, p-value = 0.08786
```

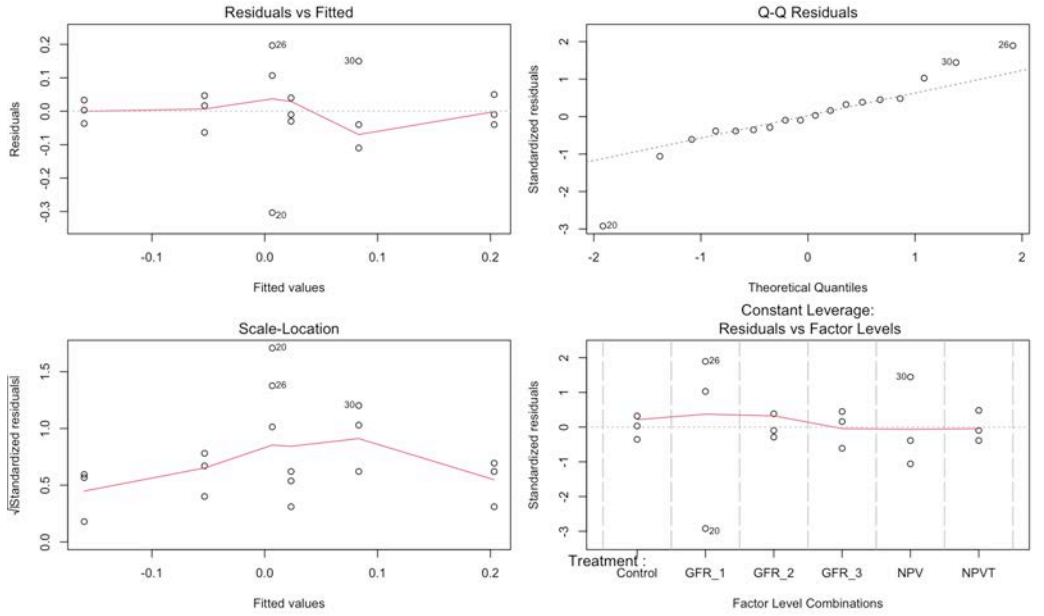

Fig. s2. Diagnostic Plots and Shapiro-Wilk Normality Test Results for Chlorophyll a at Røde Elv DCM. Diagnostic plots include Residuals vs Fitted, Q-Q plot of residuals, Scale-Location plot, and Residuals vs Factor Levels. Visual inspection of plots indicated no substantial deviations from model assumptions. Shapiro-Wilk test for normality showed no significance with p = 0.08786.

Model Assumptions for Chlorophyll a at Fast Station Surface Layer

```
---- Fast Station SL ----

        Shapiro-Wilk normality test

data:  residuals(model)
W = 0.94489, p-value = 0.3506
```

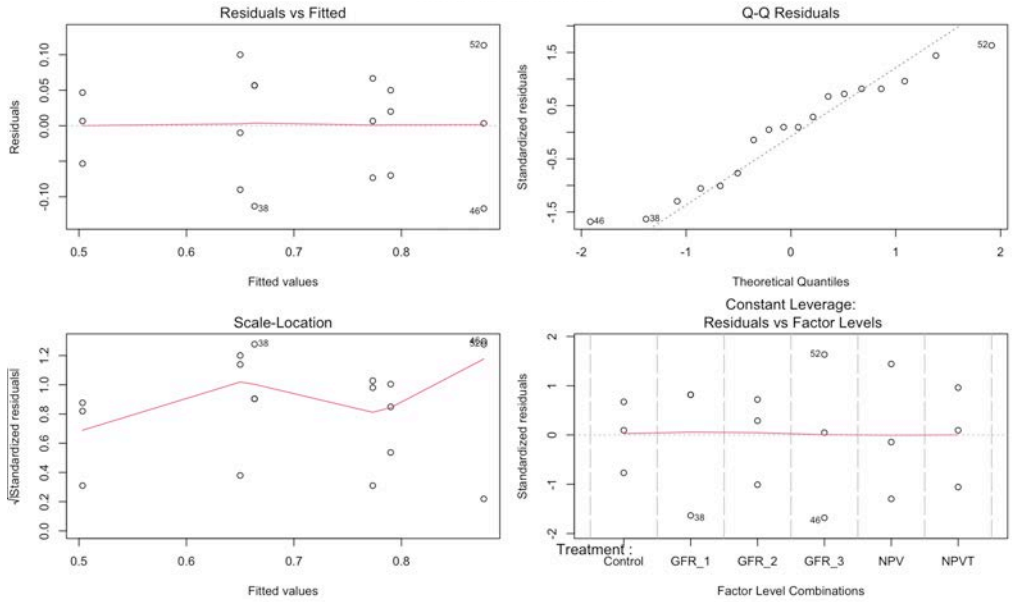

Fig. S1. Diagnostic Plots and Shapiro-Wilk Normality Test Results for Chlorophyll a at Fast Station SL. Diagnostic plots include Residuals vs Fitted, Q-Q plot of residuals, Scale–Location plot, and Residuals vs Factor Levels. Visual inspection of plots indicated no substantial deviations from model assumptions. Shapiro-Wilk test for normality showed no significance with p = 0.3506.

Model Assumptions for Chlorophyll a at Fast Station Deep Chlorophyll Max

```
---- Fast Station DCM ----

        Shapiro-Wilk normality test

data:  residuals(model)
W = 0.96674, p-value = 0.7347
```

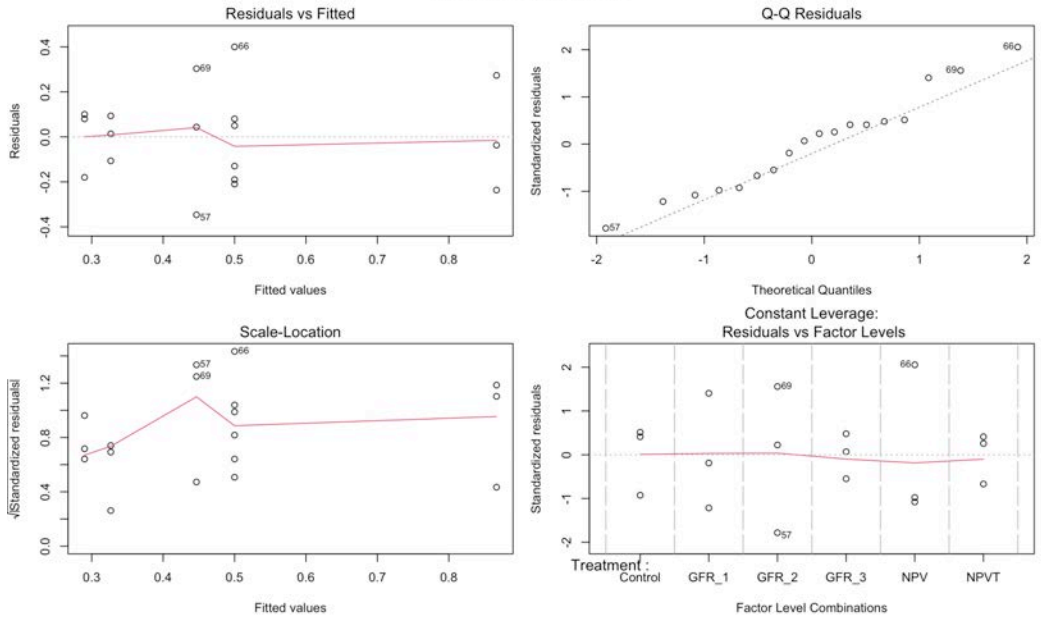

Fig. S2. Diagnostic Plots and Shapiro-Wilk Normality Test Results for Chlorophyll a at Fast Station DCM. *Diagnostic plots include Residuals vs Fitted, Q-Q plot of residuals, Scale-Location plot, and Residuals vs Factor Levels. Visual inspection of plots indicated no substantial deviations from model assumptions. Shapiro-Wilk test for normality showed no significance with p = 0.7347.*

Model Assumptions for F_v/F_m

1.2. Model Assumptions for F_v/F_m at Røde Elv Surface Layer

```
---- Røde Elv SL ----

        Shapiro-Wilk normality test

data:  residuals(model)
W = 0.91041, p-value = 0.08747
```

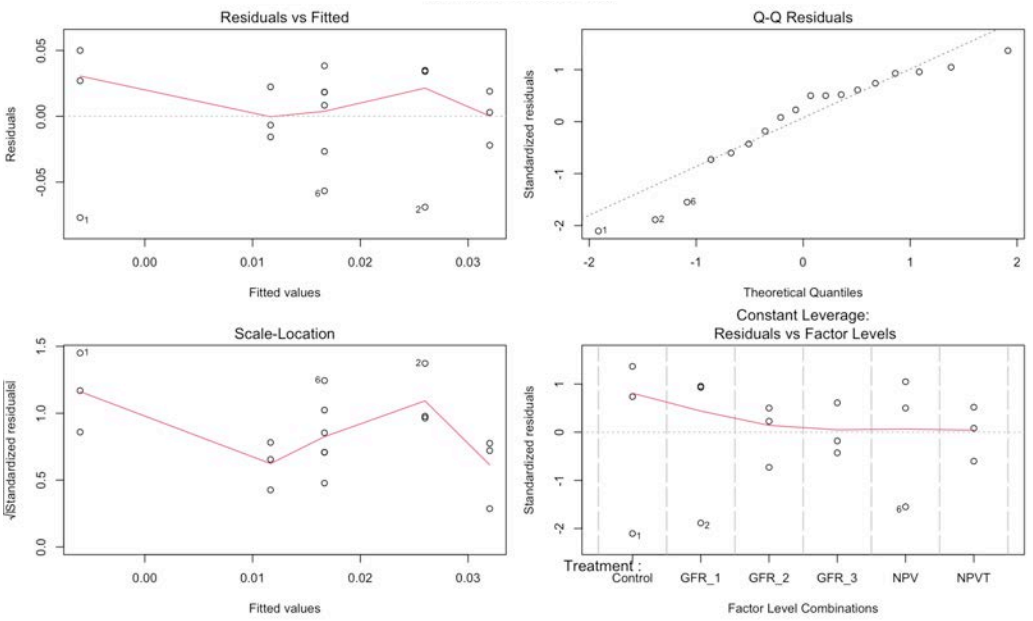

Fig. S3. Diagnostic Plots and Shapiro-Wilk Normality Test Results for F_v/F_m at Røde Elv SL. Diagnostic plots include Residuals vs Fitted, Q-Q plot of residuals, Scale-Location plot, and Residuals vs Factor Levels. Visual inspection of plots indicated no substantial deviations from model assumptions. Shapiro-Wilk test for normality showed no significance with p = 0.08747.

Model Assumptions for F_v/F_m at Fast Station Surface Layer

```
---- Fast Station SL ----

        Shapiro-Wilk normality test

data:  residuals(model)
W = 0.96803, p-value = 0.76
```

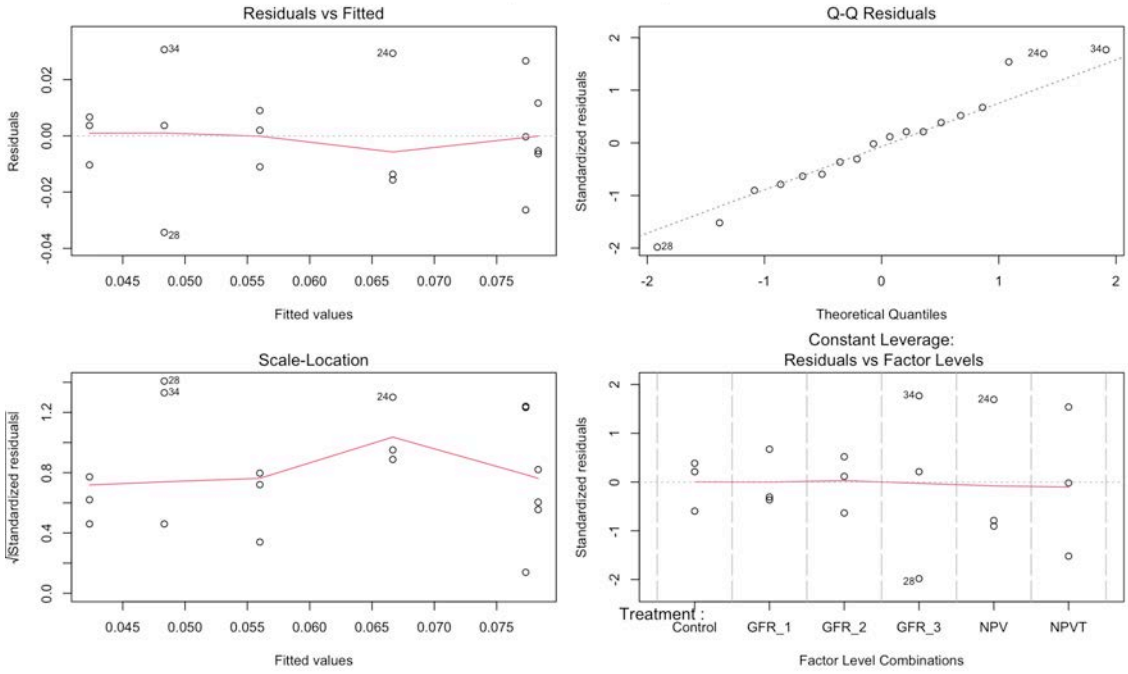

Fig. S4. Diagnostic Plots and Shapiro-Wilk Normality Test Results for F_v/F_m at Fast Station SL. Diagnostic plots include Residuals vs Fitted, Q-Q plot of residuals, Scale-Location plot, and Residuals vs Factor Levels. Visual inspection of plots indicated no substantial deviations from model assumptions. Shapiro-Wilk test for normality showed no significance with p = 0.76.

Model Assumptions for F_v/F_m at Fast Station Deep Chlorophyll Max

```
---- Fast Station DCM ----

        Shapiro-Wilk normality test

data:  residuals(model)
W = 0.94193, p-value = 0.3126
```

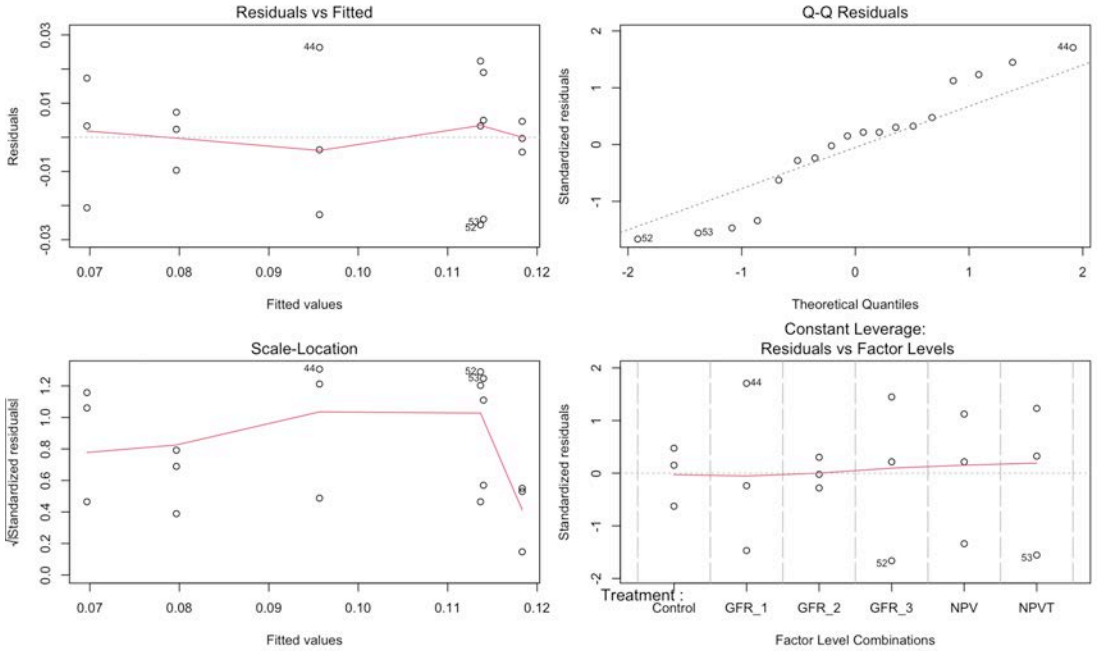

Fig. S5. Diagnostic Plots and Shapiro-Wilk Normality Test Results for F_v/F_m at Røde Elv DCM. Diagnostic plots include Residuals vs Fitted, Q-Q plot of residuals, Scale-Location plot, and Residuals vs Factor Levels. Visual inspection of plots indicated no substantial deviations from model assumptions. Shapiro-Wilk test for normality showed no significance with p = 0.3126.

Model Assumptions for Suspended Particulate Matter

1.3. Model Assumptions for pH at Røde Elv SL

```
---- Røde Elv SL ----

        Shapiro-Wilk normality test

data:  residuals(model)
W = 0.98684, p-value = 0.7804
```

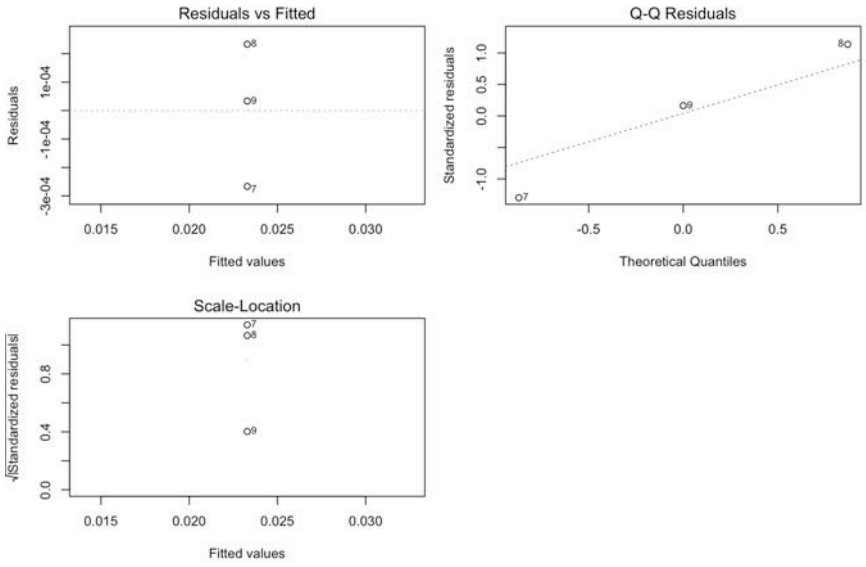

Fig. S8. Diagnostic Plots and Shapiro-Wilk Normality Test Results for Suspended Particulate Matter at Røde Elv SL. Due to only three data points, no plot of residuals vs factor levels is shown. Visual inspection indicated no substantial deviations from model assumptions. Shapiro–Wilk test for normality was non-significant (p = 0.7804).

Model Assumptions for pH at Fast Station SL

```
---- Fast Station SL ----

        Shapiro-Wilk normality test

data:  residuals(model)
W = 0.9195, p-value = 0.4506
```

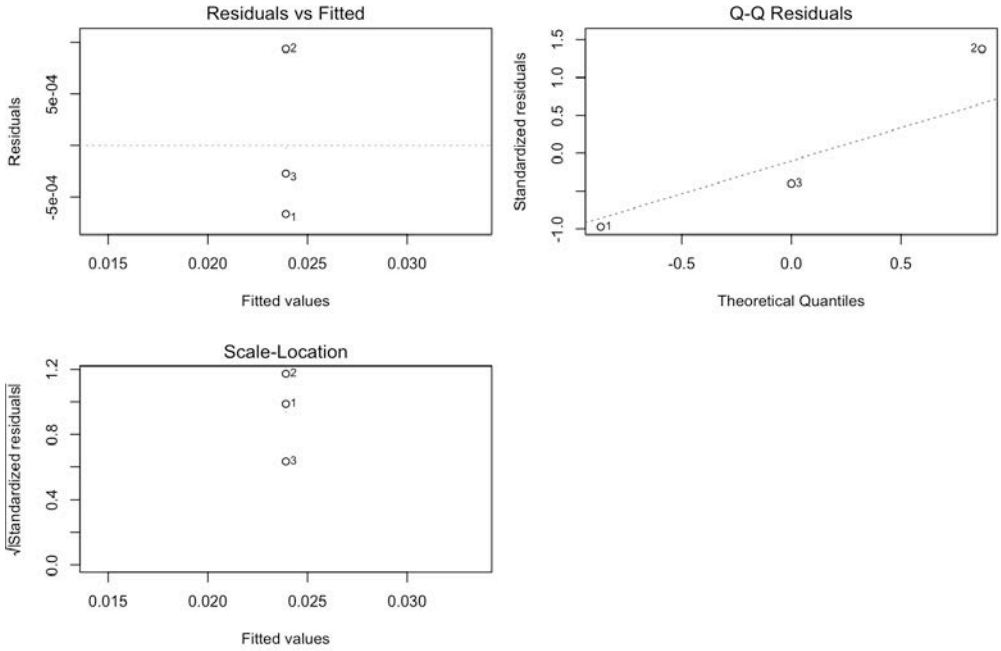

Fig. S9. Diagnostic Plots and Shapiro-Wilk Normality Test Results for Suspended Particulate Matter at Fast Station SL. Due to only three data points, no plot of residuals vs factor levels is shown. Visual inspection indicated no substantial deviations from model assumptions. Shapiro–Wilk test for normality was non-significant (p = 0.45).

Model Assumptions for pH at Fast Station DCM

```
---- Fast Station DCM ----

        Shapiro-Wilk normality test

data:  residuals(model)
W = 0.82418, p-value = 0.1736
```

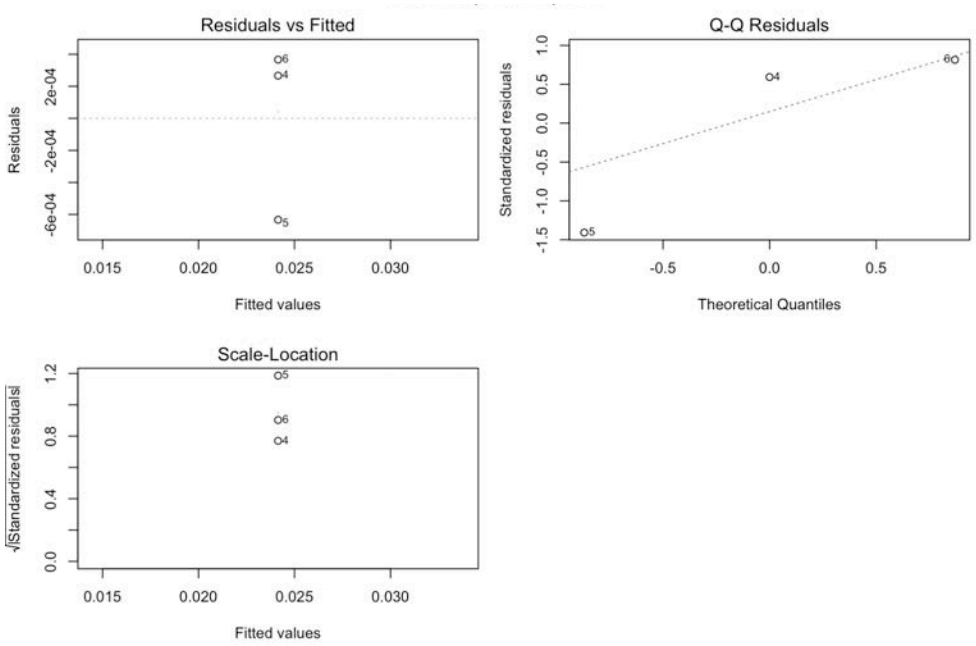

Fig. S10. Diagnostic Plots and Shapiro-Wilk Normality Test Results for Suspended Particulate Matter at Fast Station DCM. Due to only three data points, no plot of residuals vs factor levels is shown. Visual inspection indicated no substantial deviations from model assumptions. Shapiro–Wilk test for normality was non-significant (p = 0.17).

1.4. Model Assumptions for pH at Røde Elv SL

```
Shapiro-Wilk (residuals):

        Shapiro-Wilk normality test

data:  residuals(model)
W = 0.94643, p-value = 0.3718
```

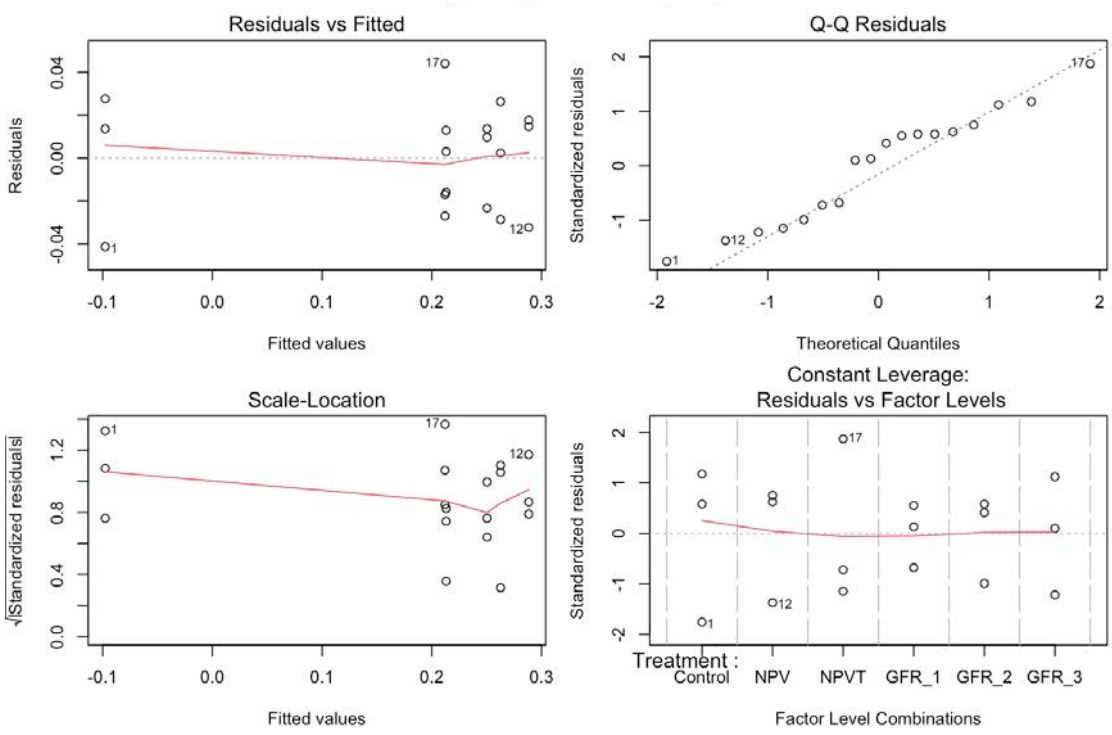

Fig. S11. Diagnostic Plots and Shapiro-Wilk Normality Test Results for pH at Røde Elv SL. Visual inspection of plots indicated no substantial deviations from model assumptions. Shapiro-Wilk test for normality showed no significance (p = 0.37).

Model Assumptions for pH at Fast Station SL

```
Shapiro-Wilk (residuals):

        Shapiro-Wilk normality test

data:  residuals(model)
W = 0.95005, p-value = 0.4257
```

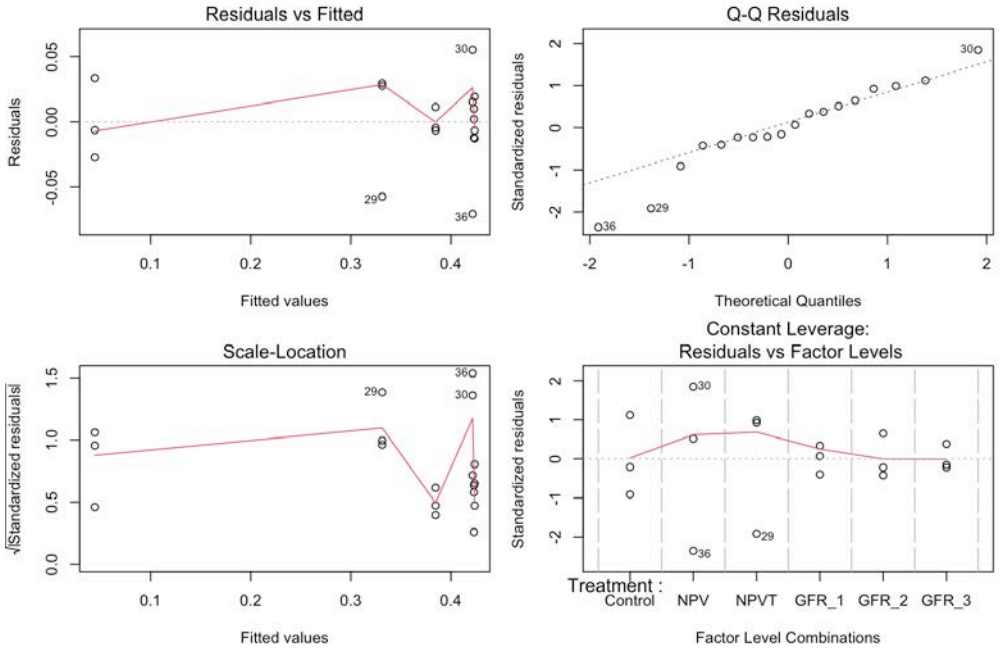

Fig. S12. Diagnostic Plots and Shapiro-Wilk Normality Test Results for pH at Fast Station SL. Visual inspection of plots indicated no substantial deviations from model assumptions. Shapiro-Wilk test for normality was not significant (p = 0.43).

Model Assumptions for pH at Fast Station DCM

```
Shapiro-Wilk (residuals):

        Shapiro-Wilk normality test

data:  residuals(model)
W = 0.96979, p-value = 0.7938
```

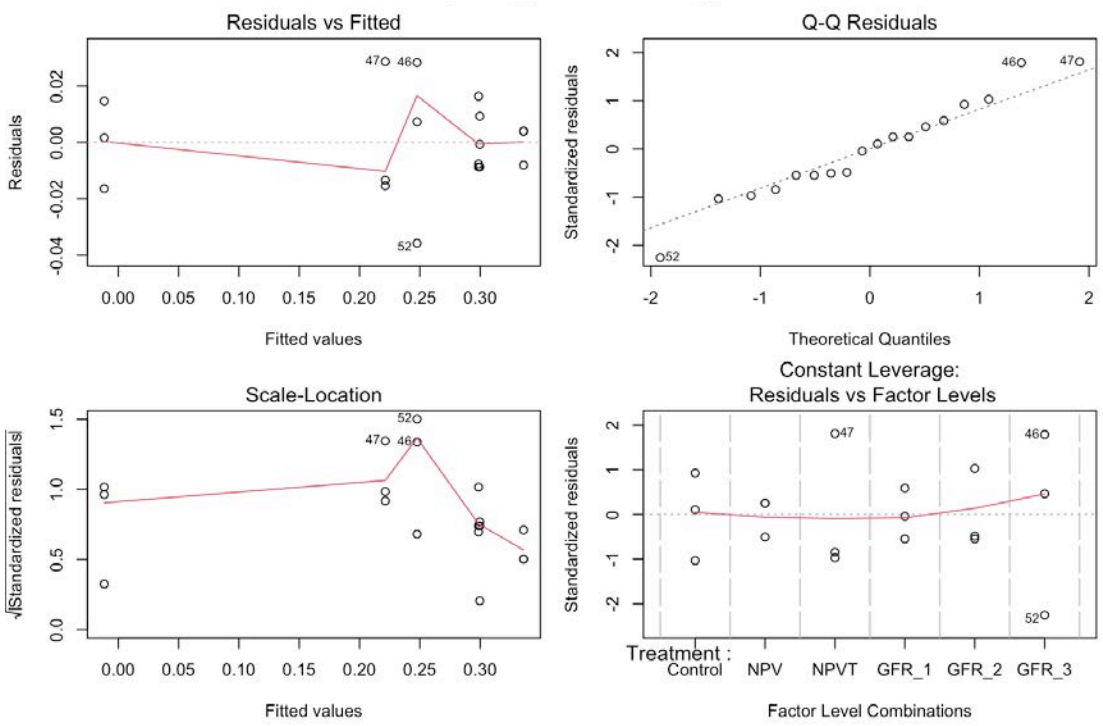

Fig. S13. Diagnostic Plots and Shapiro-Wilk Normality Test Results for pH at Fast Station DCM. Visual inspection of plots indicated no substantial deviations from model assumptions. Shapiro-Wilk test for normality showed no significance (p = 0.79).

Report 2

Emily Aileen Faye, Amalie Kargaard Jensen, Emma Nitschky Juvik, Signe Korte Petersen & Marie Ulfbeck Schovsbo (2025). Short-term effects of glacial rock flour on phytoplankton communities in Disko Bay, Western Greenland.

Short-term effects of glacial rock flour on phytoplankton communities in Disko Bay, Western Greenland

Emily Aileen Faye (wmv544)

Amalie Kargaard Jensen (lsq585)

Emma Nitschky Juvik (jxr599)

Signe Korte Petersen (rtf662)

Marie Ulfbeck Schovsbo (fts434)

15.08.2025

Preface

This report was initially designed to follow a thorough sampling and incubation plan, with the aim of assessing the response of different phytoplankton communities to varying concentrations of glacial rock flour (GRF). The original experiment included a transect with four stations, a temporal sampling scale at days 0, 3, and 5, and a microscopy-based community composition analysis. We wanted to do this to assess short- and long-term responses in biomass, physiology, and species community structure.

However, unforeseen complications hindered the full execution of this plan. Significant travel delays due to mechanical issues with a plane and bad weather shortened our stay at the research station and thus limited our sampling and laboratory time. We were therefore forced to downscale our experimental set-up to a transect with three stations and our incubation period to a sampling time scale of day 0 and 1.6. We were also unable to complete any microscopy work. In addition, a packing error led to the omission of essential vitamins in two treatments, limiting our ability to compare across treatments and with previous studies. Finally, the failure of the cooler, an essential part of the equipment, during measurements of F_v/F_m, resulted in missing data for two treatments.

In response to these complications and changes, we refined our hypotheses. Originally, we expected to observe a time- and dose-dependent response to GRF, including differences in community structure across stations and depths, and a shift in phytoplankton size classes. Now, with the shortened incubation period and limited available data, we instead focused on short-term physiological responses. We are now interested in whether phytoplankton can even utilize trace metals from GRF within this shortened timeframe. This shift in focus reflects both the logistical constraints that we encountered during the fieldwork and the opportunity to still test ecologically meaningful responses to GRF.

Despite all these complications, we are incredibly grateful to have had the opportunity to carry out fieldwork in such a remote and unique place as Greenland. We learned a lot - not only during the months of preparation leading up to the trip, but also during our unexpected (and very long) stay in Nuuk, and once we finally reached the Arctic Station and were able to conduct work in the field and the laboratory. This trip taught us many valuable lessons, we did

not expect to be taught - above all: the importance of adaptability and resilience! We are incredibly proud to present this report as a reflection of our efforts. Enjoy!

Abstract

Glacial rock flour (GRF) has been proposed as a marine carbon dioxide removal (mCDR) strategy by supplying phytoplankton communities with limiting nutrients such as iron, thereby stimulating growth and enhancing the biological carbon pump. This study investigated the short-term effects of GRF addition on natural phytoplankton communities in Disko Bay, West Greenland. Water samples were collected from three stations along a glacial sediment gradient and from two depths: surface and deep chlorophyll maximum (DCM). Incubation experiments were conducted using three GRF concentrations; L1 media with nitrate, phosphate, silicate and trace metals; a negative control with nitrate, phosphate and silicate (NPS); and a water control (C) as treatments over a short incubation period of 38 h. Phytoplankton biomass and photosynthetic efficiency were assessed via chlorophyll *a* concentration and F_v/F_m ratios, respectively. Results showed inconsistent responses across stations and treatments. A positive dose-response in chlorophyll *a* was observed at some stations, suggesting possible GRF utilization, while other stations exhibited negative or no effects. Fv/Fm ratios remained largely unaffected by GRF treatments, indicating no short-term increase in photosynthetic efficiency. No clear patterns emerged in relation to proximity to glacial discharge or depth. The short incubation time may have limited phytoplankton acclimation, highlighting the need for longer-term experiments to better assess GRF utilization across different phytoplankton communities

1. Introduction

Glacial rock flour (GRF) is a fine-grained material produced by the mechanical grinding of bedrock beneath glaciers, particularly those associated with large ice sheets, including the Greenland Ice Sheet (Bendtsen et al., 2024). The annual production of suspended sediments of the Greenland Ice Sheet accounts for around 7-9% of the global sediment load. GRF is transported by meltwater through rivers or lakes, or directly into marine environments via subglacial discharges at the front of glaciers. In Greenland, it has been deposited in large amounts along the coast since the beginning of the Holocene; especially Western Greenland is a main producer of sediments to the ocean (Ray Sarkar, 2023).

The mineral composition of GRF mainly includes biotite, oligoclase/andesine, amphibole, anorthite, quartz, and trace metals like iron and zinc, depending on the region (Bendtsen et al., 2024). The GRF found in Greenland has one of the finest grain sizes, typically around 2-5 μm, due to the cold glacier temperatures and bedrock composition (Bendtsen et al., 2024). The small grain size results in a high surface area to volume ratio, which facilitates rapid weathering. When exposed to water and CO_2, the minerals undergo slow dissolution reactions that sequester carbon in the form of bicarbonate, while also releasing essential nutrients (Ray Sarkar, 2023).

These physical and chemical properties of GRF have made it gain growing attention for its potential role in environmental and climate related applications (Bendtsen et al., 2024). GRF may act as a natural fertilizer in ocean ecosystems, potentially enhancing phytoplankton growth and strengthening the ocean's biological carbon pump. Phytoplankton play a key role in the marine carbon pump by converting dissolved organic carbon into particulate organic matter, which is subsequently transported to the deep ocean, facilitating long-term carbon sequestration (Bendtsen et al., 2024). Thus, GRF may be used in marine carbon dioxide removal (mCDR) strategies to help mitigate climate change by stimulating oceanic primary productivity, thereby enhancing their natural capacity for CO_2 sequestration. (Bendtsen et al., 2024).

Experimental studies have demonstrated how primary productivity in the open ocean is enhanced by the addition of limiting nutrients and trace metals, particularly iron (de Baar et al., 2005). This has been further supported by mesoscale iron enrichment experiments (FeAXs), which confirmed iron's role in stimulating phytoplankton growth (Boyd et al., 2007). Therefore, GRF may have the same effect, although this appears to be highly context dependent. In a study by Maselli et al. (2023), the effect of GRF on photoautotrophic, heterotrophic, and mixotrophic microplankton was investigated by analyzing natural communities and incubation experiments in four Greenlandic fjords in the summer. They found that autotrophic microplankton were negatively affected in areas influenced by glacial meltwater, likely due to reduced light availability and stratification induced nutrient limitation in the surface layer. Heterotrophic and mixotrophic microplankton appeared largely unaffected, and no trophic group responded to the direct addition of GRF in incubation settings. In contrast, (Bendtsen et al., 2024) demonstrated that GRF can stimulate phytoplankton growth in the open ocean of the subtropical North Atlantic. In 14 incubation experiments conducted with surface water, 12 of them showed a significant increase in phytoplankton growth following GRF addition, suggesting that the availability of trace metals, particularly iron, plays a key role in enhancing primary production. These contrasting results suggest that GRF may inhibit autotrophic production in arctic coastal waters due to turbidity and stratification, while promoting phytoplankton growth in open-ocean environments where light is abundant and trace metals are limiting. Additionally, in terrestrial systems, GRF has also shown promising results. Field experiments have demonstrated increased crop yields following GRF application (Gunnarsen et al., 2023), and Dietzen and Rosing (2023) found that the weathering of silicate minerals in GRF contributes to long-term CO_2 removal via the formation of stable bicarbonate ions. Together, these findings highlight the broader potential of using GRF as an mCDR strategy. However, the ecological consequences of the increased phytoplankton activity and biomass and how it affects the ecosystem structure and higher trophic levels remain unknown.

This study focuses on the short-term influence of GRF addition to phytoplankton communities. The study was conducted in Disko Bay, Western Greenland, in July 2025. Samples were collected at three stations along a transect where the gradient was the proximity to glacial discharge (Røde Elv) carrying sediment consisting mainly of GRF. Water samples were taken to assess whether the phytoplankton communities can utilize the trace metals from the GRF in a short (~38-h) incubation

period. This is assessed by determining changes in biomass (using chlorophyll *a* concentration as a proxy) and photosynthetic efficiency (using F_v/F_m ratio as a proxy) in the incubation period.

We hypothesize that:

1) If the phytoplankton can utilize the trace metals in the GRF in the short incubation period, an increase in chlorophyll *a* concentration and the F_v/F_m ratio is expected in response to the added GRF concentrations. Furthermore, external literature (Bendtsen et al., 2024) suggests a positive dose response to the GRF, such that higher GRF concentrations should result in a higher chlorophyll *a* concentration and F_v/F_m ratio.
2) The microbial communities appearing at the different stations will differ in their ability to utilize GRF. The microbial communities closest to the glacial discharge have already developed mechanisms (including enzymes) allowing them to mobilize GRF. In contrast, the microbial communities in the stations furthest away first will need to upregulate the production of the given enzymes before they can utilize the GRF. Thus, in a short incubation period, we expect a greater response in chlorophyll *a* concentration and F_v/F_m in the phytoplankton communities from the station closest to the glacier, as more nutrients will be available for them.
3) There will be different microbial and phytoplankton communities appearing at the two depths, and therefore, (like 2), we expect a bigger response in chlorophyll *a* concentration and F_v/F_m in the phytoplankton communities in the DCM samples, where more GRF is available due to sedimentation.

2. Materials and methods

2.1. Regional setting and location of field sampling

The study was carried out at Disko Bay (Western Greenland), where seawater was sampled from three different locations along the coast (Figure 1): Røde Elv (69.2445 N, -53.5022 W), Fortuna Bay (69.2423 N, -53.7092 W), and Laksebugten (69.2607 N, -53.8985 W).

The following section (2.1) is based on the descriptions of Disko Bay and its surroundings provided by Latuta et al., (2025) and the references cited therein. Disko Bay (locally known as Qeqertarsuup Tunua) is the largest open-water embayment found in Western Greenland. This embayment is bordered to the east by many glacial fjord systems and to the west by Baffin Bay, resulting in a complex interplay between waters from glacial outflow and water-mass exchange coming from the west. In Baffin Bay, the three major currents characterizing the region include the West Greenland Current (WGC), the West Greenland Coastal Current (WGCC), both of which flow northward, and the Baffin Island Current, which flows in the opposite direction to the south. The WGC consists of warm and saline subsurface waters from the North Atlantic, which subduct under the fresher and colder waters from polar origin after crossing the Davis Strait; while the WGCC, following the Greenland Coast all the way from the East Greenland Coast, consists of fresh and cold meltwaters from the Arctic Ocean and Greenland Ice Sheet. The bathymetry of Disko Bay is shallow and complex, and the circulation within the bay is thought to follow this bathymetry cyclonically. Dense and warm waters from Baffin Bay enter Disko Bay via a trough known as Egedesminde Dyb (ED), with a depth ≥ 900m (Krawczyk et al., 2022), while Egedesminde Dyb Sill (EDS) presents a boundary to the passage of these waters – the western boundary of Disko Bay. East and south of the embayment, the coast creates boundaries; a noteworthy mention is the Ilulissat Icefjord on the eastern coast, exchanging waters with Disko Bay. Disko Island (DI) creates the northern boundary; Vaigat Strait separates the island in the east from the mainland, which happens to be an outflow passage of Disko Bay waters. In (Latuta et al., 2025), they further describe a seasonal hydrographic cycle in Disko Bay, which is said to be influenced by the interplay of glacial input (from eastern glacial fjord systems) and inflowing water masses (from Baffin Bay and the WGC). This cycle is found to be quite consistent and impacts the surface as well as the deep waters. Warming and freshening of the surface begin with sea ice melt during the springtime, creating a stratified surface layer. The Polar Water, below the surface layer, also shows seasonal variability, mainly driven by freshwater input from glacial melt. The consistent seasonal variability in temperature and salinity, driven by the interplay of glacial inputs and water mass exchange from the west, provides important context for our investigation into phytoplankton responses to GRF, as it highlights the dynamic nature of Disko Bay's hydrography throughout the year.

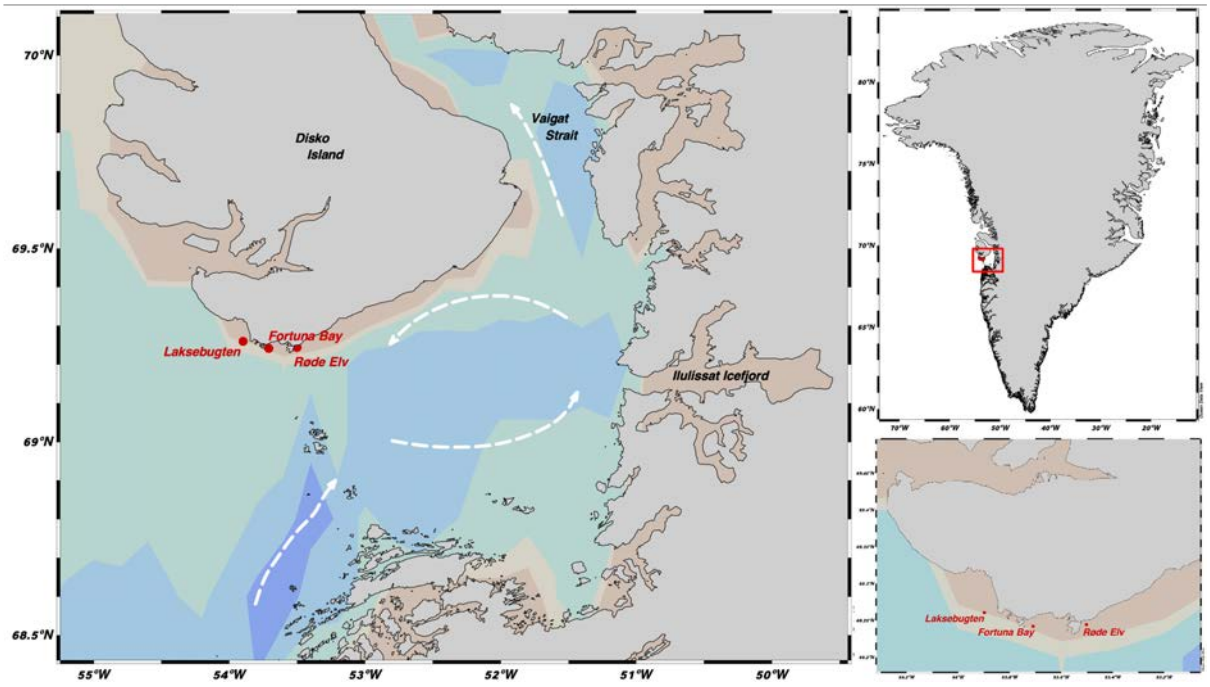

Fig. 1. Map of the Disko Bay area, West Greenland, showing the three sample sites: Laksebugten (Station 3), Fortuna Bay (Station 2) and Røde elv (Station 1). The main surface circulation patterns are indicated by white arrows. Adapted from Latuta et al., (2025).

2.2. Field sampling

Water was sampled as a transect with a gradient from Røde Elv, which carries sediment largely containing GRF, and ending in Laksebugten, furthest away from the glacial discharge. Sampling was carried out from the research vessel Porsild at the following stations and depths: Station 1 (Røde Elv) at the deep chlorophyll *a* maximum (DCM) at 12 m (1D) and at the surface at 2 meters (1S); Station 2 (Fortuna Bay) at the DCM at 18 m (2D); and Station 3 (Laksebugten) at the DCM at 25 m (3D) and at the surface at 2 m (3S). The DCM depths were determined based on the corresponding CTD profile taken just before sampling (see figures 3, 4, & 5 in the results section 3.1). Sea water was collected twice at each station and depth using a 10 L Niskin bottle. The water was transferred into 20 L carboys, whilst filtered with a 200 µm mesh filter to ensure that there would not be any metazooplankton in the samples, grazing on the phytoplankton. Stations 1, 2, and 3 were sampled at 10:35 AM, 1:34 PM, and 12:22 PM, respectively. Weather conditions on the sampling day were relatively wind still, with no rain and partly cloudy.

2.3. Sample preparation

Upon returning from the field, the 20 L carboys were immediately transported to a cold lab, where they were stored at a constant temperature of ca 5 °C. Water samples were then collected directly from the 20 L canisters for baseline measurements (T_0) of turbidity, F_v/F_m ratio, and chlorophyll *a* concentration at 16:00 on the 13th of July 2025.

Hereafter, incubation bottles were prepared by transferring water from each of the 20 L carboys into separate 2 L blue cap bottles for each station. The appropriate treatments were then added to the 2 L bottles and mixed thoroughly before being aliquoted into three replicate 0.5 L incubation bottles per treatment. The six different treatments included three different concentrations of GRF (GRF1, GRF2 & GRF3) each supplemented with nitrate (NO_3), phosphate (PO_4), and silicate (Si); a control with nitrate, phosphate, silicate and trace metals (L1); a negative control with nitrate, phosphate and silicate (NPS); and lastly a water control (C). The NPS was added as a negative control to assess whether trace metals, in particular iron, were the controlling factor of phytoplankton growth in GRF, while the L1 treatment served as a positive control to assess the response to available trace metals. The concentrations of the treatments are given in Table 1.

Table 1. Concentrations of the applied treatments. GRF1, GRF2 and GRF3 were applied (g L^{-1}), while L1, NPS, and C were applied (mL L^{-1}).

Treatment	GRF1	GRF2	GRF3	L1	NPS	C
Concentration	0.0506 g L^{-1}	0.3256 g L^{-1}	0.82539 g L^{-1}	1 mL L^{-1}	1 mL L^{-1}	1 mL L^{-1}

The treatments were prepared in the following order to ensure that the concentration of trace metals increased progressively: Water control, NPS, L1 media, GRF1, GRF2, and GRF3. Between each preparation, the 2 L blue cap bottles were rinsed with water from the respective stations to prevent contamination. The prepared incubation bottles were incubated until 18:30 on July 15th, where T_2 measurements were made, resulting in an incubation period of 38.5 hours (~1.6 days). The incubation bottles were placed beneath a light setup with lamps that emitted approximately ~120 µmol photons m^{-2} s^{-1}. During the entirety of the incubation time, the bottles were turned every second hour to avoid sedimentation. During each turning, bottles were also reassigned to new positions under the lamps to ensure even light exposure and prevent consistent shading of the same areas.

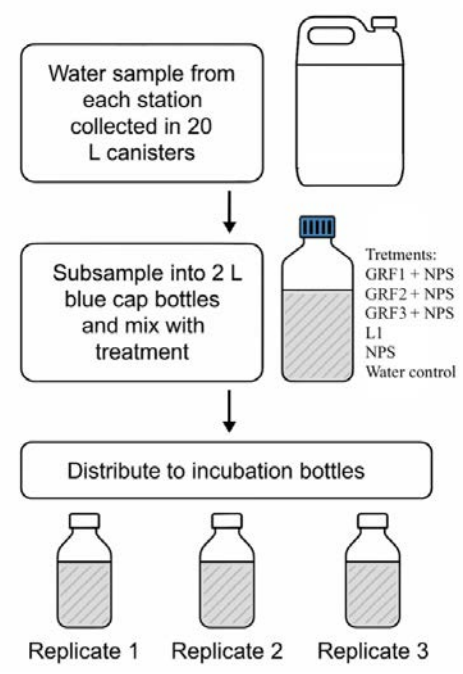

Fig. 2. Flowchart illustrating the sample preparation procedure.

2.4. Turbidity

Water samples of 2 L were collected at T_0 from the 20 L carboys from each station and depth for turbidity measurements. In the laboratory, turbidity was measured using a Millipore vacuum pump and GF/F filters (Whatman™). Before filtration, each filter was labeled according to station and depth and weighed on a METTLER AT261 DeltaRange weight. Each sample was filtered in triplicate (3 × 0.5 L). Following filtration, filters were carefully removed with tweezers and dried in an oven at 65 °C for 4 h. After drying, the filters were reweighed, and the initial filter weight was subtracted to determine the sediment mass, assumed to be primarily GRF. Turbidity was expressed as sediment mass per liter (g/L), and for each triplicate, the mean and standard error were calculated and visualized as a bar plot by station.

2.5. F_v/F_m ratio

The ratio of variable (F_v) and maximum (F_m) fluorescence represents the maximum quantum yield of photochemistry in photosystem II (PSII), measured in a dark-adapted state (Gorbunov & Falkowski, 2021). The photon energy absorbed by chlorophyll *a* can follow three possible fates: it can drive photochemistry, be re-emitted as fluorescence, or dissipate as heat through non-photochemical quenching (NPQ) (Gorbunov & Falkowski, 2021). The F_v/F_m ratio quantifies the fraction of absorbed energy directed toward photochemistry and is widely used as a proxy for

assessing photochemical efficiency and stress in photosynthetic organisms. The ratio is calculated as the variable fluorescence (F_v), which is the difference between maximum (F_m) and minimum fluorescence (F_o) measured in a dark-adapted state, normalized to F_m:

$$\frac{F_v}{F_m} = \frac{F_m - F_o}{F_m}$$

In darkness, NPQ is minimal, reducing thermal dissipation and allowing the maximum fraction of absorbed light energy to be allocated to photochemistry (Gorbunov & Falkowski, 2021). Under these conditions, a weak measuring light is used to determine the baseline fluorescence yield (F_o), where all PSII reaction centers are open, i.e., all primary electron acceptors are oxidized. A strong, short saturating pulse of light called the single turnover (ST) flash is then applied, reducing all primary electron acceptors and thus closing all PSII reaction centers. Consequently, the excitation energy cannot be directed to photochemistry, leading to a maximum fluorescence yield, F_m. The ratio can attain a value between 0-1, with high values (0.55-0.65) indicating efficient photosynthetic function. In contrast, lower values suggest physiological stress, such as nutrient limitation or photoinhibition, which reduces the proportion of energy used in photochemistry (Gorbunov & Falkowski, 2021).

The F_v/F_m ratio was measured with a LabSTAF (Chelsea Technologies Ltd) instrument using the fast repetition rate fluorometry technique, where the ST flash was delivered with a 100-µs excitation pulse. For baseline measurements, 80 mL samples were collected in glass vials from the 20 L canisters from each station. Three 20 mL aliquots were then taken from the 80 mL vials, and the mean F_v/F_m ratio was calculated based on these triplicates. For T_2 measurements, 20 mL samples were taken from the 0.5 L incubation bottles containing the different treatments, which were already made in three replicates. All samples were stored in the dark for 30 minutes before being loaded into the instrument for measurements. However, due to a malfunction of the equipment, the baseline measurement of the F_v/F_m ratio for Station 3D was first measured on the 14th of July at 13:30 instead. Consequently, the samples from Station 3D were placed in the cold lab with limited light for 21.5 hours before T2 measurements were made. Furthermore, the malfunction resulted in missing Fv/F_m values for the GRF1 and NPS treatments, which were therefore excluded from the analysis.

2.6. Chlorophyll *a* concentration

Chlorophyll *a* (chl *a*) was measured in the laboratory using GF/F filters (pore size 0.7 µm, Whatman™) and a laboratory vacuum pump (VWR). Before the filtration, a sample of 100 ml was taken from each replicate. After the replicates were filtered, the filters were removed using a tweezer and then placed in a tube. The tube was thereafter filled with 5 ml of ethanol. The tube was then turned upside down a couple of times to ensure that the content was thoroughly mixed, and the filter did not clog the tube. The tube with the replicates was placed in a fridge at 2 °C for 24 h.

After 24 h, the tubes were removed from the fridge and then prepared to measure the concentration of chl *a*. The tubes were turned upside down a couple of times, and then by using a pipette, a small sample was taken out of the tubes and squeezed into small glass vials. The samples were measured using a fluorometer (Trilogy Laboratory Fluorometer by Turner Designs) and then measured using the most recent calibration (2025). After placing the small glass vials, the amount of water used in the filtration sample (100 ml) was typed in, and the amount of ethanol was also typed in (5 ml). Then the chlorophyll *a* could be measured, and if the F value was above 0.4, the sample was used.

2.7. Statistical data analysis

Two-way ANOVAs (Analysis of Variance) were performed to test whether the F_v/F_m ratio and chlorophyll *a* concentration varied with treatment and time as independent variables, while also accounting for their interaction (Treatment * Time). The models were applied separately within each station, rather than including station as a third factor in a three-way ANOVA, due to the limited dataset (only two time points per station). Prior to the ANOVAs, it was tested that the data conformed to all assumptions for the test. Data were collected randomly and were independent of each other. Normality was assessed using the Shapiro-Wilk test and visually inspected with Q-Q plots. Homogeneity of variance was tested using Levene's test. Data that did not meet the assumption of normality were log-transformed. Following a significant treatment effect in the ANOVAs, Tukey's HSD (Honestly Significant Difference) post hoc test was conducted to determine pairwise differences between treatment groups. A post hoc test was not applied for the time variable, as it only included two levels (T_0 and T_2). To support interpretation of the statistical analyses, raw (untransformed) F_v/F_m and chl *a* values were visualized as box plots, showing differences across treatments and time points separately for each station.

3. Results

3.1. CTD profiles

At Station 1 (Røde Elv), both temperature and salinity profiles on the day of sampling (13.07.2025) show a clear stratification at ~12 meters, matching the presence of the DCM at the same depth (Figure 3). Photosynthetically Active Radiation (PAR) declines steadily until ~20 m, where it reaches near zero levels. The samples taken at the surface layer (2m) and the DCM were exposed to approximately 140 and 40 µmol m^{-2} s^{-1}, respectively. However, just two days later, all measured parameters changed, and the stratification was observed at ~9 m, and the DCM had shifted to ~25 m. These rapid changes highlight how dynamic the sampling area is.

At Station 2 (Fortuna Bay), the CTD profile from 13.07.2025 shows stratification at ~18 m with the DCM matching closely to the same depth (Figure 4). By 15.07.2025, the stratification had moved upwards towards ~10 meters. However, the chl *a* and the PAR were both relatively steady, with only small differences. The DCM sample measured ~50 µmol m^{-2} s^{-1} from the PAR on the day of sampling.

At Station 3 (Laksebugten), only one CTD profile was collected on 13.07.2025 (Figure 5). Here, the DCM was present at ~25 m, which is below the stratification line that appeared around 18 meters. The PAR increases first before it starts decreasing at ~18 m, giving the surface layer sample and the DCM sample an irradiation at ~100 and 30 µmol m^{-2} s^{-1}, respectively.

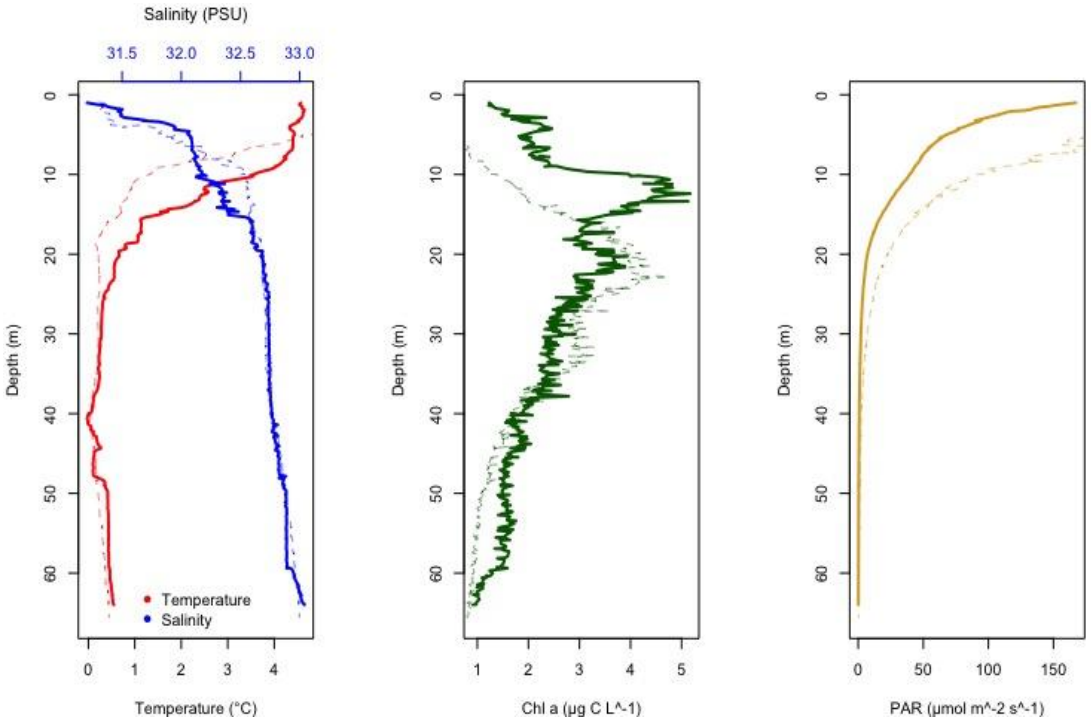

Fig. 3. CTD data from Station 1 (Røde Elv). Bold lines show data from sampling on 13.07.2025, while dashed lines show data from 15.07.2025 for comparison. Red lines indicate salinity, blue lines temperature, green lines chlorophyll a, and orange lines Photosynthetically Active Radiation (PAR). DCM is present at 12 meters.

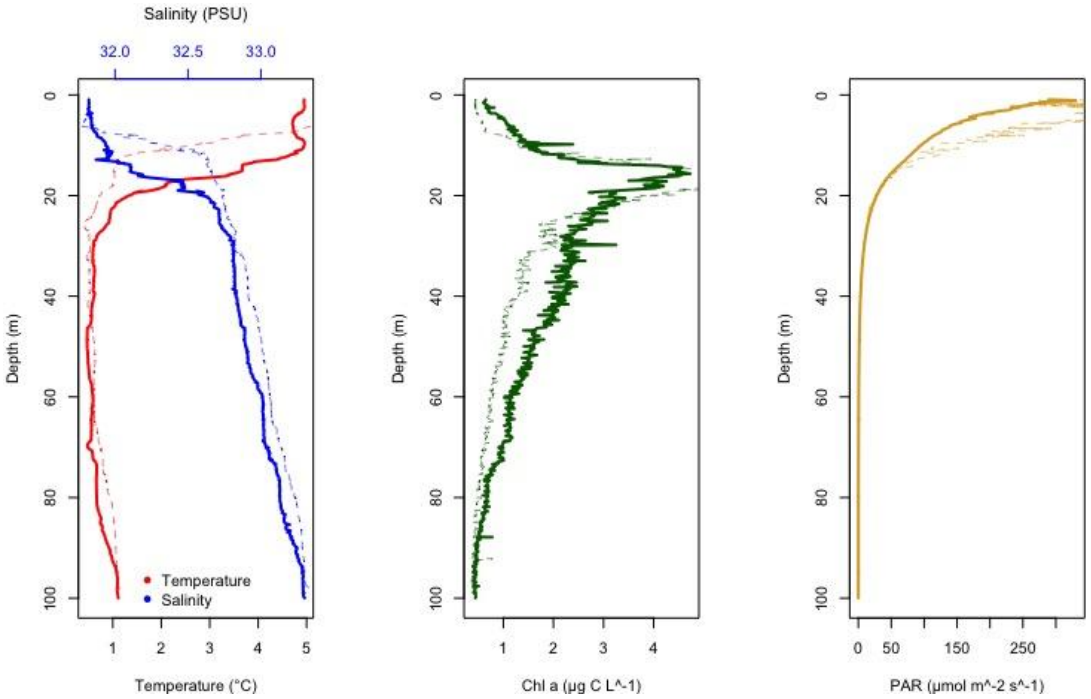

Fig. 4. CTD data from Station 2 (Fortuna Bay). Bold lines show data from sampling on 13.07.2025, while dashed lines show data from 15.07.2025 for comparison. Red lines indicate salinity, blue lines temperature, green lines chlorophyll a, and orange lines Photosynthetically Active Radiation (PAR). DCM is present at 18 meters.

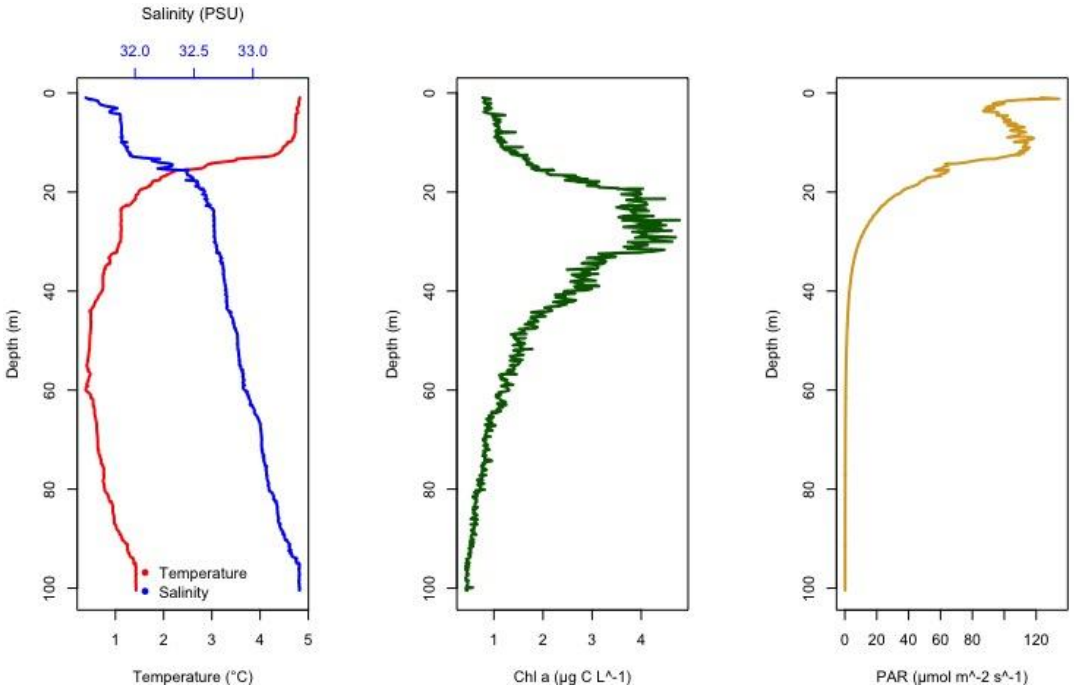

Fig. 5. CTD data from Station 3 (Laksebugten) taken on 13.07.2025. Red lines indicate salinity, blue lines temperature, green lines chlorophyll a, and orange lines Photosynthetically Active Radiation (PAR). DCM is present at 25 meters.

3.2. Turbidity

Turbidity levels were measured across all five stations (Figure 6). All stations show similar turbidity values, ranging from approximately 0.045 to 0.055 g L^{-1}. Station 1D has a large variability shown by the large error bar, while the remaining stations show relatively similar values with smaller variations.

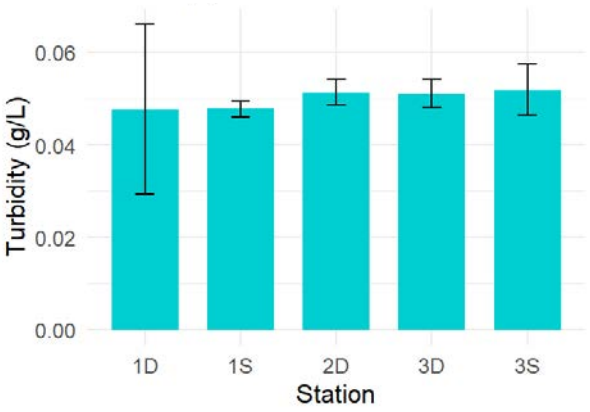

Fig. 6: Mean turbidity measurements (gL^{-1}) for each of the five sampling stations including error bars. Station 1D (Deep Chlorophyll Maximum) and 1S (surface layer) correspond to station 1, "Røde Elv"; 2D to station 2, "Fortuna Bay"; and 3D and 3S to station 3, "Laksebugten".

3.3. The effect of treatment and time on the F_v/F_m ratio

Raw (untransformed) F_v/F_m values are presented as boxplots grouped by time and treatment for each station in Figure 7, to provide an initial visual overview of the data. The corresponding ANOVA results and significant pairwise differences are reported later in Tables 2 and 3. The boxplots illustrate a higher F_v/F_m in the L1 treatment compared to the control in Stations 1D and 3S. Moreover, in Station 3D, the GRF3 treatment showed significantly lower F_v/F_m values than the water control (C), L1, and GRF2. Regarding the effect of time, F_v/F_m increased significantly from T_0 to T_2 in Stations 1D and 3D, whereas the opposite trend was observed in 1S, 2D, and 3S. However, as described previously in section 2.6, due to the malfunction of equipment, the F_v/F_m baseline measurement in Station 3D was made 21.5 hours later than at the other stations and has resulted in very low T_0 values, likely due to the low light environment during storage. Furthermore, GRF1 and NPS were excluded as treatments due to missing F_v/F_m values.

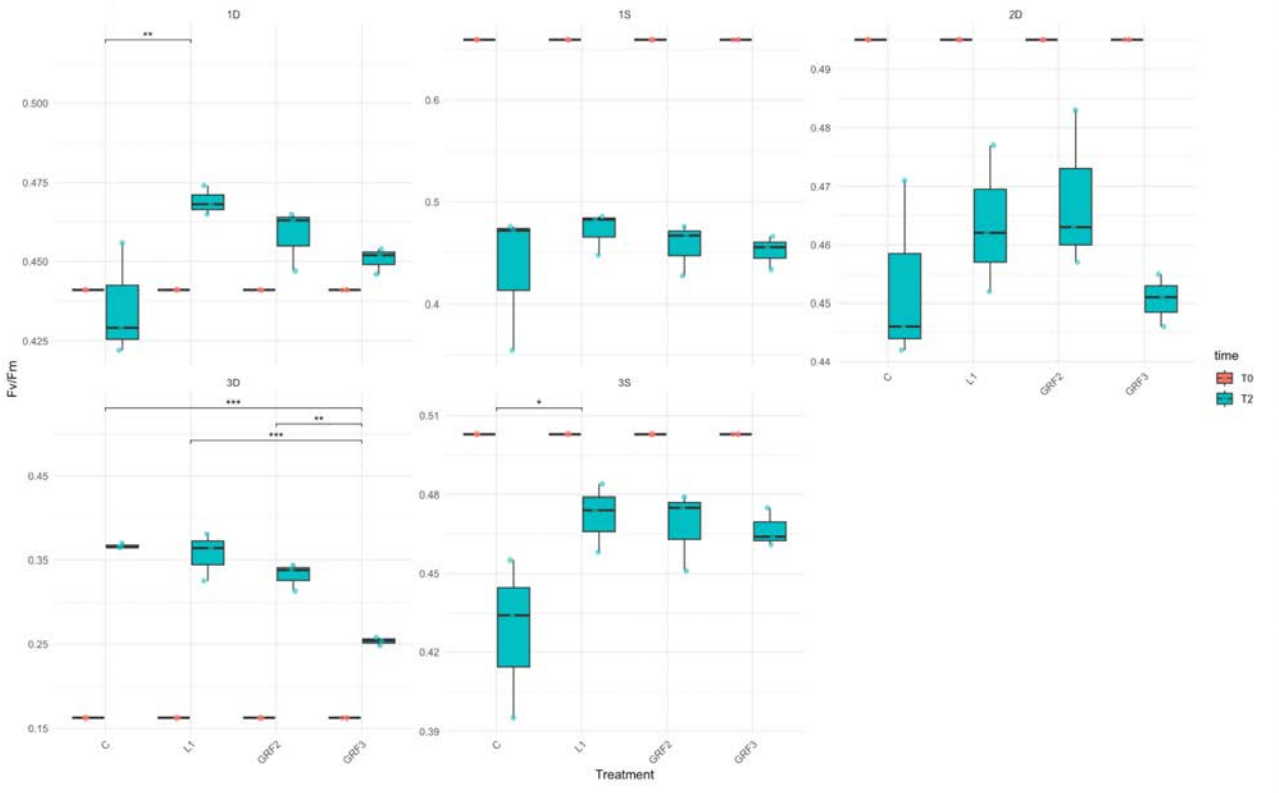

Fig. 7. Boxplots of untransformed F_v/F_m values by treatment and time across all stations. Note that F_v/F_m values are missing for GRF1 and NPS treatments and are thus excluded from the analysis. Time points are distinguished by color: T0 (Red) and T2 (Blue). Statistically significant pairwise treatment differences based on Tukey's HSD test are indicated with brackets and annotated using the following significance code: '' 0.05, '**' 0.01, '***' 0.001.*

To statistically assess these patterns, two-way ANOVAs were performed separately for each station to examine the effects of treatment and time on F_v/F_m. Assessment of the model assumptions showed deviations from normality in all cases, as indicated by the Shapiro–Wilk tests and Q–Q plots. Log transformations were applied to the F_v/F_m data to improve normality, though normality was still not fully achieved (Table A1 in the appendix). Levene's test confirmed that the assumption of homogeneity of variance was met across all stations ($p > 0.05$). Therefore, the statistical analyses were conducted on the log-transformed data.

The ANOVA results revealed significant effects ($p < 0.05$) of treatment, time, and their interaction in stations 1D, 3D, and 3S (Table 2). In station 1S, significant effects of time and the interaction between time and treatment were observed ($p < 0.05$), while in Station 2D, only time had a significant effect with no detectable treatment or interaction effects.

*Table 2. Results from the ANOVA models testing the effect of treatment, time, and their interaction (treatment * time) on F_v/F_m ratio at each station. Significance code: '*' 0.05, '**' 0.01, '***' 0.001.*

Station 1D	**DF**	**P-value**	
Treatment	3	0.01185	*
Time	1	0.00123	**
Treatment * Time	3	0.01185	*

Station 1S	**DF**	**P-value**	
Treatment	3	0.684	
Time	1	2.08E-10	***
Treatment * Time	3	0.684	*

Station 2D	**DF**	**P-value**	
Treatment	3	0.297	
Time	1	3.10E-08	***
Treatment * Time	3	0.297	

Station 3D	**DF**	**P-value**	
Treatment	3	2.81E-07	***
Time	1	< 2e-16	***
Treatment * Time	3	2.81E-07	***

Station 3S	**DF**	**P-value**	
Treatment	3	0.0368	*
Time	1	1.08E-06	***
Treatment * Time	3	0.0368	*

Where a significant treatment effect was found, Tukey's HSD post hoc test was used to identify significant differences among the treatments (Table 3). In Stations 1D and 3S, a significant

difference was observed between the L1 treatment and the water control. In Station 3D, GRF3 differed significantly from the water control, L1, and GRF2.

Table .3 Pairwise comparisons from Tukey's HSD post hoc test showing significant differences in F_v/F_m between treatments at each station. Note that F_v/F_m values are missing for GRF1 and NPS treatments and are thus excluded from the analysis. Only comparisons with $p < 0.05$ are included.

Station	Treatment comparison	P-value
1D	L1 – C	0.0080356
3D	GRF3 – C	0.0000005
	GRF3 – GRF2	0.0000281
	L1 – GRF3	0.0000015
3S	L1 – C	0.0465277

3.4. The effect of treatment and time on chlorophyll a (chl a)

To provide a visual overview of the chl *a* data, Figure 8 shows raw (untransformed) concentrations as boxplots, grouped by time and treatment for each station. The corresponding ANOVA results and significant pairwise comparisons are reported later in Tables 4 and 5.

The plots reveal that, in Station 1D, chl *a* concentration was significantly higher in the L1 treatment compared to the water control.

In Station 1S, significantly higher chl *a* concentrations were observed in L1, NPS, and GRF3 compared to the control, while GRF1 showed significantly lower concentrations. GRF2 showed significantly higher values than GRF1, and GRF3 was significantly higher than both GRF1 and GRF2, indicating a positive dose-response pattern.

Looking at Station 2D, all treatments except GRF3 resulted in significantly higher Chl *a* concentrations than the water control. Interestingly, in contrast to Station 1S, a significant decline in chl *a* was observed with increasing GRF concentration, suggesting a negative dose-response. L1 and NPS also showed significantly higher values than GRF3.

In Station 3D, Chl *a* concentrations were significantly higher in GRF2 and GRF3 compared to the control. A positive dose-response was indicated, as GRF3 exhibited higher concentrations than both

GRF1 and GRF2. Furthermore, GRF2 and GRF3 had significantly higher concentrations than both L1 and NPS.

Lastly, in Station 3S, all treatments showed significantly higher chl *a* concentrations than the control.

Regarding the effect of time, chlorophyll *a* concentrations were significantly higher at time point T2 compared to baseline T0 in Stations 1S, 2D, and 3S. In contrast, Station 3D showed a significant decrease in chl *a* concentration at T2, while Station 1D showed no significant variation over time, consistent with the ANOVA results.

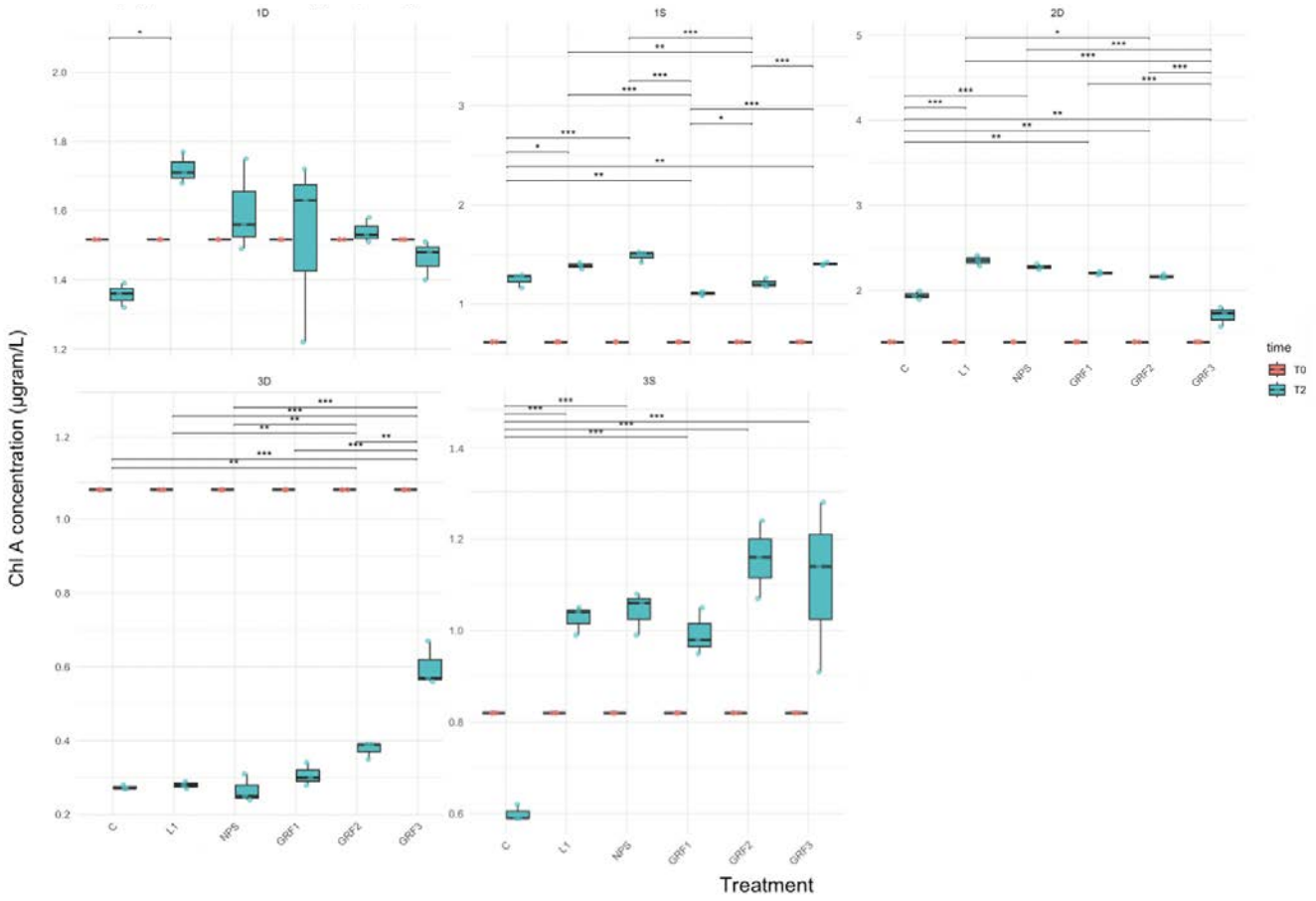

Fig. 8. Boxplots of untransformed chl a values by treatment and time across all stations. Time points are distinguished by color: T0 (Red) and T2 (Blue). Statistically significant pairwise treatment differences based on Tukey's HSD test are indicated with brackets and annotated using the following significance code: '' 0.05, '**' 0.01, '***' 0.001.*

To evaluate these patterns statistically, two-way ANOVAs were carried out for each station to test the effects of treatment and time on chl *a* concentration. Examination of model assumptions revealed deviations from normality across all stations, as shown by the Shapiro–Wilk tests and Q–Q plots. Additionally, the assumption of homogeneity of variance was violated in Station 3S. To address these issues, a log transformation was applied to the chlorophyll *a* data. The log-transformation improved normality slightly and Levene's test confirmed that homogeneity of variance was met in all models post-transformation ($p > 0.05$) (Table A2 in the appendix). Therefore, the statistical analyses were conducted on the log-transformed data.

The ANOVA results showed significant effects of treatment, time, and their interaction in all stations except in Station 1D, where no significant differences were observed (Table 4).

*Table 4. Results from the ANOVA models testing the effect of treatment, time, and their interaction (treatment * time) on chl a concentration at each station. Significance code: '*' 0.05, '**' 0.01, '***' 0.001.*

Station 1D	DF	P-value	
Treatment	5	0.0507	
Time	1	0.0507	
Treatment * Time	5	0.0507	

Station 1S	DF	P-value	
Treatment	5	< 2e-1	***
Time	1	< 2e-16	***
Treatment * Time	5	1.40E-09	***

Station 2D	DF	P-value	
Treatment	5	8.50E-11	***
Time	1	< 2e-16	***
Treatment * Time	5	8.50E-11	***

Station 3D	DF	P-value	
Treatment	5	7.46E-11	***
Time	1	< 2e-16	***
Treatment * Time	5	7.46E-11	***

Station 3S	DF	P-value	
Treatment	5	1.09E-08	***
Time	1	1.80E-08	***
Treatment * Time	5	1.09E-08	***

However, the treatment effect in Station 1D was marginally non-significant ($p = 0.0507$), and Tukey's post hoc analysis revealed a significant pairwise difference between the L1 treatment and the water control (C) ($p = 0.0267$) (Table 5). In the other stations, Tukey's HSD confirmed multiple significant treatment differences, consistent with the patterns observed in Figure 8.

Table 5. Pairwise comparisons from Tukey's HSD post hoc test showing significant differences in chl a concentrations between treatments at each station. Only comparisons with $p < 0.05$ are included.

Station	Treatment comparison	P–value
1D	L1 – C	2.67E-02
1S	GRF1 – C	4.50E-03
	GRF3 – C	3.27E-03
	L1 – C	1.10E-02
	NPS – C	2.93E-05
	GRF2 – GRF1	4.80E-02
	GRF3 – GRF1	2.00E-07
	L1 – GRF1	6.00E-07
	NPS – GRF1	0.00E+00
	GRF3 – GRF2	9.18E-04
	L1 – GRF2	9.18E-04
	NPS – GRF2	2.60E-06
2D	GRF1 – C	1.22E-03
	GRF2 – C	6.28E-03
	GRF3 – C	8.45E-04
	L1 – C	3.60E-06
	NPS – C	6.40E-05
	GRF2 – GRF1	9.83E-01
	GRF3 – GRF1	0.00E+00
	GRF3 – GRF2	1.00E-07
	L1 – GRF3	0.00E+00
	NPS – GRF3	0.00E+00
3D	GRF2 – C	1.54E-03
	GRF3 – C	0.00E+00
	GRF3 – GRF1	0.00E+00
	GRF3 – GRF2	1.01E-05
	L1 – GRF2	3.55E-03
	NPS – GRF2	5.15E-04
	L1 – GRF3	0.00E+00
	NPS – GRF3	0.00E+00
3S	GRF1 – C	1.80E-06
	GRF2 – C	0.00E+00
	GRF3 – C	1.00E-07
	L1 – C	4.00E-07
	NPS – C	4.00E-07

4. Discussion and conclusion

4.1. Limitations: Experimental design and statistical analysis

This study investigated whether different phytoplankton communities in Disko Bay, Greenland, could utilize trace metals from GRF during a short (~38-h) incubation period. Given the limited dataset, it is important to acknowledge several underlying caveats and limitations of the experimental design and statistical analysis when interpreting the results.

One major limitation is the short duration of the experiment and the limited number of timepoints. From a statistical standpoint, the small sample size challenged the assumptions underlying an ANOVA test, reducing the robustness of the analyses. With so few data points, it was not possible to confidently assess normality for either F_v/F_m or chl *a* data, despite slight improvements after log-transformation. Consequently, the statistical power of the analyses is low, increasing the risk of both type I and type II errors.

With a larger dataset, it would also have been possible to include *station* as an additional factor in the ANOVA models to test for significant differences across locations and depths. However, adding this variable with the current sample size would have introduced too many interaction terms, increasing model complexity and the risk of overfitting. Therefore, analyses were performed separately within each station, allowing for comparison of findings afterwards.

Furthermore, if time had permitted, growth rate would ideally have been calculated to track changes in biomass over time. However, with just two time points, only a single growth rate could be derived, preventing assessment of changes in growth rates over time. Instead, chl *a* concentration and F_v/F_m were used as proxies for phytoplankton biomass and photosynthetic efficiency, respectively. While both are widely used proxies, they have important limitations, which must be taken into consideration when interpreting the results. chl *a* can vary independently of biomass due to photoacclimation, particularly in stratified water columns. In deeper layers (e.g., at the DCM), phytoplankton may increase chl *a* content per cell to adapt to low light conditions (i.e., the pigment packaging effect), while surface populations may reduce pigment content to avoid photoinhibition (Zonneveld, 1998). In this experiment the samples received ~120 µmol photons m^{-2} s^{-1} when incubating, which does not correspond to the light available at the surface or at the DCM at either of the stations that was sampled. The PAR values (Figure 3-5) varied between ~100-140 µmol m^{-2} s^{-1} for the surface samples and ~30-50 µmol m^{-2} s^{-1} for the DCM samples across all stations. This suggests that only the surface layer samples received approximately optimal conditions in terms of light availability in the incubations. However, these surface samples are most likely nutrient limited, so when adding nutrients, this could lead to increased cellular levels of chl *a* (pers. comm. Per Juel Hansen, MBS). For the DCM samples this excess amount of light received in the incubations compared to the ocean could result in a reduction of chl *a* content per cell to avoid photoinhibition. Furthermore, F_v/F_m reflects the efficiency of Photosystem II and responds rapidly to nutrient availability, but high values may not correspond to increases in growth or chl *a* over short incubations (Kruskopf & Flynn, 2006). Despite these limitations, combining the two proxies

improves interpretation, and a concurrent increase in both is considered a stronger indication of a positive treatment response.

4.2. Interpreting the statistical results considering the hypotheses

Hypothesis 1 proposed that if phytoplankton could utilize trace metals from GRF in the short incubation time, we would observe increases in chl *a* concentration and F_v/F_m ratio with increasing GRF concentration.

Looking specifically at the Chl *a* concentrations, a somewhat pattern aligning with the hypothesis was observed. All stations except Station 1D showed significant changes in chl *a* concentration with time (Table 6). Visualization of these changes in Figure 8 showed significant increases in most of the stations (1S, 2D, and 3S) between timepoints T0 and T2. However, the temporal change was negative in Station 3D, thus deviating from the pattern. Furthermore, in Station 1S and 3D, chl *a* increased significantly with GRF concentration (GRF1 < GRF2 < GRF3), suggesting a positive dose-response consistent with the pattern reported by Bendtsen et al. (2024). Therefore, it may be indicated that GRF was mobilized and that the phytoplankton communities were able to utilize GRF within the short incubation period in these given samples. In contrast, in Station 2D, a negative dose response was observed, where chl *a* decreased with increasing GRF concentration, thus making the pattern unclear. Furthermore, the NPS treatment was included as a negative control to assess trace metals (particularly iron) being the controlling factor in GRF. However, no strong pattern indicated higher chl *a* concentrations in the GRF or L1 media treatments, which all contained trace metals. Therefore, these results could not further elucidate this relationship.

The results for the changes in F_v/F_m in the incubation period did not provide evidence to support the hypothesis. In Station 1D and 3S, F_v/F_m was significantly higher in the L1 treatment than in the water control, indicating improved photochemical efficiency. However, GRF treatments did not show significantly higher values than the water control, possibly reflecting that 38 hours was insufficient for the communities to potentially upregulate GRF-mobilizing enzymes. Interestingly, in Station 3D, GRF3 showed significantly lower F_v/F_m values than all other treatments, possibly due to turbidity-induced light stress at high GRF concentrations.

Hypothesis 2 proposed that the phytoplankton communities closer to the glacial discharge (Station 1**)** would show the greatest response to GRF in a short incubation period, as the communities

present here were naturally preadapted (e.g., through upregulation of specific enzymes) to utilize GRF due to higher exposure in their natural environment.

However, no clear patterns in F_v/F_m or chl *a* values were seen along the gradient in the transect. Nevertheless, a slight tendency was seen in the chl *a* data, where Station 3 showed somewhat lower values than Station 1. Even so, the turbidity data challenges the foundational assumption of this hypothesis. The highest turbidity (as a proxy for GRF) was expected at Station 1, and a declining gradient towards Station 3. Yet turbidity levels were surprisingly similar across all stations (Figure 6), suggesting that the distribution of GRF was more homogeneous than anticipated. This complicates the interpretation, as it is not certain that the communities at each station were exposed to different GRF levels in situ prior to the experiment.

Lastly, **Hypothesis 3** predicted that DCM communities would show a greater response to GRF than surface communities due to pre-existing exposure to sinking particles and preadapted microbial communities capable of trace metal mobilization from GRF. No evidence was found for this hypothesis, as the DCM samples with GRF treatments did not show consistently higher values than surface samples treated with GRF. In contrast to our anticipation, the DCM community at Station 3D showed markedly lower chl *a* values than the surface community in 3S in response to GRF treatments. Moreover, chl *a* values were quite similar in the GRF treatments from Stations 1D and 1S. Following this pattern, when looking at F_v/F_m, the values were also (slightly) lower in the GRF treatments in Station 3D than in Station 3S, while being quite similar in the GRF treatments in Station 1S and 1D.

5. Conclusion and further perspectives

Based on the results of this study, no clear or consistent pattern emerged that strongly supports any of the three hypotheses. While Hypothesis 1 received limited support, the variability across stations and treatments makes the overall picture inconclusive. Hypotheses 2 and 3 were not supported by the data, as no consistent trends were observed along the transect or between surface and DCM communities. Furthermore, turbidity measurements did not follow the expected gradient along the transect, suggesting that GRF exposure in situ may have been more homogenous than anticipated, complicating the interpretation of hypothesis 2. However, it is important to recognize that the

experiment was likely constrained by biological limitations due to the short incubation period, which may have masked or distorted potential treatment effects. Phytoplankton communities typically require between 0 and 3–4 days to acclimate to new environmental conditions and exit the lag phase before entering exponential growth (pers. comm. Niels Daugbjerg, MBS). With only ~1.6 days of incubation, many of the phytoplankton populations may still have been in the lag phase, and the measured responses could therefore reflect short-term fluctuations rather than sustained growth. This constraint is particularly relevant for communities naturally exposed to lower concentrations of GRF, which likely would require more time to upregulate enzymes needed to mobilize and assimilate trace metals. A longer incubation period would therefore be necessary to detect treatment effects more reliably. However, in such a study with longer incubation time, less-exposed communities would be expected to show the strongest responses to GRF treatments, thereby reversing the expected trends of a short-term study. Findings from Bendtsen et al. (2024) support this, as their longer incubations (6 days) conducted on phytoplankton communities from the open ocean in the subtropical North Atlantic (i.e., limited abundance of trace metals) show significant stimulation of phytoplankton growth in response to GRF. However, as noted previously, Maselli et al. (2023) find no such effect in Arctic coastal systems, where GRF exposure likely is higher. Thus, future studies including longer incubation periods would allow for a more accurate assessment of GRF utilization across different phytoplankton communities and environmental gradients, ultimately improving our understanding of GRF's potential role in stimulating phytoplankton productivity.

7. References

Bendtsen, J., Daugbjerg, N., & Hansen, J. L. S. (2024). Glacial rock flour increases photosynthesis and biomass of natural phytoplankton communities in subtropical surface waters: a potential means of action for marine CO2 removal. *Frontiers in Marine Science*, *11*. https://doi.org/10.3389/fmars.2024.1416421

Boyd, P. W., Jickells, T., Law, C. S., Blain, S., Boyle, E. A., Buesseler, K. O., Coale, K. H., Cullen, J. J., De Baar, H. J. W., Follows, M., Harvey, M., Lancelot, C., Levasseur, M., Owens, N. P. J., Pollard, R., Rivkin, R. B., Sarmiento, J., Schoemann, V., Smetacek, V., … Watson, A. J. (2007). *Mesoscale Iron Enrichment Experiments 1993-2005: Synthesis and Future Directions*. https://www.science.org

de Baar, H. J. W., Boyd, P. W., Coale, K. H., Landry, M. R., Tsuda, A., Assmy, P., Bakker, D. C. E., Bozec, Y., Barber, R. T., Brzezinski, M. A., Buesseler, K. O., Boyé, M., Croot, P. L., Gervais, F., Gorbunov, M. Y., Harrison, P. J., Hiscock, W. T., Laan, P., Lancelot, C., … Wong, C. S. (2005). Synthesis of iron fertilization experiments: From the iron age in the age of enlightenment. In *Journal of Geophysical Research: Oceans* (Vol. 110, Issue 9, pp. 1–24). https://doi.org/10.1029/2004JC002601

Dietzen, C., & Rosing, M. T. (2023). Quantification of CO2 uptake by enhanced weathering of silicate minerals applied to acidic soils. *International Journal of Greenhouse Gas Control*, *125*. https://doi.org/10.1016/j.ijggc.2023.103872

Gorbunov, M. Y., & Falkowski, P. G. (2021). *Using Chlorophyll Fluorescence to Determine the Fate of Photons Absorbed by Phytoplankton in the World's Oceans*. https://doi.org/10.1146/annurev-marine-032621

Gunnarsen, K. C., Jensen, L. S., Rosing, M. T., & Dietzen, C. (2023). Greenlandic glacial rock flour improves crop yield in organic agricultural production. *Nutrient Cycling in Agroecosystems*, *126*(1), 51–66. https://doi.org/10.1007/s10705-023-10274-0

Krawczyk, D. W., Yesson, C., Knutz, P., Arboe, N. H., Blicher, M. E., Zinglersen, K. B., & Wagnholt, J. N. (2022). Seafloor habitats across geological boundaries in Disko Bay, central West Greenland. *Estuarine, Coastal and Shelf Science*, *278*. https://doi.org/10.1016/j.ecss.2022.108087

Kruskopf, M., & Flynn, K. J. (2006). Chlorophyll content and fluorescence responses cannot be used to gauge reliably phytoplankton biomass, nutrient status or growth rate. *New Phytologist*, *169*(3), 525–536. https://doi.org/10.1111/j.1469-8137.2005.01601.x

Latuta, L., Smedsrud, L. H., Darelius, E., Hansen, P. J., & Willis, J. K. (2025). *Drivers of seasonal hydrography in Disko Bay, Greenland*. https://doi.org/10.5194/egusphere-2025-1492

Maselli, M., Meire, L., Meire, P., & Hansen, P. J. (2023). Effects of Glacial Flour on Marine Microplankton: Evidences from Natural Communities of Greenlandic Fjords and Experimental Studies. *Protist*, *174*(1). https://doi.org/10.1016/j.protis.2022.125928

Ray Sarkar, S. (2023). *Glacial Rock Flour its Characteristics and Enhanced Weathering Potential*.

Zonneveld, C. (1998). *Photoinhibition as Affected by Photoacclimation in Phytoplankton: a Model Approach. Journal of Theoretical Biology, 193(1), 115–123. https://doi.org/10.1006/JTBI.1998.0688*.

Appendix

Table A1. Testing of assumptions for the two-way ANOVA assessing the effect of treatment, time, and their interaction on F_v/F_m.

Station 1D
Levene's Test for Homogeneity of Variance (center = median)
DF = 7, p-value = 0.2767
Shapiro-Wilk normality test
W = 0.81931, p-value = 0.00062

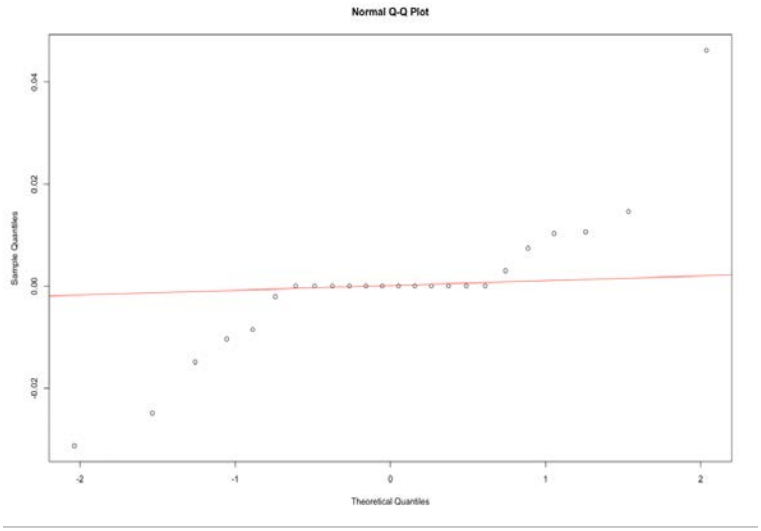

Station 1S
Levene's Test for Homogeneity of Variance (center = median)
DF = 7, p-value = 0.5439
Shapiro-Wilk normality test
W = 0.78083, p-value = 0.0001455

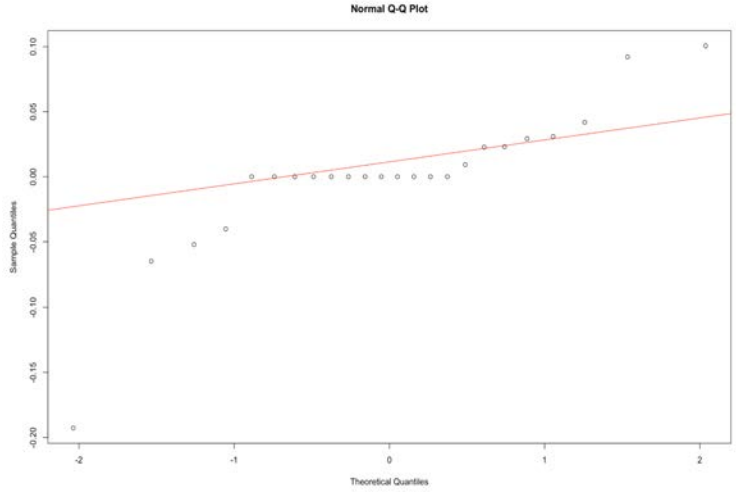

Station 2D
Levene's Test for Homogeneity of Variance (center = median)
DF = 7, p-value = 0.2913
Shapiro-Wilk normality test
W = 0.83428, p-value = 0.001132

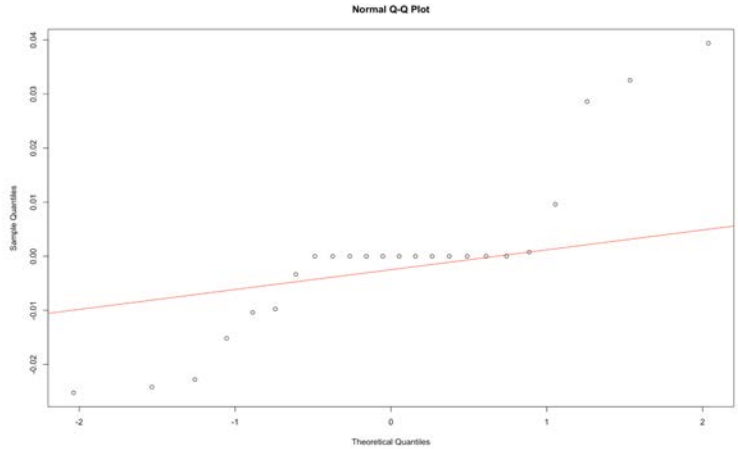

Station 3D
Levene's Test for Homogeneity of Variance (center = median)
DF = 7, p-value = 0.1533
Shapiro-Wilk normality test
W = 0.78028, p-value = 0.0001427

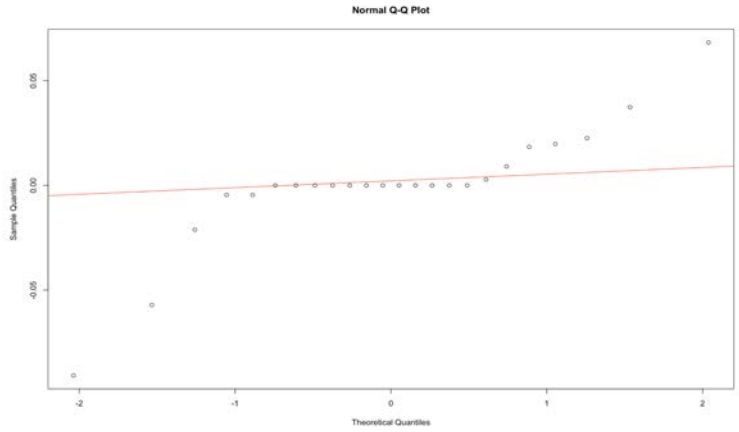

Station 3S
Levene's Test for Homogeneity of Variance (center = median)
DF = 7, p-value = 0.1332
Shapiro-Wilk normality test
W = 0.82241, p-value = 0.0007009

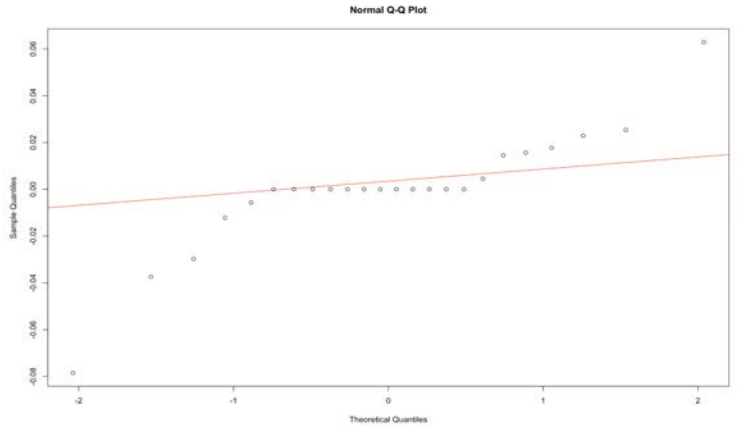

Table A2. Testing of assumptions for the two-way ANOVA assessing the effect of treatment, time and their interaction on chlorophyll *a* concentration

Station 1D
Levene's Test for Homogeneity of Variance (center = median)
DF = 11, p-value = 0.2236
Shapiro-Wilk normality test
W = 0.71567, p-value = 5.032e-07

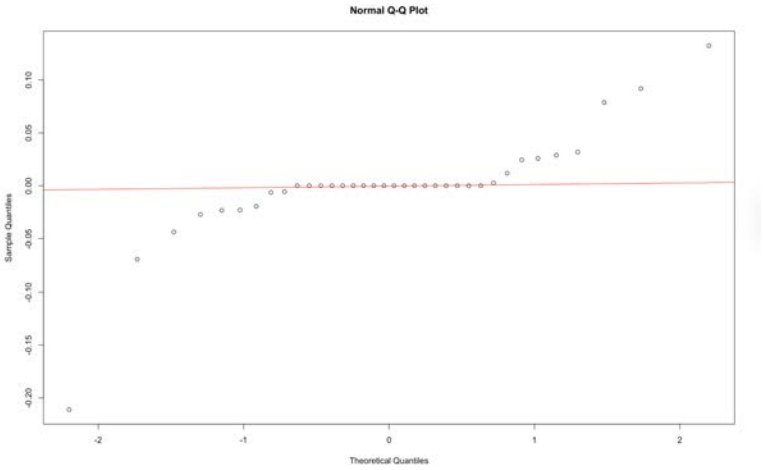

Station 1S
Levene's Test for Homogeneity of Variance (center = median)
DF = 11, p-value = 0.4798
Shapiro-Wilk normality test
W = 0.86078, p-value = 0.0003403

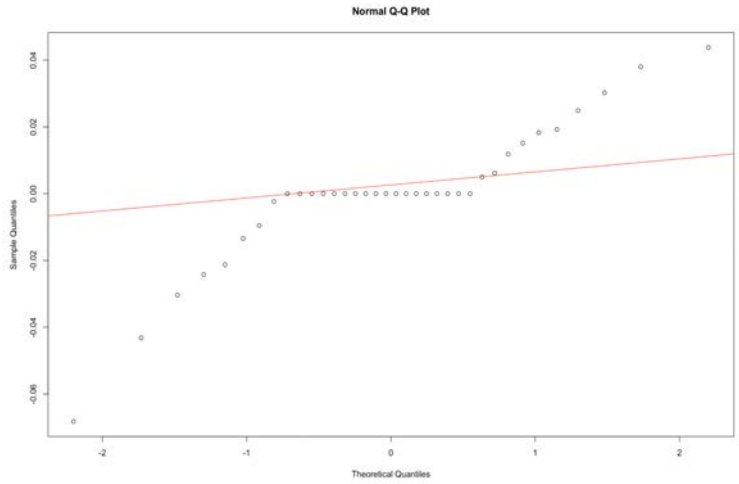

Station 2D
Levene's Test for Homogeneity of Variance (center = median)
DF = 11, p-value = 0.06099
Shapiro-Wilk normality test
W = 0.7389, p-value = 1.226e-06

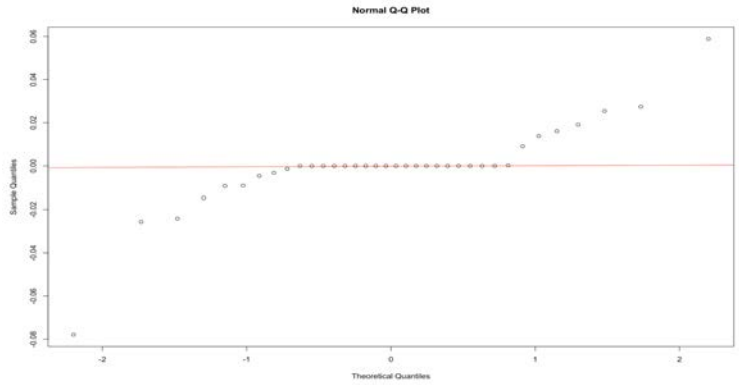

Station 3D
Levene's Test for Homogeneity of Variance (center = median)
DF = 11, p-value = 0.3671
Shapiro-Wilk normality test
W = 0.83356, p-value = 8.142e-05

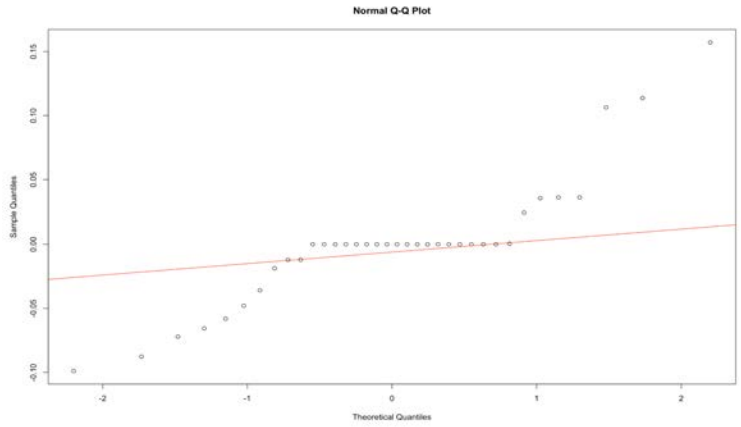

Station 3S
Levene's Test for Homogeneity of Variance (center = median)
DF = 11, p-value = 0.0546
Shapiro-Wilk normality test
W = 0.76752, p-value = 3.923e-06

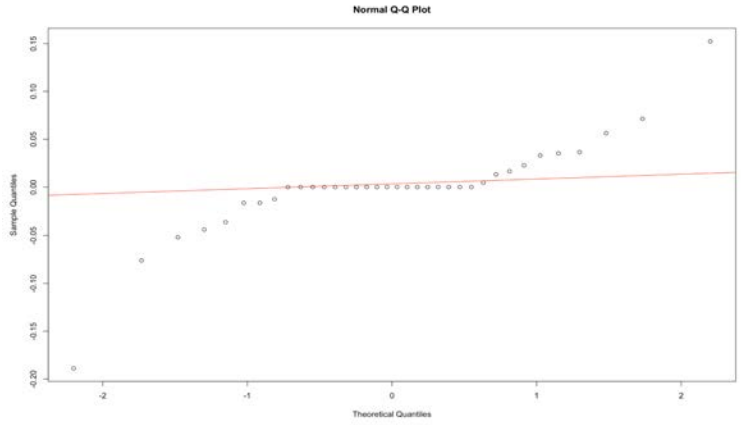

Report 3

Ane Stendal Svendsen, Ida Valbjørn Christensen & Julie Elisabeth Brantley Boesen (2025). Diversity and biomass of macroalgae at non-exposed and exposed sites in Qeqertarsuaq harbour (western Green-land) in July 2025.

Diversity and biomass of macroalgae at non-exposed and exposed sites in Qeqertarsuaq harbour (western Greenland) in July 2025

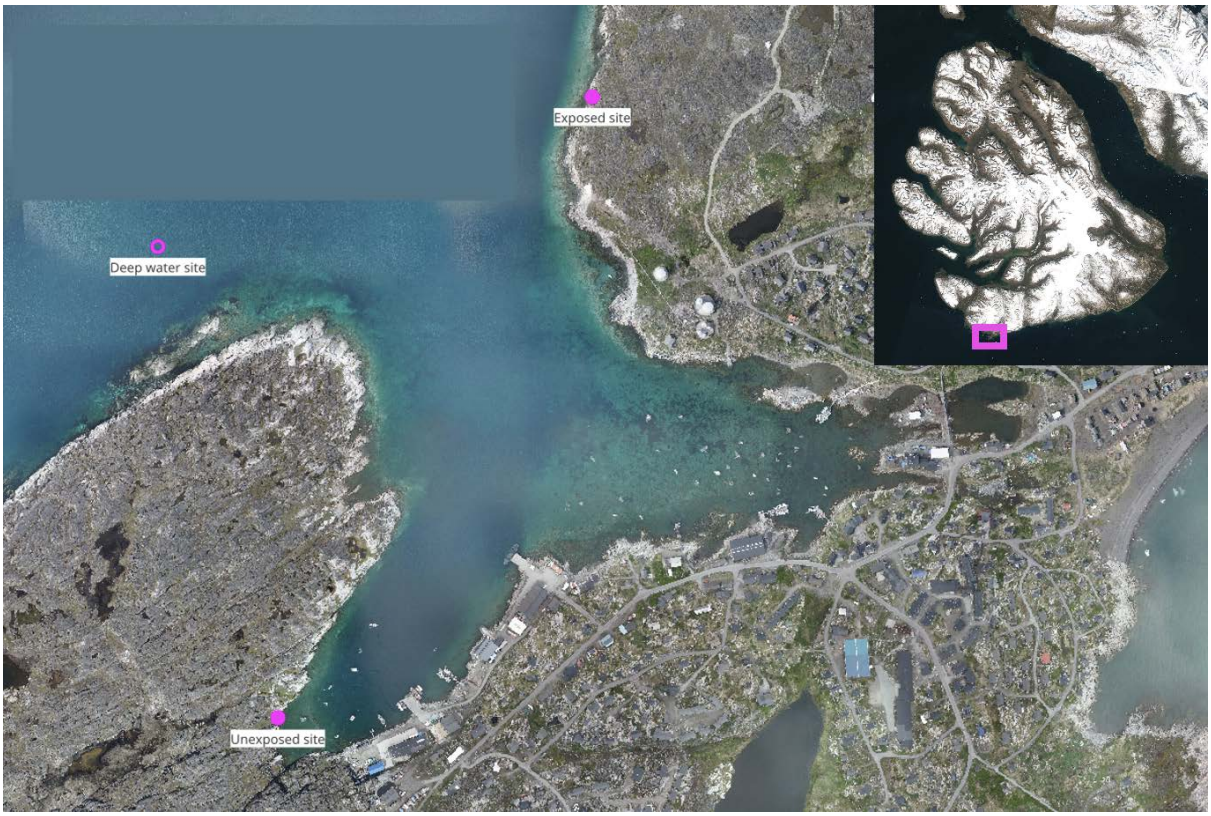

Arctic Biology Field Course 2025

Ane Stendal Svendsen (kfl705)
Ida Valbjørn Christensen (wkj174)
Julie Elisabeth Brantley Boesen (rbs305)

Supervisors: Niels Daugbjerg and Per Juel Hansen

July 2025

Abstract

Macroalgae are among the most productive and ecologically important habitats in the coastal ocean. In Arctic fjords, where other types of marine vegetation are largely absent, they play a crucial role in primary production, carbon cycling, and habitat formation. Their distribution, however, is strongly shaped by physical stressors such as wave exposure and drifting ice. Therefore, this study examines how wave exposure and ice scouring affects macroalgal vegetation in Qeqertarsuaq harbour, West Greenland, during the summer period (July). We compared a non-exposed and an exposed site to assess differences in macroalgal biomass and species diversity and examined how these patterns vary across the two tidal zones (littoral and sublittoral).

At both exposure levels, macroalgae were sampled along 3 transects using quadrats of 0.5 or 0.25 m^2 placed in the upper, middle, and lower littoral zones, as well as in the sublittoral down to a depth of approx. 1 meter. All individuals within each quadrat were collected, identified to the lowest possible taxonomic level, and weighed to calculate species specific biomasses and Shannon-Weaver diversity index for each zone and site.

Macroalgal biomass showed to be strongly influenced by exposure, with the non-exposed site showing much higher total biomass, due to the dominance of perennial species of *Fucus* (brown algae). In contrast, species diversity was slightly higher at the exposed site, likely due to reduced canopy dominance and increased niche availability under moderate disturbance.

Vertical patterns also varied between the sites. At the exposed site, diversity was highest in the sublittoral zone, supporting the hypothesis that deeper areas offer more stable conditions and reduced physical stress. At the non-exposed site, diversity was slightly higher in the littoral zone, possibly due to reduced light, limited nutrient supply, or limited hard substrate for anchoring in the sublittoral zone. The biomass was higher in the littoral than in the sublittoral zone at both sites, and increased from the upper to the lower littoral, especially at the non-exposed site, likely due to longer immersion times and more favorable growing conditions near the low tide line. Together, these patterns highlight how exposure and tidal depth interact to shape macroalgal communities in Arctic environments.

1.0. Introduction

1.1. Macroalgae

Macroalgal habitats are among the most widespread and productive vegetated ecosystems in the coastal ocean, covering approximately 7 million km² globally (Assis et al., 2022). Macroalgae are found across all climate zones on Earth and are particularly dominant as primary producers in Arctic fjords, where other types of marine vegetation such as seagrasses, marshes and mangroves are limited or absent (Ørberg et al., 2023).

In areas where macroalgae occur in high densities, they form underwater forests that increase structural complexity and contribute to coastal protection (Ager et al., 2023). These forests also provide essential habitats for a wide range of marine organisms, offering shelter from UV radiation and desiccation during low tide (Ager et al., 2023). Their high primary production supports coastal food webs and plays a substantial role in marine carbon sequestration (Ager et al., 2023; Wiktor et al., 2022). Macroalgae remove CO_2 from the water column through photosynthesis and incorporate it into their biomass. In fact, the net primary production (NPP) per unit area of many macroalgal forests ranks among the highest of any habitat worldwide (Ager et al., 2023). Although most macroalgae are anchored to hard substrates, which prevents local carbon burial, they still contribute significantly to the export of carbon in the form of dissolved organic carbon (DOC) and particulate organic carbon (POC). This exported material sustains lateral carbon flows and can contribute to long term carbon storage in sediments (Ager et al., 2023).

Finally, macroalgae are gaining increasing attention as a food resource, particularly in Arctic countries, where they are being harvested both for local human and animal consumption and thus constitute an economic resource (Kreissig et al., 2021).

1.2. Macroalgal diversity in Greenland

The diversity of macroalgae in Greenland is relatively limited, with around 200 species recorded, including approx. 80 species of brown algae (Phaeophyta), 50 species of red algae (Rhodophyta), and 50 species of green algae (Chlorophyta) (Pedersen, 2022). These three major groups differ in pigment composition, which determines the wavelengths of light (400-700 nm) they can absorb and utilize for photosynthesis, allowing them to occupy different light niches depending on water depth and clarity (Berge et al., 2020).

Most macroalgae grow on hard substrates, anchoring to bedrock, boulders, stones, or biogenic surfaces such as mussels and corals (Ager et al., 2023). While the littoral zone is a key habitat, macroalgae are also found at depths exceeding 200 meters, where light levels remain sufficient to support photosynthesis (Duarte et al., 2022).

1.3. Fucoids

Within the Arctic intertidal zone, macroalgal communities are often dominated by fucoids (Fucales), an order of intertidal brown algae (Lebrun et al., 2022). These species are well adapted to the varying conditions typical of Arctic shorelines. Their resilience allows them to colonize a wide range of coastal habitats, making them one of the most widespread and abundant macroalgal groups on tidal rocky shores across the Northern Hemisphere (Lebrun et al., 2022).

Fucoids consist of a disc-like holdfast, a short stipe and a flattened blade (Lebrun et al., 2022). The holdfast anchors the alga to the substrate, while the stipe provides support and flexibility. The blade performs most of the photosynthesis and the uppermost part may contain reproductive structures. In some species, air bladders enhance buoyancy and improve light access during high tide (Lebrun et al., 2022). Their dense structures offer shelter, substrate, and food for a variety of small marine organisms, including both epiphytic and endophytic communities. In this way, they play a key role in maintaining intertidal biodiversity and structuring of the food web (Lebrun et al., 2022).

Several fucoid species are common in Arctic regions, including *F. spiralis, F. vesiculosus, F. serratus,* and *F. distichus.* Among these, *F. distichus* is particularly well adapted to Arctic environments, capable of tolerating cold temperatures and surviving extended periods of darkness (Lebrun et al., 2022).

1.4. Factors influencing macroalgae distribution and biomass

The distribution of macroalgae is influenced by a variety of biological and physical factors, including wave exposure, ice scouring, tidal zone, light availability, temperature, sedimentation, daylength and in some areas, grazing pressure (Ager et al., 2023; Wiktor et al., 2022).
Wave exposure and ice scouring significantly impact macroalgal communities (Pedersen, 2022). Ice from marine-terminating glaciers and seasonal sea ice can scour the coastline, disrupt the benthic habitats and remove algae from the substrate (Ager et al., 2023).
Vegetation composition is closely tied to exposure level. Non-exposed coasts are typically dominated by perennial brown algae, particularly fucoids. Exposed shores are dominated by fast-

growing, short-lived species, often ephemeral green algae, such as members of the class Ulvophyceae (Hansen, 1998; Pedersen, 2022).

1.5. Stressors in the littoral zone

Within the littoral zone the vertical zonation is shaped by varying exposure to stressors such as desiccation, UV radiation, and temperature.

Intertidal macroalgae are highly adapted to dynamic coastal environments. Many have soft and flexible tissues that allow them to bend with the water movement, minimizing the risk of breakage (DiNenno, 2022). Some species, such as *F. vesiculosus*, also develop air bladders, which provide buoyancy and help keep the fronds upright during high tide and afloat during low tide, improving access to sunlight (Garbary et al., 2006).

In the upper littoral zone, macroalgae are regularly exposed to air during low tides, leading to frequent desiccation and temperature fluctuations. These conditions limit photosynthetic activity and increase metabolic costs for stress tolerance, resulting in lower biomass accumulation (Bischof et al., 2006). Species in this zone often exhibit morphological and biochemical adaptations, such as thicker cell walls and increased production of UV-screening compounds, to mitigate these damages (Hanelt et al., 1997).

In the mid and lower littoral zones, species such as *F. vesiculosus* and *F. evanescens* benefit from longer submersion periods, which buffer against drying and temperature variations. These zones experience reduced UV exposure due to water submersion and more stable thermal conditions, allowing for higher growth rates and biomass production (Wulff et al., 2009).

1.6. Abiotic factors

Light is among the most limiting resources for macroalgal growth. In Arctic regions, sea ice reduces the amount of light reaching the seafloor, and silt from melting glaciers further increases light attenuation in the water column (Ager et al., 2023). In fjords, river input adds suspended sediment that reduces the depth of visibility in the water (Pedersen, 2022). Sediment can also cover algae or rocky surfaces, making attachment and growth difficult (Pedersen, 2022).

Although salinity around Greenland generally remains stable at a salinity of 33, seasonal freshwater input from melting ice can cause local fluctuations, particularly in spring (Pedersen, 2022). However, low salinity is not typically a major constraint in Greenlandic waters. Temperature, on the

other hand, strongly influences macroalgal growth rates and species distribution (Pedersen, 2022). For many species, reproduction is regulated by a combination of temperature and daylength, and climate changes leading to changes in the sea temperature are expected to narrow the reproduction success of some species (Pedersen, 2022). Grazing can also affect macroalgal abundance. In some regions, sea urchins in high densities, can completely graze down macroalgal vegetation (Pedersen, 2022).

1.7. Coastal types

To investigate how exposure influences macroalgal diversity and biomass, this study compared two sites at and near Qeqertarsuaq harbour, one non-exposed and one exposed to waves and ice. The used sites were selected based on prior knowledge of local exposure conditions and visual assessment. The area experiences sea ice cover from December/January to May/June, limiting wave action in winter (Luetzenburg et al., 2023). In summer, ice retreats and wave exposure increases in the area (Luetzenburg et al., 2023).

The coastline of Greenland can be broadly categorized into four coastal types based on their degree of exposure, as outlined by Pedersen (2022). This classification provides a useful framework for understanding differences in macroalgal communities.
We used this typology to categorize and describe our selected study sites. We classified our study sites as coastal type 1 (non-exposed) and type 2 (exposed), based on both observed physical conditions at the sites, and species composition and biomass (Figure 1).

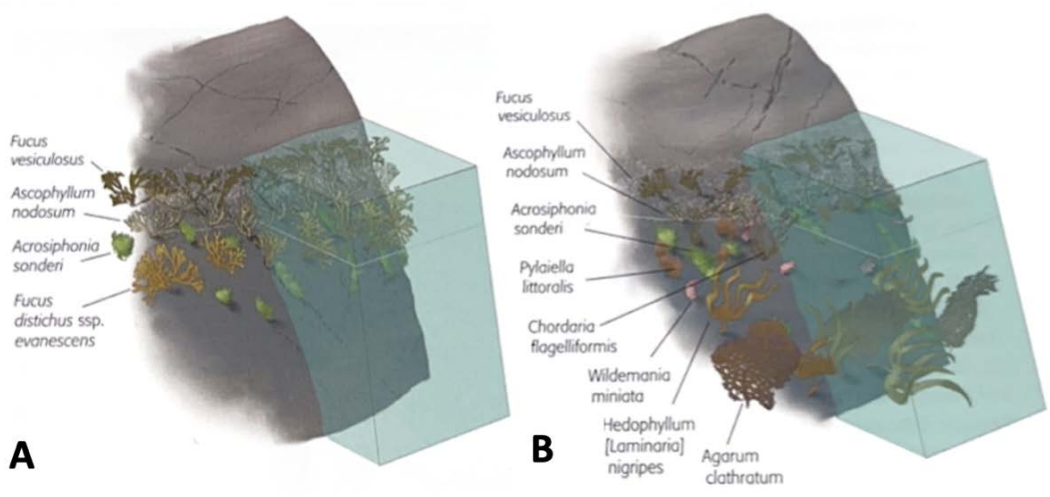

Fig. 1. Illustration of 2 coastal types, based on degree of exposure, with associated macroalgal species in the littoral and sublittoral zone. (A) shows coastal type 1, representing the most sheltered environment. (B) shows coastal type 2, which is more exposed to sea ice but protected against strong waves. From Pedersen (2022).

Coastal type 1 represents the most sheltered coastal environment, with no drift ice and protection from strong waves (Pedersen, 2022). *Fucus vesiculosus* dominates the upper littoral zone, *Ascophyllum nodosum* the middle part, and *F. evanescens* the lower part (Figure 1A). In very sheltered inlets, *Ascophyllum* may be absent. In areas where brown algal cover is less dense, an under-vegetation composition of red and green algae can develop. In addition, epiphytic algae are often found growing on larger specimens of *Fucus* (Pedersen, 2022).

Coastal type 2 is slightly more exposed, with occasional drift ice and currents, but still sheltered from strong waves (Pedersen, 2022). The same species occur in the littoral zone, as in type 1, but are often smaller, more scattered, and show signs of physical damage. Sometimes they might only remain as stumps or be restricted to cracks in rocks. Other species present in the littoral zone are short-lived algae, especially green algae (Figure 1B). The sublittoral zone is dominated by annual brown algae like *Pylaiella littoralis, Dictyosiphon foeniculaceus* and *Chordaria flagelliformis* (Pedersen, 2022).

At depths of 1.5-2 meters, the influence of sea ice declines, and more robust, perennial brown algae begin to dominate. These include species of Laminariales such as *Agarum clathratum, Saccharina latissima,* and *Hedophyllum nigripes.* In areas with mobile substrates like small stones, large algae cannot anchor, and more flexible species such as *Desmarestia aculeata* and *Desmarestia viridis* may dominate (Pedersen, 2022).

1.8. Aims and hypotheses

This study aims to investigate how wave exposure and drift ice influence macroalgal vegetation at different sites in Qeqertarsuaq harbour, West Greenland, during summer (July). We compare a non-exposed and an exposed site, to assess differences in macroalgal biomass and species diversity. Furthermore, we aim to examine how the macroalgal species composition changes across tidal zones at each site.

Based on previous studies, we expect the non-exposed site to have higher biomass and species diversity than the exposed site, due to lower physical disturbance. These more stable conditions likely favor more species, and especially perennial brown algae, like species of *Fucus,* which can accumulate substantial biomass over multiple years. In contrast, the exposed site is expected to be dominated by ephemeral, fast-growing green algae, with fewer and smaller individuals of *Fucus*.

At both sites, we expect biomass to peak in the lower littoral and upper sublittoral zones, where prolonged submersion, good light availability, and stable substrate favor macroalgal growth, especially of the large species of *Fucus*. We also expect biomass to increase again at greater depths (>1.5 meters), where larger sublittoral species such as *Desmarestia* spp. and *Laminariales* spp. dominate. Species diversity is expected to be highest in the sublittoral zone, where stable underwater conditions support a broader range of taxa, and where competition from dominant brown algae in the littoral zone is reduced.

We test the following null hypotheses (H0) in our statistical analyses:

H1: There is no difference in the macroalgal species diversity index between the non-exposed and exposed sites.

H2: The is no difference in macroalgal species diversity index between littoral (plots 1-3) and sublittoral zones (plot 4) at non-exposed and exposed sites, respectively.

H3: There is no difference in total biomass between non-exposed (plots 1-4) and exposed (plots 1-4) sites.

H4: There is no difference in biomass between littoral (plots 1-3) and sublittoral (plot 4) zones at non-exposed and exposed sites, respectively.

H5: There is no difference in biomass between the three plots in the littoral zone at non-exposed and exposed sites, respectively.

2. Materials and methods

For this study, macroalgae species diversity and biomass were investigated between littoral and sublittoral zones at two sites in and around Qeqertarsuaq harbour, West Greenland, between the 11th and 15th of July 2025 (Figure 2). The sites were selected based on two contrasting exposure levels of ice scoring and wave action, as well as accessibility and safety criteria.

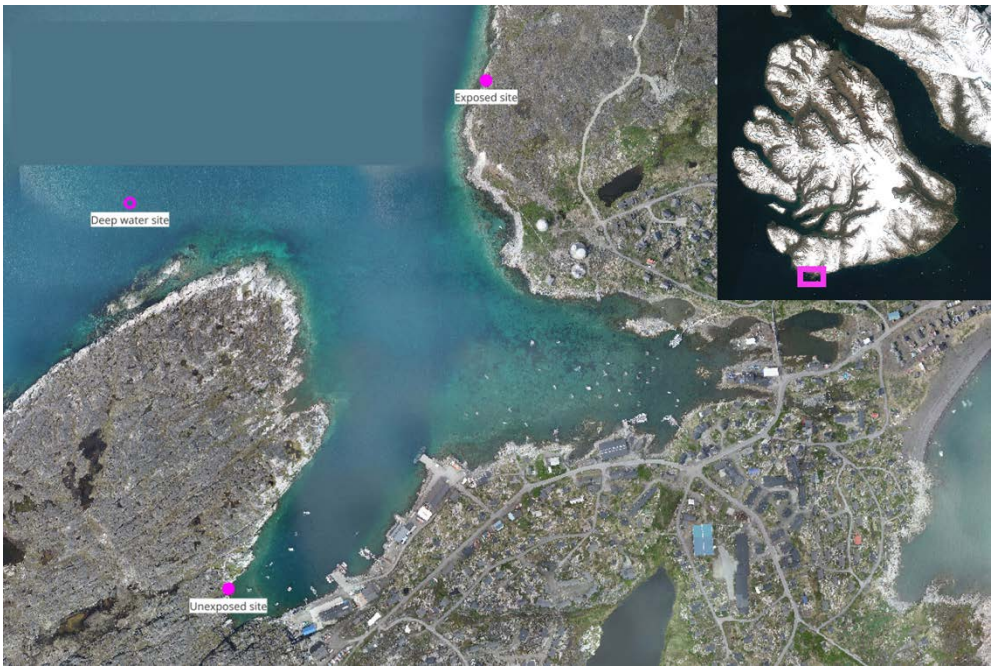

Fig. 2. Map of the harbour in Qeqertarsuaq showing the locations of non-exposed and exposed sites, as well as the deep-water sample location. Scale is 1:4800. The map to the top right shows Disko Island, West Greenland, and the location of the harbour in Qeqertarsuaq marked with a pink square. Geodata from (Klimadataforsyningen, 2022).

The map showing the sampling sites was created using the free and opensource QGIS (version 3.34.15). The map of the harbour is an orthophoto layer (Asiaq, 0.2 m) and the map of Disko Island is a satellite layer (Sentinel2, 2022, 10 m). Both layers are from Klimadataforsyningen (2022).

The non-exposed site was located in a rocky inlet within the harbour, offering protection from wave action and ice scouring. In contrast, the exposed site was positioned closer to the open water, exposing the site to ice scouring and higher wave activity (Figure 3).

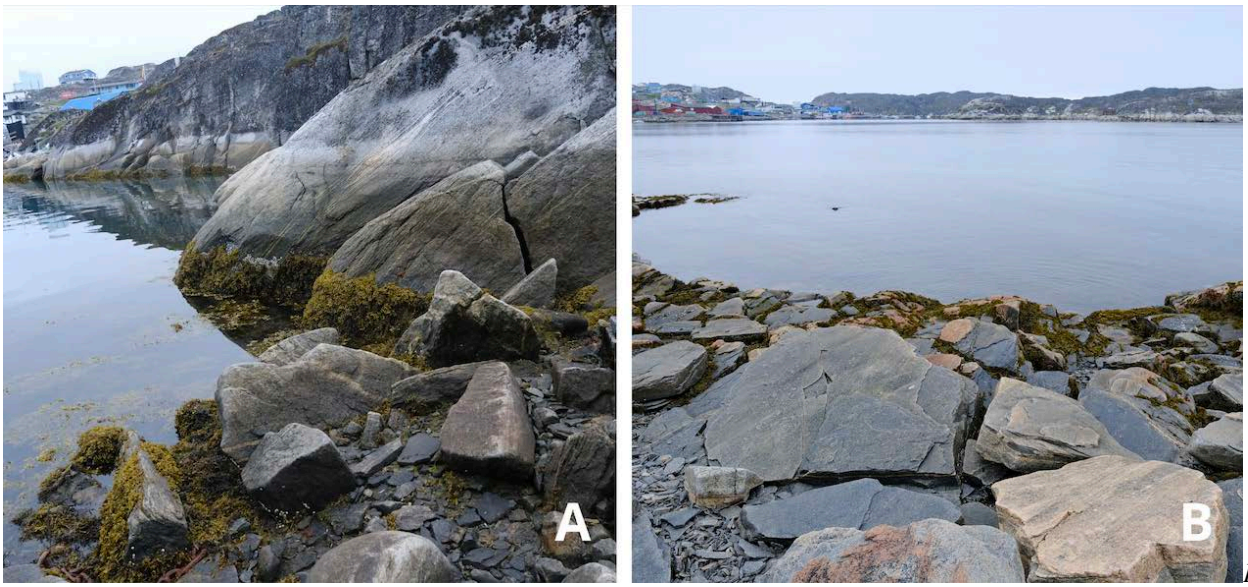

Fig. 3. The sampling area at the non-exposed (A) and exposed (B) site.

Additionally, a deep-water location was included to provide better understanding of the species diversity in the sublittoral zone. This site was accessed by the research vessel *Porsild* and allowed sampling of macroalgae at a depth of approximately 8 meters. A metal frame forming a triangle was used for this sampling (each side approx. 50 cm).

Coordinates for the non-exposed and exposed sites were recorded using an Apple Watch, while the deep-water site coordinates were obtained using the GPS system on the research vessel. Abiotic factors, including salinity and temperature, were measured at the two sites. Temperature was measured in both air and water using a digital thermometer, and salinity was measured with a refractometer (Table 1).

Salinity and temperature were not measured at the deep-water site but given the position close to the non-exposed and exposed sites, salinity is assumed to be 32-33.

Table 1. Site, sampling date, coordinates, water and air temperature, salinity and length of transects.

Site	Sampling date	Plots sampled	Coordinates	Water temp. (°C)	Air temp. (°C)	Salinity	Length of transect (m)
Non-exposed	11.07.25	1, 2, 3	69.24524 N, 53.55544 W	5.5	8.5	33	7 m
Non-exposed	13.07.25	4	69.24524 N, 53.55544 W	5.5	8.5	33	7 m
Exposed	13.07.25	1, 2, 3, 4	69.25268 N, 53.54589W	6.1	7.7	32	10 m
Deep water location	15.07.25	--	69.25071 N, 53.56005 W	--	--	--	--

2.1. Experimental setup

2.1.1 Determining the littoral and sublittoral zone

Sampling of macroalgae was carried out during low tide. Tidal conditions were determined using the app “Tide Charts Near Me”. Occurrence of barnacles and *Fucu*s species were used as indicators of the upper limit of the littoral zone. The sublittoral zone was determined as the water level at low tide, representing the transition point where the substrate remains consistently submerged.

2.1.2. Transect and plots

At each site, three transects were established perpendicular to the shoreline, in order to replicate each plot three times and to capture the variation across sites.

Along each transect, four sampling plots (plot 1-4) were established using a 1 x 1 m frame. The frame consisted of a 2-meter folding yardstick broken at the midpoint, forming a right angle with sides measuring one meter each. Plot 1 was placed in the upper littoral zone at the top of the transect. The remaining plots (plot 2-4) were subsequently placed along the transect 1 meter apart at the non-exposed site and 2 meters apart at the exposed site, ending at approximately 1 meter depth in the sublittoral zone (Table 2). The distance between plots and the total length of transects varied between the two sites due to a steeper slope at the non-exposed site. The total transect length measured 7 meters at the non-exposed site and 10 meters at the exposed site.

Table 2. Depth of plots 4 in transects at sheltered sites (1-3), exposed sites (4-6) and the depth of deep-water sampling.

	Sheltered site			Exposed site			Deep waters
Transect	1	2	3	4	5	6	--
Depth	114 cm	93 cm	105 cm	73 cm	77 cm	71 cm	8 m

2.1.3 Sampling: non-exposed and exposed site

Sampling was done by placing the 1 m^2 quadrat on the rocks and removing macroalgae from inside the quadrat. To minimize disturbance while also ensuring representative results, only half of the biomass (0.5 m^2) inside the quadrats were removed for plots 1-3. The quadrats were halved either at the 50 cm mark or the 150 cm mark randomly to minimize observer bias. In the sublittoral zone (plot 4), only 0.25 m^2 could be effectively sampled due to difficulty sampling under water. All biomass data were later extrapolated to 1 m^2 for comparison across sites and zones.

Sampling of plots 1-3 were conducted using knives and by hand to collect as much macroalgal material as possible. Only macroalgae that were attached to the substrate inside the rectangle were sampled; dead or washed-up material was discarded. Sampling was done on a three-dimensional scale, as the surface consisted of rocks which created an uneven surface.

Photographs were taken before and after sampling to document the extent of collection (Figure 4, Figure A1-7). Sampling of plot 4 was collected by hand by a single person wearing a 7 mm wetsuit and using snorkel equipment. Sampling of plot 4 at the non-exposed site was repeated as the initial attempt was hindered by poor visibility caused by bad weather. At the exposed site an additional dive was conducted at 2 meters depth, collecting additional species as an extension of the samples in the sublittoral zone (plot 4). This was only a qualitative sample and was used as a supplement for the species list (Table 6).

All samples were collected in plastic bags, transported to the Arctic Field Station and subsequently sorted, identified, blotted and weighed.

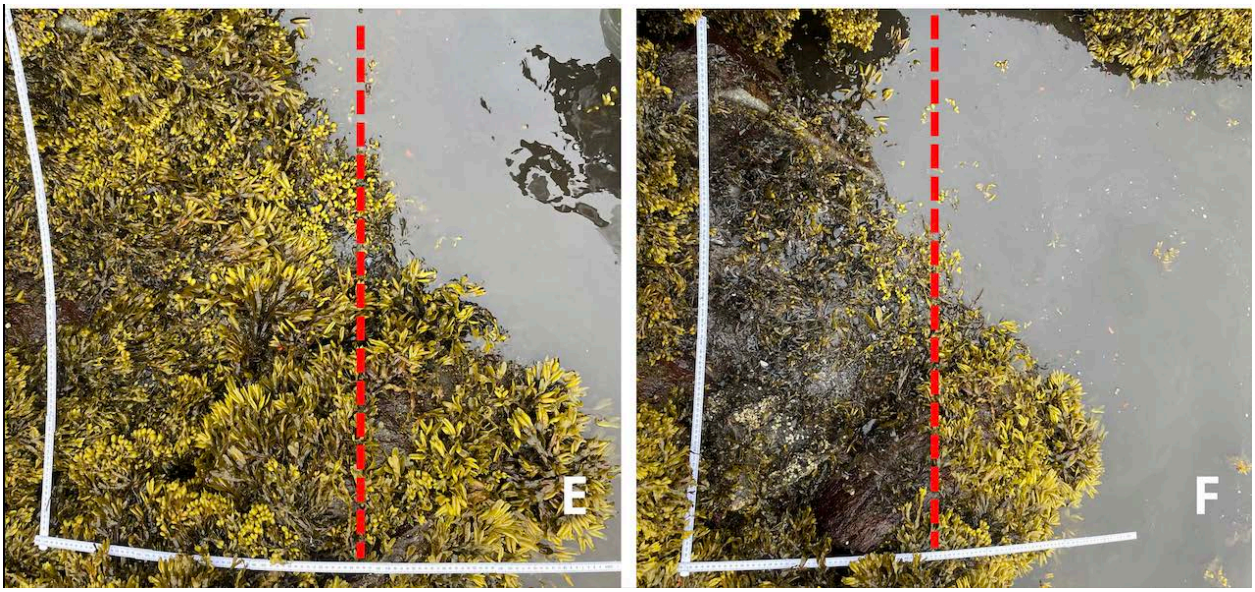

Fig. 4. Sampling before (E) and after (F) at the non-exposed site (Figure A2). The red dashed line indicates the specific area in the plot where sampling took place.

2.1.4 Sampling: deep waters

To study species of macroalgae in the sublittoral zone at greater depths, sampling was conducted using the research vessel *Porsild*. A triangle scraper was used to collect samples at a depth of 8 meters in the Qeqertarsuaq harbour. Some species were identified onboard the vessel, while others were brought back to the Arctic Field Station for identification. This sampling was qualitative and was only used as a supplement to the species list (Table 6).

2.2. Species identification

The collected macroalgae were identified to the lowest taxonomic level possible, using the identification guide *Marine Algae of Greenland* (Pedersen, 2022). Identification was conducted by visual inspection and a light microscope (Olympus BX51) equipped with a DP10 digital camera.

Fucus species were identified as either *F. evanescens, F. vesiculosus* or non-fertile. *Fucus evanescens* were identified based on long receptacles, the absence of floats and by being monoecious. *Fucus vesiculosus* was identified based on often having two floats on either side of the midrib and by being dioecious. Some *Fucus* individuals were not fertile and therefore species identification was not possible. These were labeled as non-fertile *Fucus*.

Small algae were sorted to the best extent possible. Due to time constraints, this process was not carried out as thoroughly as intended. Species identification was conducted as accurately as

possible under the given conditions. In cases where identification was not possible due to the absence of an identification guide or reference images, specimens were labeled as unknown. A group of brown algae, including *P. littoralis*, *Hincksia ovata* and *Ectocarpus fasciculatus,* could not be distinguished for use in estimates of biomass and were collectively labelled as a mixed group called brown filaments. Furthermore, *Cladophora rupestris* was identified both at its species level and as unidentified *Cladophora* spp. and was then grouped for biomass calculation as *Cladophora* spp. Lastly, a group of species were entangled in a gelatinous mass and were difficult to separate into distinct taxa. These were labeled as unidentified algal material.

2.3. Biomass calculation

To estimate the carbon biomass of macroalgae, excess surface water was gently removed by blotting each species with paper towels. The wet weight of each species was then measured using a precision scale with an accuracy of 0.001 grams, up to a maximum of 300 grams.

In cases where species occurred in dense clumps that hindered accurate identification, random subsamples were collected. These subsamples were subsequently analyzed to estimate the species composition within the clump. For example, a subsample might consist of 95% *Rhizocloniumn tortuosum*, 2% *Pylaiella varia*, 3% *Percursaria percursa*. Based on these proportions, the wet weight was divided accordingly among the identified species.

Carbon biomass (CB) was calculated using the following formula:

$$CB = WW \cdot 0.195 \cdot 0.36 \cdot P$$

Where CB is the carbon biomass (g C m^{-2}), WW is the wet weight (g 0.5 m^{-2} /0.25 m^{-2}). 0.195 is the conversion factor for wet weight to dry weight, and 0.36 is the conversion factor for dry weight to carbon biomass (Ager et al., 2023; Wickham et al., 2019). P is a plot-specific scaling factor used to extrapolate the results to m^2 (2 for plot 1-3, and 4 for plot 4).

Although these conversion factors were originally derived for *Fucus* species, they were applied to all species due to the biomass being predominantly composed of *Fucus*.

2.4. Data analysis

Data analyses were done in the statistical program R Studio (2023.12.1+402). Prior to data analysis, the dataset was filtered to remove observations with zero biomass, ensuring that only species

present at each plot contributed to the analysis. A subset of the data used for the following analyses are shown in Appendix 8.

2.4.1 Comparing sites and zones – diversity (H1 and H2)

To compare species diversity between non-exposed and exposed sites, we calculated the Shannon-Weaver diversity index based on biomass. The function *diversity ()* from the 'vegan' package (Oksanen et al., 2025) was used to calculate the Shannon-Weaver diversity index at both sites. The same was done to compare species diversity in the littoral and sublittoral zones at the non-exposed and exposed sites, respectively.

For the following hypothesis regarding biomass, differences between sites, zones and plots were tested using non-parametric tests. Biomass was the dependent variable and n = 3 for all statistical tests, due to the three transects which serve as replicates. For each transect biomass is either summed or averaged depending on the hypothesis.

2.4.2 Comparing sites – biomass (H3)

To assess differences in biomass between sites, the dataset was grouped by site and transect, and total biomass was calculated by summing all biomass values at each transect within each site. A one-sided Wilcoxon rank-sum test was then performed to test whether total biomass at the non-exposed site was significantly higher than that at the exposed site.

2.4.3 Comparing zones – biomass (H4)

For both sites, the difference in biomass between littoral and sublittoral zones was tested. The dataset was filtered to only include observations where 'site' = "non-exposed" and data was grouped by site, transect and zone. The average biomass was calculated for each zone (littoral and sublittoral) at each transect. A one-sided Wilcoxon rank-sum test was then performed to test whether average biomass at the littoral zone was significantly higher than at the sublittoral zone.

2.4.4 Comparing plots in littoral zone – biomass (H5)

The difference in biomass between plots (1-3) in the littoral zone was assessed for both sites, respectively. A Kruskal-Wallis rank-sum test was performed to test whether average biomass between plots 1-3 was significantly different from each other. Pairwise comparisons were subsequently analyzed with Dunn's post hoc test, to determine which plots were different from each other.

2.4.5 Fucus plots

The distribution of the three *Fucus* species were plotted to show the distribution of dominant species at the tidal zone, from the upper littoral zone (plot 1) to the sublittoral zone (4) at both sites. The average biomass and standard deviation of each *Fucus* species, for each plot at both sites, were calculated and plotted using ggplot () function.

3. Results

A total of 38 species were found and identified during this project, collected from both non-exposed and exposed sites, as well as from the additional deep-water location to enhance better insights into the sublittoral zone. Of the 38 species, 11 were green algae (Chlorophyceae), 18 were brown algae (Phaeophyceae), 6 were red algae (Rhodophyceae), 2 were cyanobacteria, and 1 was an unidentified species (Table 6).

At the non-exposed site, 27 species were identified, including 3 unidentifiable species. At the exposed site, 28 species were identified, also including 3 unidentifiable species with 3 species found at the additional dive. From the deep-water location, a total of 4 species were identified. In terms of unique species, the non-exposed site had 8 species not found at other locations, the exposed site had 6 unique species, and the deep-water location with 2 unique species (Table 3).

3.1. Species diversity index

For the species diversity index, 24 species from the non-exposed site were included. This count reflects the grouping of brown filaments, which consist of 3 species, as a single taxonomic unit. At the exposed site, 22 species were included in the diversity index (Table 3). This also followed the same grouping as above. Moreover, 3 species were found exclusively during the additional dive and were outside the sampling plot. Due to the absence of biomass-per-area data, these species were not included in the diversity index calculation.

Table 3. Overview of species composition and biomass for the species diversity index. Unique species refers to species found exclusively at one site.

	Total species	Unknown species	Unique species	Total biomass (g C m^{-2})
Non-exposed	24	3	8	2503
Exposed	22	3	6	1077
Deep-water	4	0	2	-

3.2. Species distribution based on biomass on the two sites

At the non-exposed site, the biomass was dominated by species of the *Fucus* genus, which accounted for 99% of the total (Figure 5). The most abundant species was *F. vesiculosus* (56%), followed by *F. evanescens* (29%) and non-fertile *Fucus* individuals (14%). The remaining 1% of biomass was primarily comprised of *Chordaria chordaeformis* (49% of the residual fraction) and *Cladophora* spp. (27%), with additional contributions from brown filamentous algae (10%) and unidentified algal material (6%).

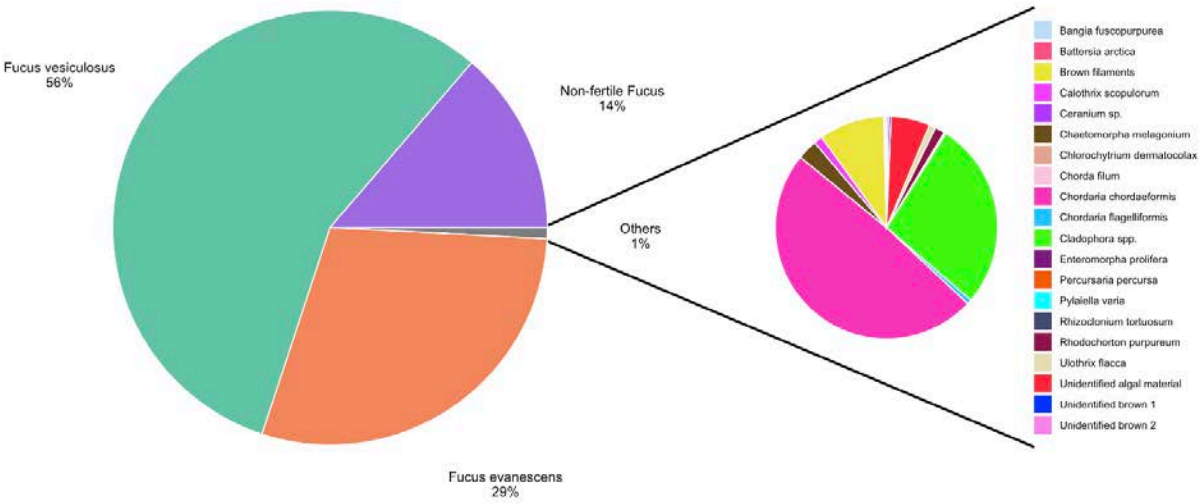

Fig. 5. Distribution of total species biomass (in %) at the non-exposed site. The outer pie shows that 99 % of the total biomass consists of Fucus species, while the remaining 1 % consists of 20 other species.

At the exposed site, species within the *Fucus* genus made up 98% of the total biomass (Figure 6). The dominant contributors were *F. vesiculosus* (46%) and non-fertile *Fucus* (43%), with *F. evanescens* accounting for the remaining 9%. Non-*Fucus* species represented just 2% of the biomass, primarily consisting of *Cladophora* spp. (30% of this fraction), *C. chordaeformis* (29%),

and *Chorda filum* (14%), along with smaller contributions from unidentified algal material (11%) and brown filamentous algae (9%).

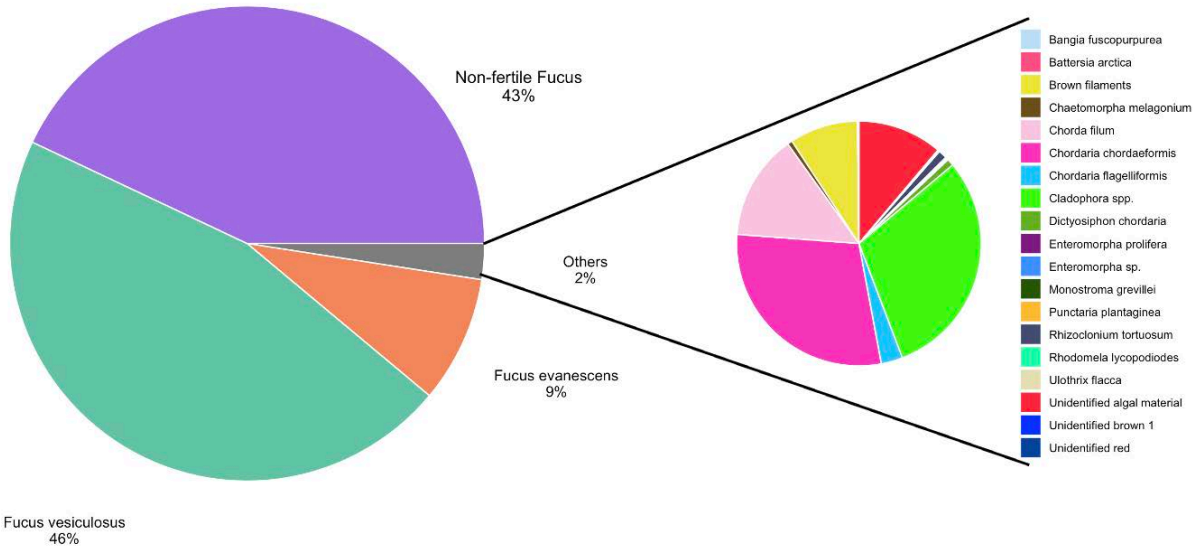

Fig. 6. Distribution of total species biomass (in %) at the exposed site. The outer pie shows that 98 % of the total biomass consists of Fucus species, while the remaining 2 % consists of 19 other species.

3.3. Comparing sites – diversity (H1)

The Shannon-Weaver diversity index was 0.89 at the exposed site and 0.80 at the non-exposed site (Table 4).

Table 4. Shannon-Weaver diversity index at the exposed and non-exposed site.

	Shannon-Weaver diversity index	SD	n
Exposed	0.890	0.421	12
Non-exposed	0.805	0.296	12

3.4. Comparing zones – diversity (H2)

The Shannon-Weaver diversity index at the non-exposed site was 0.83 in the littoral zone and 0.72 in the sublittoral zone. At the exposed site, the index was 0.70 in the littoral zone and 1.47 in the sublittoral zone (Table 5).

Table 5. Shannon-Weaver diversity index at the littoral zone (plot 1-3) and sublittoral (plot 4) zone at the non-exposed and exposed site, respectively.

Site	Zone	Plot	Shannon-Weaver diversity index	SD	n
Non-exposed	Littoral	1-3	0.83	0.185	9
	Sublittoral	4	0.72	0.576	3
Exposed	Littoral	1-3	0.70	0.249	9
	Sublittoral	4	1.47	0.241	3

3.5. Species list

A total of 38 species were recorded at non-exposed and exposed sites, including additional deep-water location. A complete list of all identified species during this project is shown in Table 6 and the presence at a site is indicated by the symbol x.

Table 6. Species list at non-exposed and exposed site, including additional deep-water location. All species are written as in algaebase.org. Species marked as (x) indicate those observed during the additional dive at the exposed site.

Phylum	Latin	Non-exposed	Exposed	Deep-water
Chlorophyta	*Chaetomorpha melagonium*	x	x	
	Chlorochytrium dermatocolax	x		
	Cladophora rupestris	x	x	
	Cladophora spp.	x	x	
	Enteromorpha prolifera	x	x	
	Enteromorpha sp.		x	
	Monostroma grevillei		x	
	Percursaria percursa	x		
	Rhizoclonium tortuosum	x	x	
	Ulothrix flacca	x	x	
	Ulva lactuca		(x)	
Cyanobacteria	*Calothrix scopulorum*	x		
	Oscillatoria sp.	x		
Ochrophyta	*Agarum clathratum*			x
	Battersia arctica	x	x	
	Chorda filum	x	x	
	Chordaria chordaeformis	x	x	
	Chordaria flagelliformis	x	x	
	Desmarestia aculeata		(x)	x
	Dictyosiphon chordaria		x	
	Ectocarpus fasciculatus	x	x	
	Fucus evanescens	x	x	
	Fucus vesiculosus	x	x	
	Hincksia ovata	x	x	
	Non-fertile *Fucus*	x	x	
	Punctaria plantaginea		x	
	Pylaiella littoralis	x	x	
	Pylaiella varia	x		
	Saccharina latissima		(x)	x
	Unidentified brown 1	x	x	
	Unidentified brown 2	x		
Rhodophyta	*Bangia fuscopurpurea*	x	x	
	Ceramium sp.	x		
	Polysiphonia stricta			x
	Rhodochorton purpureum	x		
	Rhodomela lycopodiodes		x	
	Unidentified red		x	
-	Unidentified algal material	x	x	

3.6. Photographic overview of collected species

The collected species are presented in the following figures of the classes Chlorophyceae, Rhodophyceae, Phaeophyceae and Cyanophyceae. Additionally, species collected from the deep-water location and other findings are shown.

3.6.1. Chlorophyceae

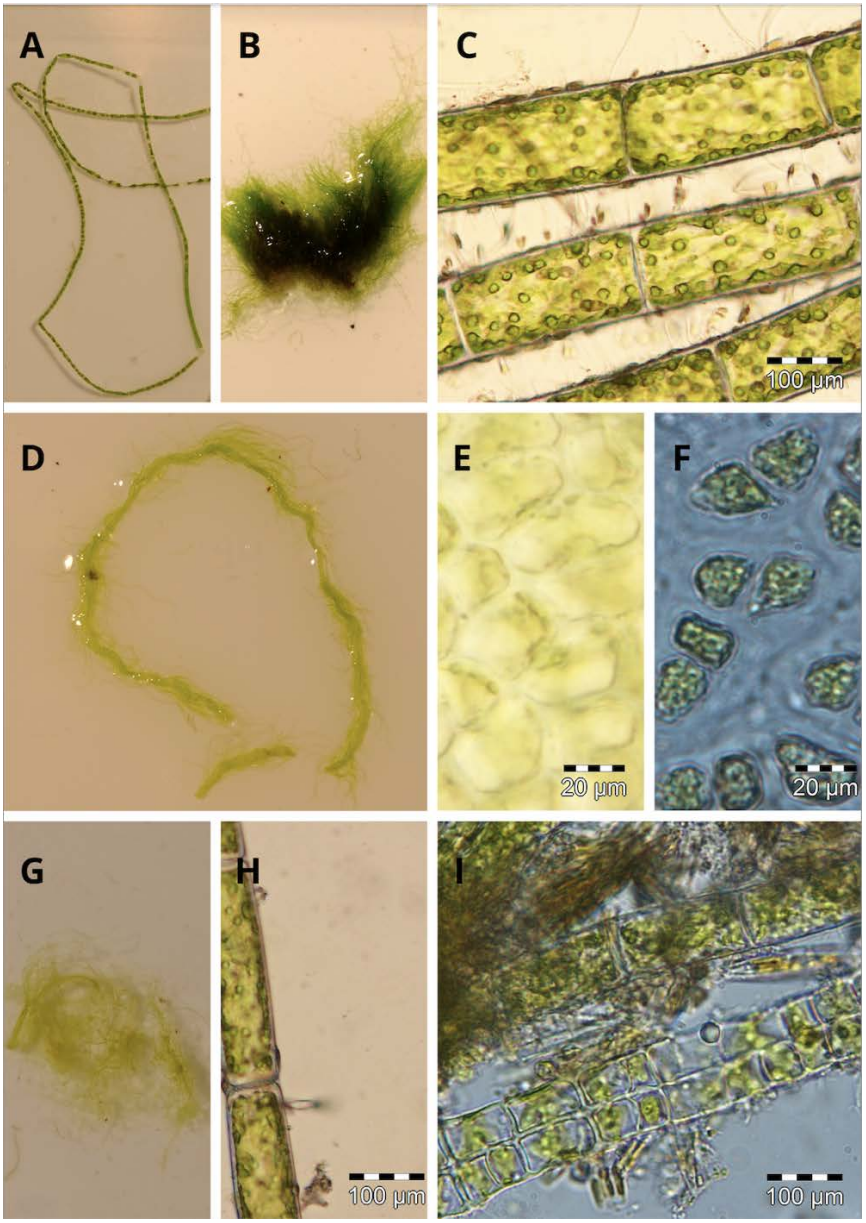

Fig, 7. Green algal species. A: C. melagonium. B: C. rupestris. C: C. rupestris, cell layer view. D: E. prolifera, cell layer view. E: Enteromorpha sp. F: M. grevillei, cell layer view. G: R. tortuosum. H: R. tortusum, cell layer view. I: P. percursam, cell layer view.

3.6.2 Rhodophyceae

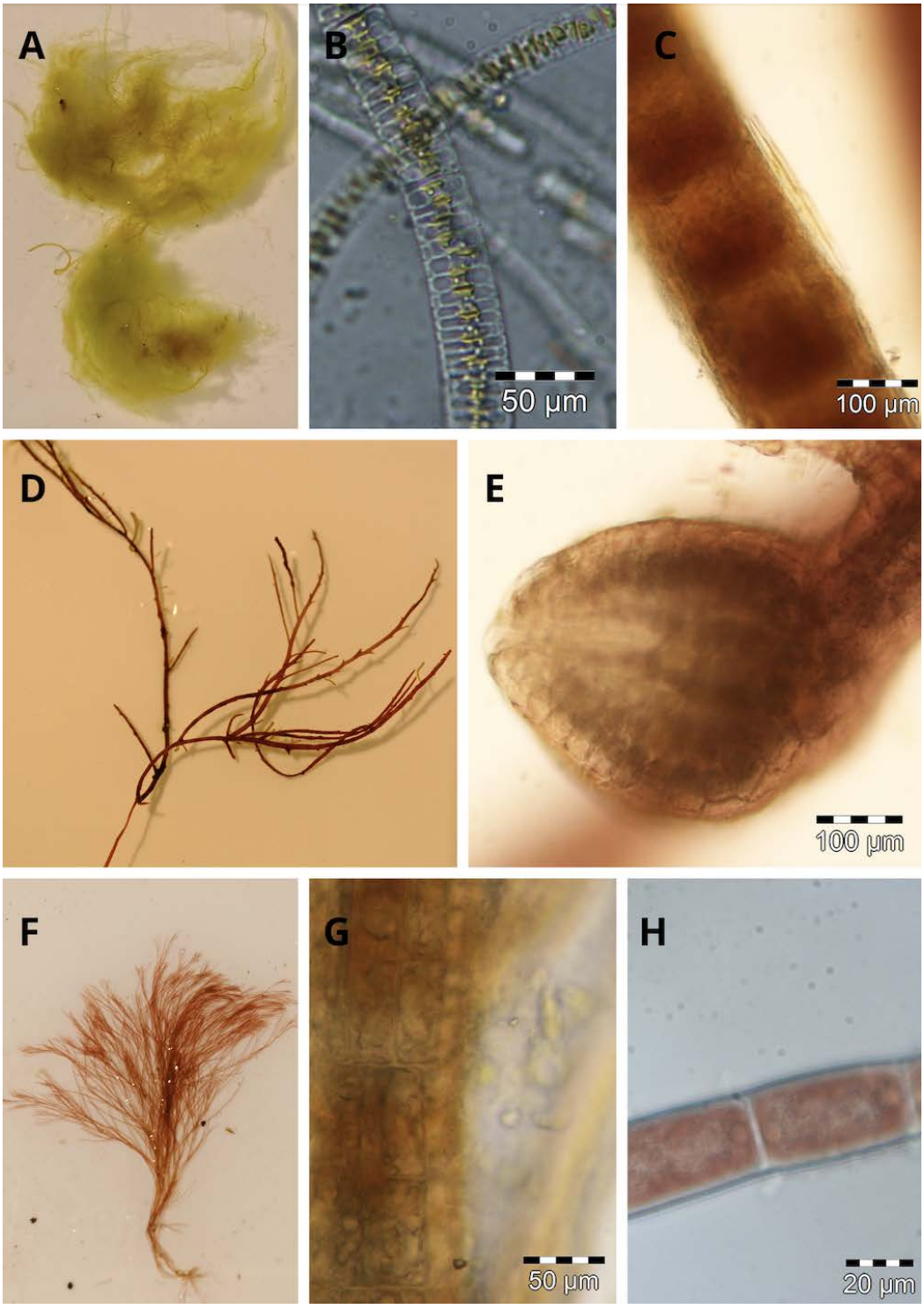

Fig. 8. Red algae. A: B. fuscopurpurea. B: B. fuscopurpurea, cell layer view. C: Ceramium sp. D: unidentified red algae. E: unidentified red algae with carpogonia. F: P. stricta. G: P. stricta, cell layer view. H: R. purpureum.

3.6.3 Phaeophyceae

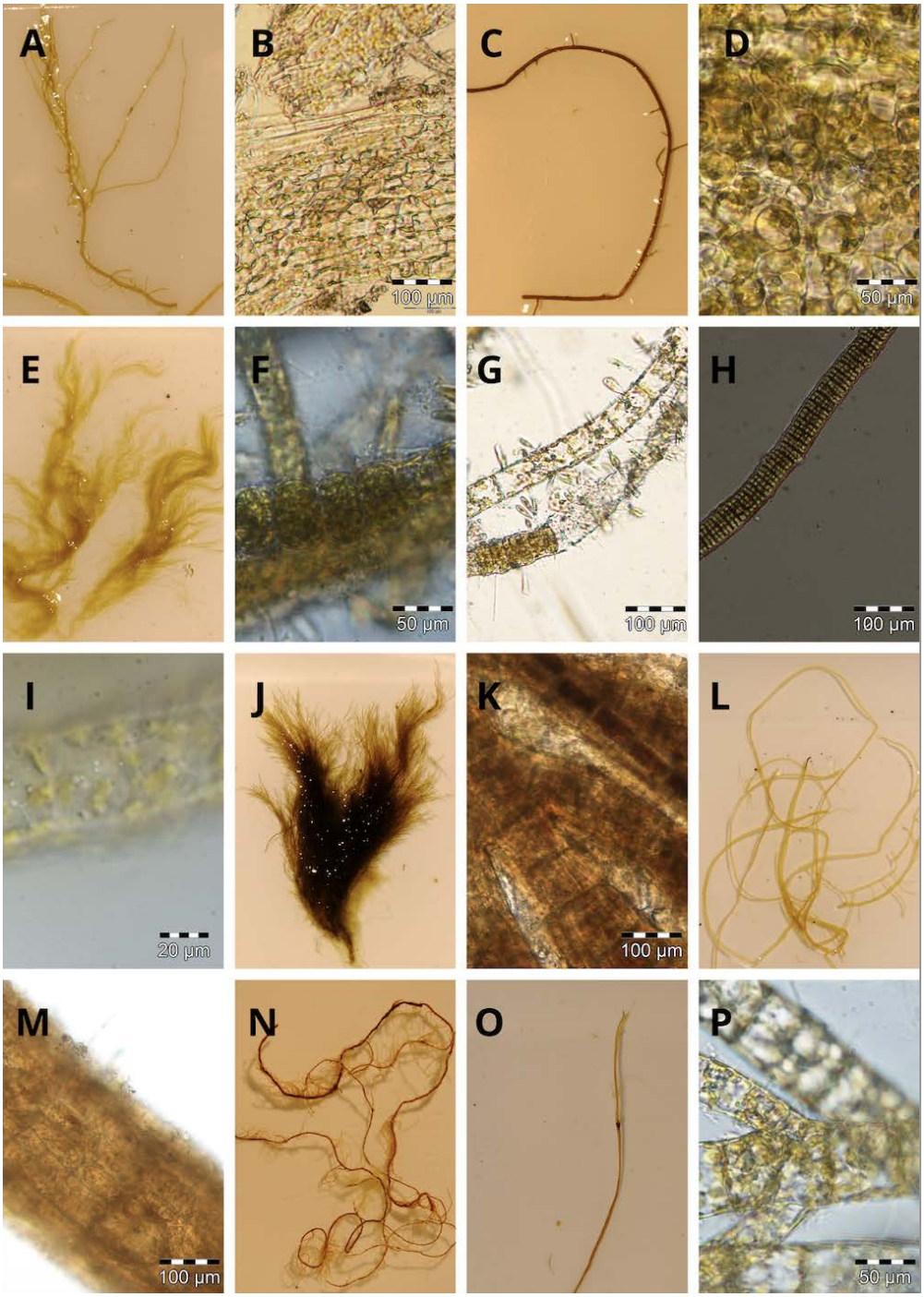

Fig. 9. Brown algae. A: C. chordaeformis. B: C. chordaeformis, cell layer view. C: C. flagelliformis. D: C. flagelliformis, cell layer view. E: P. littoralis. F: P. littoralis with sporangia. G: P. varia, cell layer view. H: H. ovata, cell layer view. I: H. ovata, cell layer view zoom. J: B. arctica. K: B. arctica, cell layer view. L: Unidentified brown 1 algae. M: Unidentified brown 1 algae, cell layer view. N: Unidentified brown 2 algae. O: C. filum. P: E. fasciculatus, cell layer view.

3.6.4 *Fucus* species

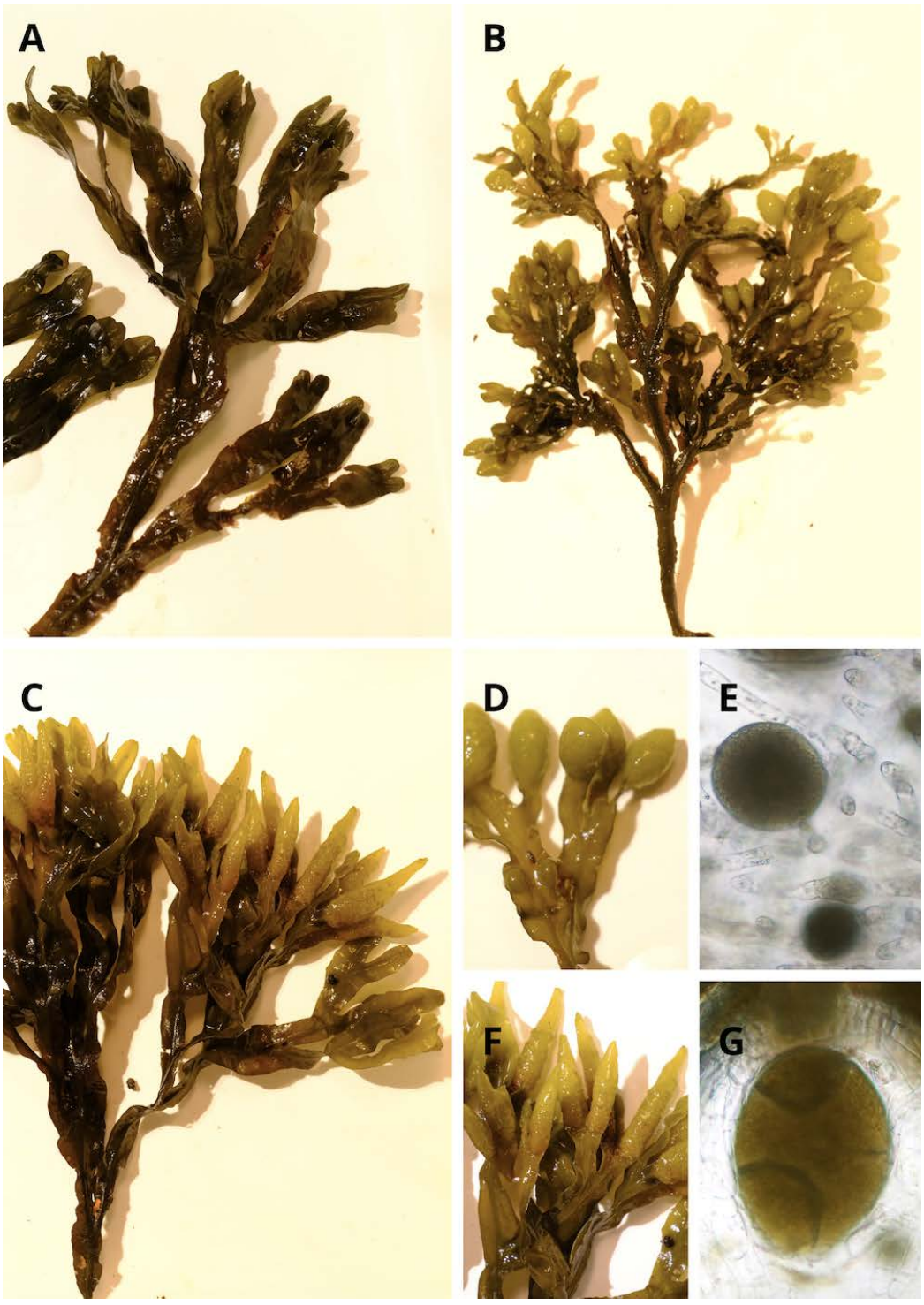

Figure 10. *Fucus species. A: Non-fertile Fucus thallus. B: F. vesiculosus, whole thallus. C: F. evanescens, whole thallus. D: F. vesiculosus, close-up. E: F. vesiculosus, cell layer view, dioecious. F: F. evanescens, close-up. G: Oogonia of F. evanescens, monoecious.*

3.6.5 Cyanobacteria and other findings

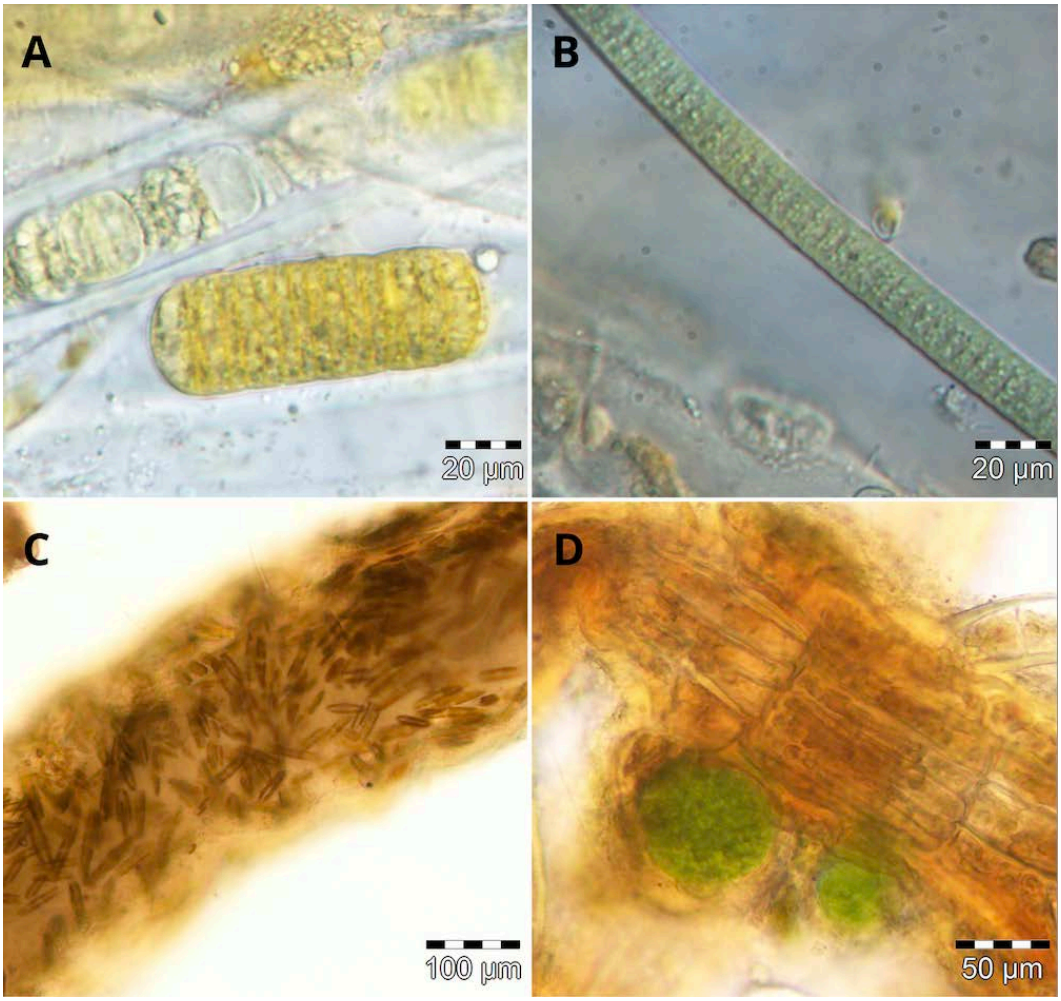

Fig. 11. Cyanobacteria and other findings. A: C. scopulorum, cell layer view. B: Oscillatoria sp., cell layer view. C: Pennate diatoms in mucus strand. D: Green parasite on B. arctica.

3.6.6 Deep-water location

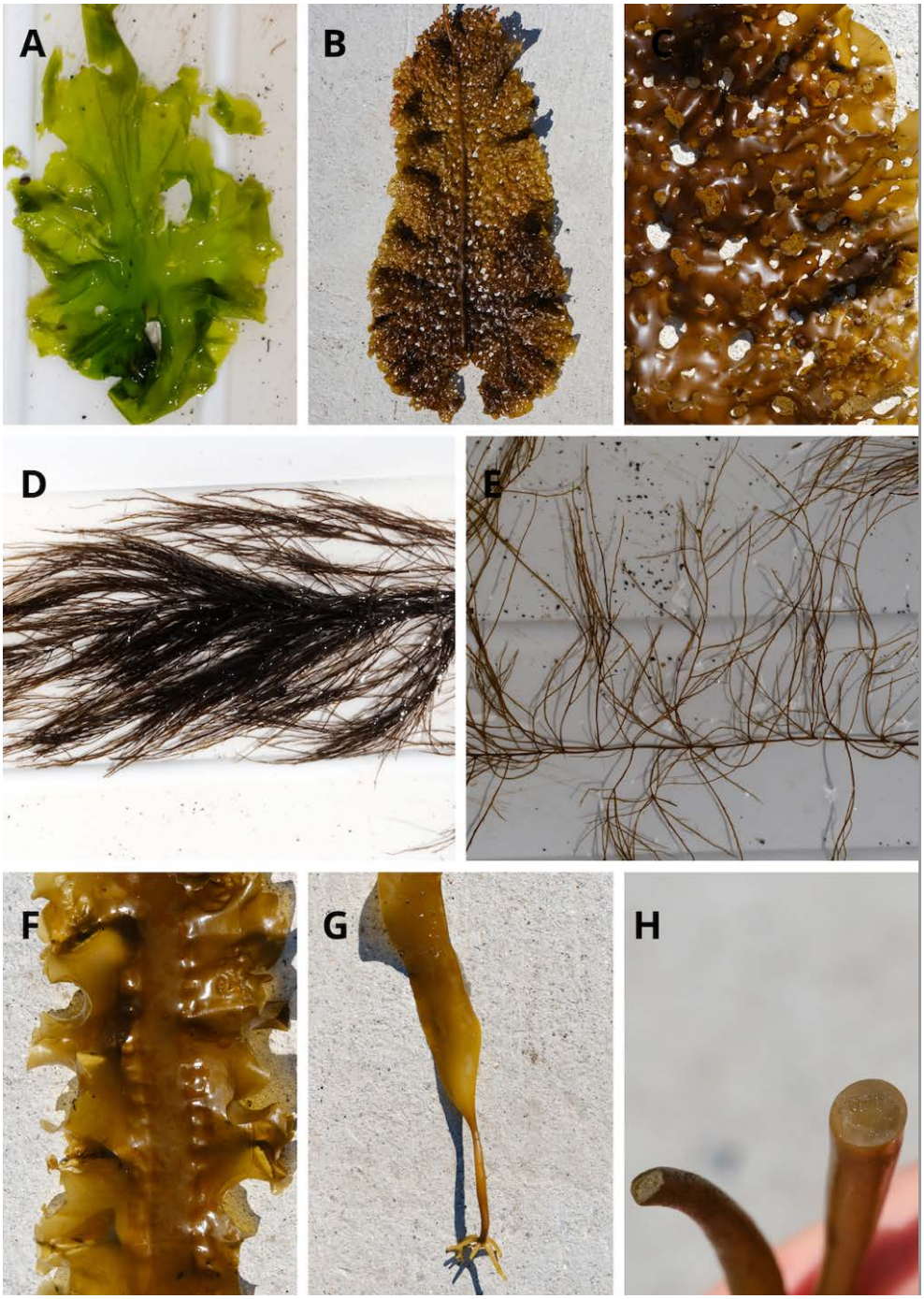

Fig. 12. Deep waters species. A: U. lactuca. B: A. clathratum. C: A. clathratum, close-up. D: D. aculeata. E: D. aculeata, close-up. F: S. latissima. E: S. latissima, small specimen with a large attachment. H: S. latissima with solid stipe.

3.7. Biomass

The biomass was dominated by *Fucus* species at exposed and non-exposed sites, accounting for 98% and 99% of the measured biomass, respectively.

At the non-exposed site, *F. vesiculosus* and non-fertile *Fucus* were observed in all plots, whereas *F. evanescens* was absent from plot 1 (Figure 11). Biomass peaked in plot 3, which contained the highest values of *F. vesiculosus* and *F. evanescens*. Non-fertile *Fucus* showed the highest biomass in plot 2. All species exhibited low biomass in plots 1 and 4. Across most plots, *F. vesiculosus* accounted for the highest biomass, except in plot 1, where non-fertile *Fucus* dominated. Mean values and standard deviation across plots are presented in Appendix 9.

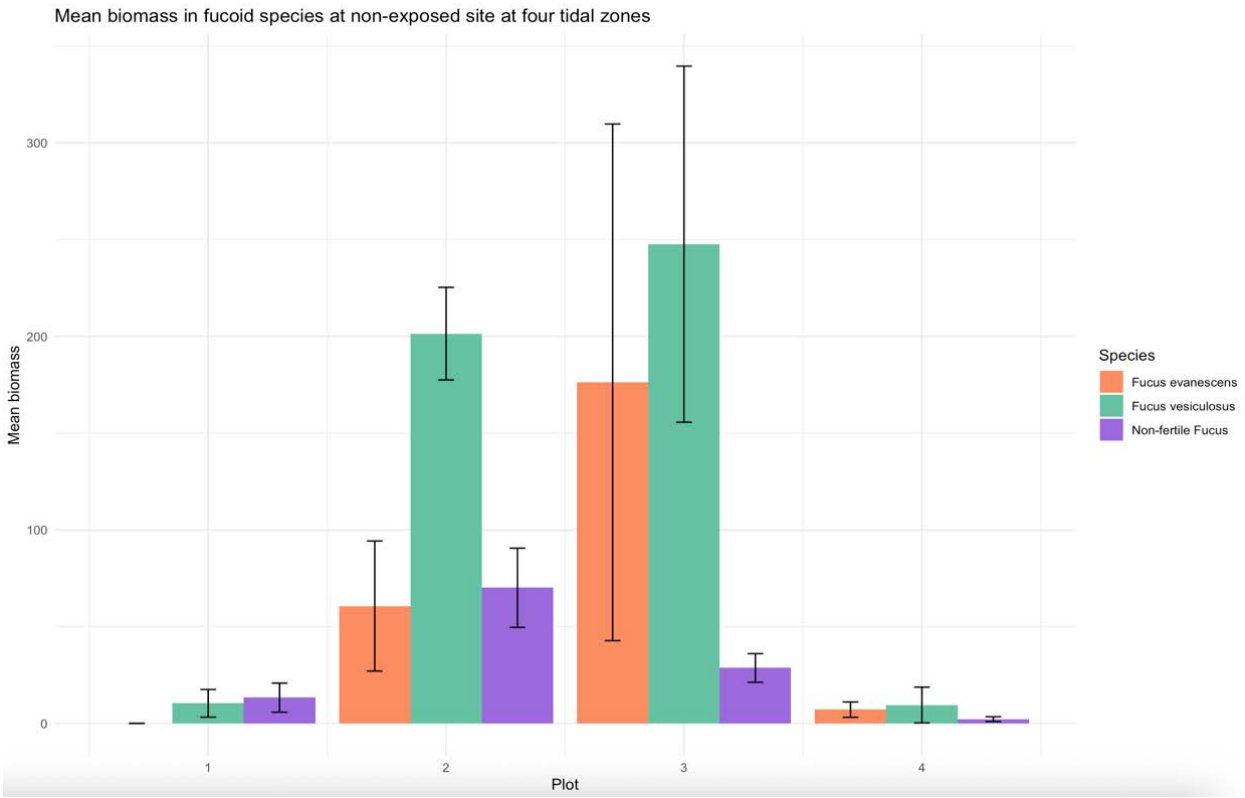

Fig. 13. Mean biomass (+/- standard deviation) of F. vesiculosus, F. evanescens and non-fertile Fucus at the non-exposed site.

At the exposed site, *F. vesiculosus* and non-fertile *Fucus* were consistently present across all plots, whereas *F. evanescens* was absent in plot 1 (Figure 12). Biomass peaked in plot 3, which also contained the highest biomass of non-fertile *Fucus* and *F. evanescens*. The maximum biomass of *F. vesiculosus* was observed in plot 2. Plot 1 exhibited generally low biomass for all species, and plot 4 showed a marginal presence. Across most plots, non-fertile *Fucus* contributed with the highest

biomass, except for plot 2, where *F. vesiculosus* dominated. Mean values and standard deviation across plots are presented in Appendix 9.

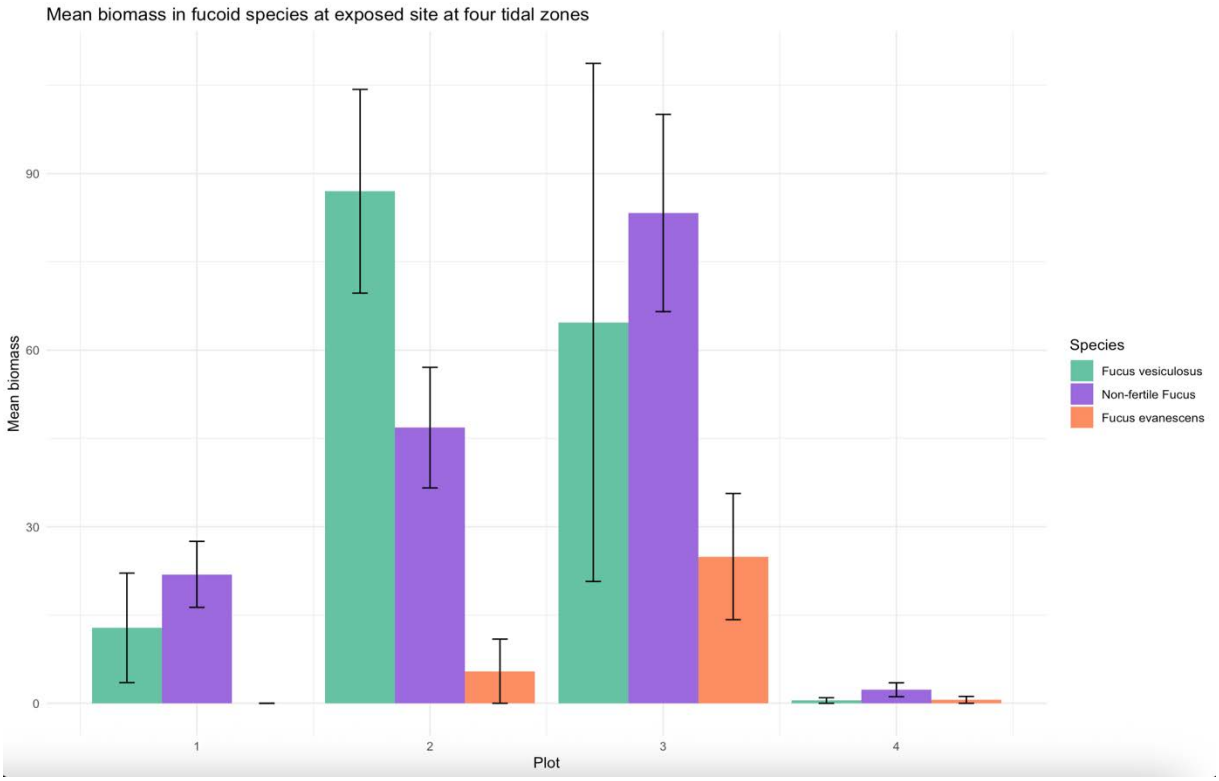

Fig. 14. Mean biomass (+/- standard deviation) of F. vesiculosus, F. evanescens and non-fertile Fucus, at the exposed site.

3.7.1. Comparing sites – biomass (H3)

Total biomass for transects at the non-exposed site (1-3) was significantly higher compared to transects of the exposed site (4-6), as determined by a Wilcoxon rank-sum test ($p = 0.05$). Biomass values at the non-exposed site ranged from 758 to 1078 g C m^{-2}, while the biomass for transects at the exposed site ranged narrowly between 355 and 366 g C m^{-2} (Table 7).

Table 7. Total biomass (g C m^{-2}) for each transects for non-exposed and exposed sites. Total biomass of transect 1-3 at non-exposed site was significantly higher than transect 4-6 at exposed site (Wilcoxon rank-sum test, p = 0.05).

Site	Zone	Plot	Transect	Total biomass (g C m^{-2})
Non-exposed	Littoral and sublittoral	1-4	1	1078
			2	667
			3	758
Exposed	Littoral and sublittoral	1-4	4	356
			5	366
			6	355

3.7.2. Comparing zones – biomass (H4)

At the non-exposed site, average biomass for each transect was significantly higher in the littoral zone (plot 1-3) compared to the biomass at the sublittoral zone (plot 4), as determined by a Wilcoxon rank-sum test (p = 0.05). Average biomass values across transects in the littoral zone ranged from 217 to 354 g C m^{-2}, while the average biomass in the sublittoral zone ranged between 14.7 and 36.1 g C m^{-2} (Table 8).

Table 8. Average biomass (g C m^{-2}) for each zone at the non-exposed site. Average biomass in the littoral zone was significantly higher than average biomass in the sublittoral zone (Wilcoxon rank-sum test, p = 0.05).

Site	Transect	Zone	Plot	Average biomass (g C m^{-2})
Non-exposed	1	Littoral	1-3	354
	2			217
	3			341
	1	Sublittoral	4	14.7
	2			15.0
	3			36.1

At the exposed site, average biomass for each transect was significantly higher in the littoral zone (plot 1-3) compared to the biomass at the sublittoral zone (plot 4), as determined by a Wilcoxon rank-sum test (p = 0.05). Average biomass values across transects in the littoral zone ranged from 114 to 118 g C m^{-2}, while the average biomass in the sublittoral zone ranged between 1.88 and 13.1 g C m^{-2} (Table 9).

Table 9. Average biomass (g C m^{-2}) for each zone at the exposed site. Average biomass in the littoral zone was significantly higher than average biomass in the sublittoral zone (Wilcoxon rank-sum test, p = 0.05).

Site	Transect	Zone	Plot	Average biomass (g C m^{-2})
Exposed	4	Littoral	1-3	118
	5			118
	6			114
	4	Sublittoral	4	1.88
	5			11.5
	6			13.1

3.7.3. Comparing plots in littoral zone – biomass (H5)

At the non-exposed site in the littoral zone, total biomass across plots 1-3 were significantly different from each other, as determined by a Kruskal Wallis rank sum test (p = 0.05) (Table 10). Based on Dunn' s pos hoc test, there is a difference in total biomass between plot 1 and plot 3 (p = 0.05. No significant differences were observed between plot 1 and plot 2 (p = 0.303), or between plot 2 and plot 3 (p = 1.00).

Table 10. Total biomass (g C m^{-2}) for each plot at the non-exposed site in the littoral zone. Total biomass in each plot is significantly different from each other (Kruskal Wallis rank-sum test, p = 0.05). Total biomass is significantly different between plot 1 and 3 (p = 0.05), while the difference is not significant between plot 1 and 2 (p = 0.30) or between plot 2 and 3 (p = 1.00).

Site	Transect	Zone	Plot	Total biomass (g C m^{-2})
Non-exposed	1	Littoral	1	18.0
	2			54.4
	3			4.26
	1		2	412
	2			356
	3			231
	1		3	633
	2			242
	3			487

At the exposed site in the littoral zone, total biomass across plots 1-3 were not significantly different from each other, as determined by a Kruskal Wallis rank sum test (p = 0.06) (Table 11). Pairwise comparisons, based on Dunn's post hoc test, revealed $p = 0.08$ for plot 1 vs. plot 3, $p = 0.22$ for plot 1 vs. plot 2, and $p = 1.00$ for plot 2 vs. plot 3.

Table 11. Total biomass (g C m^{-2}) for each plot at the exposed site in the littoral zone. Total biomass in each plot is not significantly different from each other (Kruskal Wallis rank-sum test, p = 0.06). Pairwise comparisons, based on Dunn's post hoc test, revealed p = 0.08 for plot 1 vs. plot 3, p = 0.22 for plot 1 vs. plot 2, and p = 1.00 for plot 2 vs. plot 3.

Site	Transect	Zone	Plot	Total biomass (g C m^{-2})
Exposed	4	Littoral	1	31.4
	5			12.9
	6			172
	4		2	97.8
	5			170
	6			60.1
	4		3	225
	5			149
	6			133

4. Discussion

4.1. Comparing species diversity between non-exposed and exposed sites (H1)

Our results show relatively similar macroalgal diversity between the non-exposed and exposed sites, with Shannon-Weaver diversity index of 0.81 and 0.89, respectively (Table 4). Given the small difference and overlapping standard deviations (0.42 and 0.30), we do not reject H1. This was not what we initially expected, as we had hypothesized that the more stable conditions at the non-exposed site would support a higher diversity.

One explanation could be the overwhelming dominance of *Fucus* species at the non-exposed site, where they made up 99% of the biomass (Figure 5). Dense *Fucus* canopies are known to reduce evenness by shading and outcompeting other algae (Blanc et al., 2023). In contrast, the exposed site, subject to greater wave action and ice disturbance, likely prevents such dominance, opening niches for more small, fast-growing opportunists. This pattern is consistent with the Intermediate

Disturbance Hypothesis, which suggests that moderate disturbance can enhance diversity by limiting competitive exclusion (Connell, 1978). Our observation of smaller and more often non-fertile *Fucus* individuals (43%) at the exposed site supports this (Figure 6). This pattern also reflects a classic ecological trade-off, that sheltered sites often support competitive dominants, while exposed environments restrict them and allow more diversity among disturbance-tolerant species (Connell, 1978).

We did not record *Ascophyllum nodosum* at either site, which normally is a dominant species in the tidal zone. This may reflect the specific exposure levels of our sites. While *A. nodosum* typically favors sheltered shores, it is often absent in very protected inlets where strong competition from faster growing *Fucus* species or poor water exchange limits its success (Pedersen, 2022). Thus, its absence may be another indicator of competitive dominance at the non-exposed site.

Although both sites showed relatively low Shannon-Weaver values, species numbers were quite similar (24 and 22, Table 3). The overall diversity index was likely reduced at both sites due to the strong dominance of *Fucus*, which limited evenness. Still, the comparable diversity levels suggest that while physical disturbance may shape macroalgal community structure, it does not necessarily reduce overall diversity, at least under the summer conditions sampled here. This is supported by a similar study conducted around Queqertassuaq by Hansen & Jensen (2018), where they also reported no significant differences in overall diversity measures between locations.

4.2. Species diversity between littoral and sub-littoral zones at both sites (H2)

Species diversity differed across tidal zones, but only at the exposed site. Here, the sublittoral zone had a substantially higher Shannon-Weaver index (1.47) than the littoral zone (0.70), leading us to reject H2 for the exposed site (Table 5). In contrast, diversity at the non-exposed site was slightly higher in the littoral zone (0.83) than in the sublittoral (0.72), so we do not reject the hypothesis there (Table 5).

The higher diversity in the sublittoral zone compared to the littoral zone at the exposed site aligns well with our expectations. The difference in diversity indicates that while the littoral zone experiences strong physical stress from wave action and ice scouring, the sublittoral offers a more stable refuge. The sublittoral zone remains submerged for longer periods, and provides more stable

abiotic conditions such as constant moisture, less temperature fluctuation, and reduced exposure. These conditions can support a wider range of species (Wulff et al., 2009).

At the non-exposed site, the smaller diversity difference between zones may result from several interacting factors. The dominance of large, canopy-forming *Fucus* species likely extends into the sublittoral, monopolizing space and light. In addition, reduced water exchange, increased turbidity, and low nutrient delivery in this sheltered inlet may limit sublittoral growth and diversity. These conditions likely override the benefit of reduced physical stress.

Our findings are consistent with previous research from Arctic regions such as Wulff et al., (2009). Their review highlights that macroalgal diversity is strongly influenced by depth and exposure, showing that sublittoral habitats with moderate exposure typically support the richest assemblages. They explain this pattern by noting that reduced physical disturbance, such as decreased ice scouring and wave impact, combined with sufficient light availability and nutrient flux in moderately exposed sublittoral zones, creates optimal conditions for diverse macroalgal communities to thrive (Wulff et al., 2009).

4.3. Biomasses at non-exposed and exposed site (H3)

To gain a deeper understanding of the macroalgal composition at the two sites, the total biomass was calculated. The results showed significantly higher biomass at the non-exposed site than at the exposed site ($p=0.05$, Table 7), with peak biomass nearly three times greater (1079 g C m^{-2} vs. 366 g C m^{-2}). We therefore reject H3, as there is a difference in biomass between the two sites.
The difference is likely due to reduced physical stress in the non-exposed site, where more stable conditions favour the accumulation of large, perennial species such as *F. vesiculosus* and *F. evanescens* (Hansen, 1998). In contrast, the exposed site experienced higher physical stress due to wind and potential ice-scouring. Icebergs were observed nearby, suggesting that drifting ice may shape macroalgal communities by creating harsher physical conditions. Ice scouring can damage macroalgae through mechanical disturbance and freezing, thereby hindering establishment and limiting biomass accumulation (Wiktor et al., 2022). Although ephemeral species can quickly colonize disturbed areas, they typically do not reach the same biomass as perennial species within a single growth season.

Morphological differences were also observed in the same species across the two sites. At the non-exposed site, the *F. vesiculosus* and *F. evanescens* were fully developed with a low proportion of non-fertile *Fucus* individuals (14%). In contrast, at the exposed site, 43 % of *Fucus* individuals were non-fertile. Previous studies support these findings as Hansen (1998) observed that algae at exposed sites were smaller in size, but interestingly, biomass was higher at exposed sites in that study. Høgslund et al. (2014) showed a greater occurrence of unidentifiable *Fucus* individuals at exposed sites, which plays a role in the total biomass. Unidentifiable *Fucus* individuals are non-fertile and therefore not fully developed, often smaller, which contributes to lower biomass. This aligns well with the present study, where unidentified and smaller *Fucus* individuals at the exposed site likely contributed to the lower total biomass observed.

Environmental variables such as temperature and salinity, were similar at both sites (Table 1), supporting that physical exposure rather than temperature and salinity differences, is the primary driver of biomass differences. In contrast to lower latitudes, where biological interactions like grazing and predation are key factors shaping intertidal communities, the intertidal zone in high-latitude systems appears to be primarily regulated by physical stress (Sejr et al., 2021).

4.4. Zonal differences in biomass at non-exposed and exposed site, respectively (H4)

Biomass also differed significantly between tidal zones. At both sites, the biomass in the littoral zone (plots 1-3) was significantly higher compared to the sublittoral zone (plot 4) (Wilcoxon rank-sum test, $p = 0.05$, Table 8 and 9). Therefore, we reject H4 for both sites.

At the non-exposed site, peak biomass in the littoral zone (354 g C m^{-2}) was nearly 10 times greater than in the sublittoral zone (36.1 g C m^{-2}) (Table 9). This difference reflects contrasting physical conditions. The rocky substrate in the littoral zone provided good surface area for macroalgae, to attach and grow, and the algae here were predominantly mature and fertile, contributing to the high biomass (Figure A1-3). In contrast, the sublittoral zone had a sandy bottom, limiting macroalgal attachment. Although algae were visible (Figure A7), it is uncertain whether it was attached or wash-up algae. Reduced light availability, due to suspended sediments in deeper water, may have further limited sublittoral algal growth.

A similar pattern was observed at the exposed site where littoral biomass (118 g C m^{-2}) was 9 times higher than the sublittoral biomass (13.1 g C m^{-2}) (Table 9). However, the sublittoral zone here had a more rocky bottom, compared to the non-exposed site, and clearer water, offering slightly better conditions for algal growth (Figure A7).
These patterns suggest that substrate type and light availability are critical factors influencing biomass across tidal zones. Hard substrates in the littoral zone provide essential attachment surfaces, while sandy or muddy bottoms in the sublittoral zone reduce settlement opportunities.

Despite tidal exposure, the littoral zone maintained high biomass. *Fucus* species, dominant in this zone, accounted for 98% and 99% of total biomass at both sites, but were nearly absent from the sublittoral zones. This distribution is clearly illustrated in Figure 11 and 12, where *Fucus* biomass declines sharply in plot 4 at both sites. Their dominance likely explains much of the biomass difference between the zones. Hansen & Jensen (2018) reported a similar pattern with *Fucus* dominating in the littoral zone and declining sharply in the sublittoral zone.

The dominance of *Fucus* species in intertidal zones highlights their resilience to stressors such as freezing and desiccation. For instance, *F. distichus* can recover quickly from freezing stress, showing a marked decrease in photosynthetic efficiency during freezing but rapid recovery once temperature rise (Hop et al., 2012). These species also tolerate fluctuating salinity and light, which supports their dominance in the intertidal zone and their ability to colonize after disturbance, such as ice scour (Hop et al., 2012; Thyrring et al., 2021).

4.5. Biomass differences in the littoral zones (H5)

Regarding differences in biomass between plots in the littoral zone there was a clear increase from the upper (plot 1) to the lower littoral zone (plot 3) at both sites, consistent with our hypothesis. The difference between plot 1 and plot 3 was significant ($p = 0.05$) at the non-exposed site and almost significant at the exposed site ($p = 0.08$) (Figure 11 and 12, Table 10). Therefore, we reject H5 for the non-exposed site, but not for the exposed site.

The lower biomass observed in the upper littoral zone likely results from prolonged aerial exposure during low tide. These conditions reduce photosynthetic activity and increase the metabolic costs of coping with stressors such as aerial exposure, desiccation, UV radiation and temperature variability

(Bischof et al., 2006; Hanelt et al., 1997). These environmental stressors are most intense near the high tide mark and gradually less towards the lower (Hanelt et al., 1997).

In contrast, macroalgae located in the lower littoral zones benefit from longer immersion periods that buffer against the environmental extremes (Wulff et al., 2009). These conditions support increased photosynthetic performance and reduce physiological stress, explaining the significantly higher biomass values recorded in plot 3.

5. Evaluation of methods

We used a quadrat-based method to estimate macroalgal diversity and biomass across different exposure levels and tidal zones. By combining species diversity and biomass data, it gives a more comprehensive understanding of macroalgal distribution.

Species identification

Species were identified to the lowest possible taxonomic level, but some taxa were grouped due to time constraints. For instance, the "brown filament" was a combination of *P. littoralis, H. ovata* and *E. fasciculatus.* Similarly, *Cladophora* spp. included both *C. rupestris* and other unidentifiable *Cladophora* species. However, all species within these groups were observed and included in the overall species list.

Dense clumps of algae sometimes hindered accurate species identification, also due to time constrains. In such cases, random subsamples were taken, to estimate species composition as comprehensively as possible.

While this limits taxonomic resolution, grouping was applied consistently across samples.

Biomass was calculated by converting wet weight to carbon content using *Fucus* based conversion factors. Since *Fucus* accounted for 98-99% of the total biomass at both sites, applying these factors to all samples was considered appropriate.

5.1. Site and plot selection

The selection of our two sites was based on differences in wave and predicted ice exposure. Both were located within Disko harbour, with practical considerations such as safety and accessibility influencing the selection of sites. The exposed site, while located within the harbour, was more

impacted by wind and potential ice scouring, indicated by the presence of icebergs. While not fully ocean-exposed, this site represented a contrast in exposure compared to the non-exposed site, which was sheltered in an inlet.

Transect length differed between sites due to varying coastal slopes. The steeper slope at the non-exposed site required a shorter transect compared to the flatter slope at the exposed site allowed for a longer one. While consistent transect length would have been preferable for direct comparison, adjustments were necessary to ensure sampling occurred within the same tidal zones across both sites. Additionally, challenges were met when sampling in the sublittoral zone (plot 4). In some cases, it was difficult to determine whether collected algae were attached to the substrate or were dislodged. Observational notes were taken to help interpret these uncertainties in the biomass data.

6. Summary of findings and concluding remarks

The main findings of the study can be summarized as follows: (1) overall macroalgal diversity was relatively similar between the non-exposed and exposed sites, and we did not reject the null hypothesis (H1). (2) Across tidal zones, higher species diversity was observed in the sublittoral zone at the exposed site but not at the non-exposed site, leading to a partial rejection of H2. (3) A clear difference in biomass was found between the two sites with the non-exposed site having a significantly higher macroalgal biomass than the exposed site, rejecting H3. (4) The biomass was consistently higher in the littoral zone than in the sublittoral zone at both sites, rejecting H4. (5) Biomass increased significantly from the upper to the lower littoral zone, rejecting H5 at the non-exposed site and slightly at the exposed site.

The aims of this study were to investigate how wave exposure and drift ice influence macroalgal vegetation at non-exposed and exposed sites in Qeqertarsuaq harbour, West Greenland, during summer (July), and to examine how the macroalgal composition changes across tidal zones at each site. The findings largely support the hypothesis that exposure plays a central role in shaping macroalgal communities, especially biomass distribution. The dominance of perennial *Fucus* species (98% and 99%) across both sites highlights their importance in Arctic tidal zone. However, there were some differences from expectations; species diversity was not higher at the non-exposed site, instead it was slightly higher at the exposed site, possible due to reduced dominance and

increased niche availability under disturbed conditions. Similarly, sublittoral diversity was only higher at the exposed site, and biomass did not peak in the sublittoral zone as expected.

These insights contribute to a broader understanding of how tidal ecosystems may respond to physical stressors, and important knowledge in a changing Arctic environment with less ice and more wave exposure to be expected in the future.

7. Acknowledgements

First, a great thanks to our main supervisors Niels Daugbjerg and Per Juel Hansen for giving us the opportunity to do this project.

A special thanks goes to Niels Daugbjerg for his invaluable contributions throughout the project. For his skilled guidance in species identification, his helpfulness during all stages of the work and for always bringing a positive spirit. A huge thanks to Per Juel Hansen for providing us with the necessary equipment and support for this project.

We would also like to thank the crew of the research vessel *Porsild* for their assistance in collecting samples from sublittoral zones at greater depths.

Special thanks to the entire team for bringing in the good spirit to the work. Finally, thanks to the people at Arctic Station for their hospitality and support.

8. References

Ager, T. G., Krause-Jensen, D., Olesen, B., Carlson, D. F., Winding, M. H. S., & Sejr, M. K. (2023). Macroalgal habitats support a sustained flux of floating biomass but limited carbon export beyond a Greenland fjord. *Science of the Total Environment*, *872*. https://doi.org/10.1016/j.scitotenv.2023.162224

Assis, J., Serrão, E. A., Duarte, C. M., Fragkopoulou, E., & Krause-Jensen, D. (2022). Major Expansion of Marine Forests in a Warmer Arctic. *Frontiers in Marine Science*, *9*. https://doi.org/10.3389/fmars.2022.850368

Berge, J., Johnson, G., & Cohen, J. (2020). *POLAR NIGHT Marine Ecology Life and Light in the Dead of Night: Life and Light in the Dead of Night*.

Bischof, K., Gómez, I., Molis, M., Hanelt, D., Karsten, U., Lüder, U., Roleda, M. Y., Zacher, K., & Wiencke, C. (2006). Ultraviolet radiation shapes seaweed communities. *Reviews in Environmental Science and Biotechnology*, *5*(2–3), 141–166. https://doi.org/10.1007/S11157-006-0002-3/METRICS

Blanc, J. F., Rinne, H., & Salovius-Laurén, S. (2023). Relationship between Fucus coverage and algal diversity in the northern Baltic Sea. *Journal of Sea Research*, *191*, 102312. https://doi.org/10.1016/J.SEARES.2022.102312

Connell, J. H. (1978). Diversity in Tropical Rain Forests and Coral Reefs. *Science*, *199*(4335), 1302–1310. https://doi.org/10.1126/SCIENCE.199.4335.1302

DiNenno, N. (2022). On the Edge: The Curious Lives of Intertidal Organisms and How We Monitor Them. *Klamath Kaleidoscope Newsletter*.

Duarte, C. M., Gattuso, J. P., Hancke, K., Gundersen, H., Filbee-Dexter, K., Pedersen, M. F., Middelburg, J. J., Burrows, M. T., Krumhansl, K. A., Wernberg, T., Moore, P., Pessarrodona, A., Ørberg, S. B., Pinto, I. S., Assis, J., Queirós, A. M., Smale, D. A., Bekkby, T., Serrão, E. A., & Krause-Jensen, D. (2022). Global estimates of the extent and production of macroalgal forests. *Global Ecology and Biogeography*, *31*(7), 1422–1439. https://doi.org/10.1111/geb.13515

Garbary, D., Brackenbury, A., Macdonald, A., & Morrison, D. (2006). Structure and development of air bladders in Fucus and Ascophyllum (Fucales, Phaeophyceae). *Phycologia*, *45*.

Hanelt, D., Wiencke, C., & Nultsch, W. (1997). Influence of UV radiation on the photosynthesis of Arctic macroalgae in the field. *Journal of Photochemistry and Photobiology*, *38*(1), 40–47.

Hansen, L. (1998). *The intertidal macrofauna and macroalgae at five Arctic localities (Disko, West Greenland)*.

Hansen, M. J., & Jensen, R. S. (2018). *Being exposed - How ice and waves affect macroalgae in and around Qeqertarsuaq*.

Høgslund, S., Sejr, M. K., Wiktor, J., Blicher, M. E., & Wegeberg, S. (2014). Intertidal community composition along rocky shores in South-west Greenland: a quantitative approach. *Polar Biology*, *37*(11), 1549–1561. https://doi.org/10.1007/S00300-014-1541-7/FIGURES/8

Hop, H., Wiencke, C., Vögele, B., & Kovaltchouk, N. A. (2012). Species composition, zonation, and biomass of marine benthic macroalgae in Kongsfjorden, Svalbard. *Botanica Marina*, *55*(4), 399–414. https://doi.org/10.1515/BOT-2012-0097

Klimadataforsyningen. (2022). *Satellitfoto Grønland*. Https://Dataforsyningen.Dk/Data/4783.

Kreissig, K. J., Hansen, L. T., Jensen, P. E., Wegeberg, S., Geertz, O. H., & Sloth, J. J. (2021). Characterisation and chemometric evaluation of 17 elements in ten seaweed species from Greenland. *PLoS ONE*, *16*(2 February). https://doi.org/10.1371/journal.pone.0243672

Lebrun, A., Comeau, S., Gazeau, F., & Gattuso, J.-P. (2022). Impact of climate change on Arctic macroalgal communities. *Global and Planetary Change*, *219*.

Luetzenburg, G., Townsend, D., Svennevig, K., Bendixen, M., Bjørk, A. A., Eidam, E. F., & Kroon, A. (2023). Sedimentary Coastal Cliff Erosion in Greenland. *Journal of Geophysical Research: Earth Surface*, *128*(4). https://doi.org/10.1029/2022JF007026

Oksanen, J., Simpson, G., Blanchet, F., Kindt, R., Legendre, P., Minchin, P., O'Hara, R., Solymos, P., Stevens, M., Szoecs, E., Wagner, H., Barbour, M., Bedward, M., Bolker, B., Borcard, D., Borman, T., Carvalho, G., Chirico, M., De Caceres, M., … Weedon, J. (2025). *vegan: Community Ecology Package. R package version 2.8-0,*.

Ørberg, S. B., Duarte, C. M., Geraldi, N. R., Sejr, M. K., Wegeberg, S., Hansen, J. L. S., & Krause-Jensen, D. (2023). Prevalent fingerprint of marine macroalgae in arctic surface sediments. *Science of the Total Environment*, *898*. https://doi.org/10.1016/j.scitotenv.2023.165507

Pedersen, P. M. (2022). *Marine Algae of Greenland* (L. Bruun, Ed.).

Sejr, M. K., Mouritsen, K. N., Krause-Jensen, D., Olesen, B., Blicher, M. E., & Thyrring, J. (2021). Small Scale Factors Modify Impacts of Temperature, Ice Scour and Waves and Drive Rocky Intertidal Community Structure in a Greenland Fjord. *Frontiers in Marine Science*, *7*, 607135. https://doi.org/10.3389/FMARS.2020.607135/BIBTEX

Thyrring, J., Wegeberg, S., Blicher, M. E., Krause-Jensen, D., H&oslashgslund, S., Olesen, B., Wiktor, J., Mouritsen, K. N., Peck, L. S., & Sejr, M. K. (2021). Latitudinal patterns in intertidal ecosystem structure in West Greenland suggest resilience to climate change. *BioRxiv*, 2021.01.05.419028. https://doi.org/10.1101/2021.01.05.419028

Wickham, S. B., Darimont, C. T., Reynolds, J. D., & Starzomski, B. M. (2019). Species-specific wet-dry mass calibrations for dominant Northeastern Pacific Ocean macroalgae and seagrass. *Aquatic Botany*, *152*, 27–31. https://doi.org/10.1016/j.aquabot.2018.09.006

Wiktor, J. M., Tatarek, A., Kruss, A., Singh, R. K., Wiktor, J. M., & Søreide, J. E. (2022). Comparison of macroalgae meadows in warm Atlantic versus cold Arctic regimes in the high-Arctic Svalbard. *Frontiers in Marine Science*, *9*. https://doi.org/10.3389/fmars.2022.1021675

Wulff, A., Iken, K., Quartino, M. L., Al-Handal, A., Wiencke, C., & Clayton, M. N. (2009). Biodiversity, biogeography and zonation of marine benthic micro- and macroalgae in the Arctic and Antarctic. In *Botanica Marina* (Vol. 52, Issue 6, pp. 491–507). https://doi.org/10.1515/BOT.2009.072

Appendices

Appendix 1: Non-exposed site, transect 1 plot 1-3

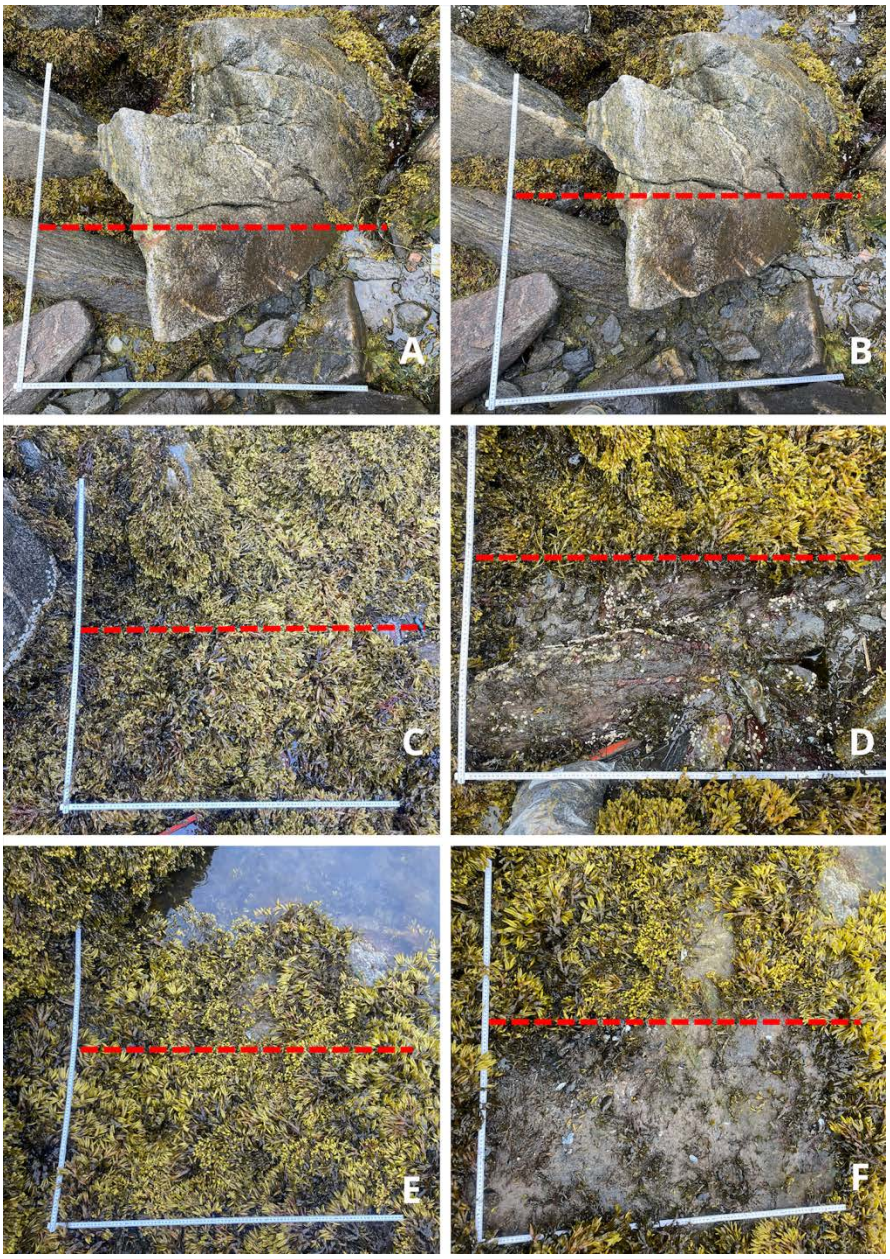

Fig. A1. Non-exposed site for transect 1, plot 1-3, shown before sampling (A, C, D) and after sampling (B, D, F). The top row shows plot 1, the middle row shows plot 2, and the bottom row shows plot 3. Red stripes indicate the area where sampling was conducted in each plot.

Appendix 2: Non-exposed site, transect 2 plots 1-3

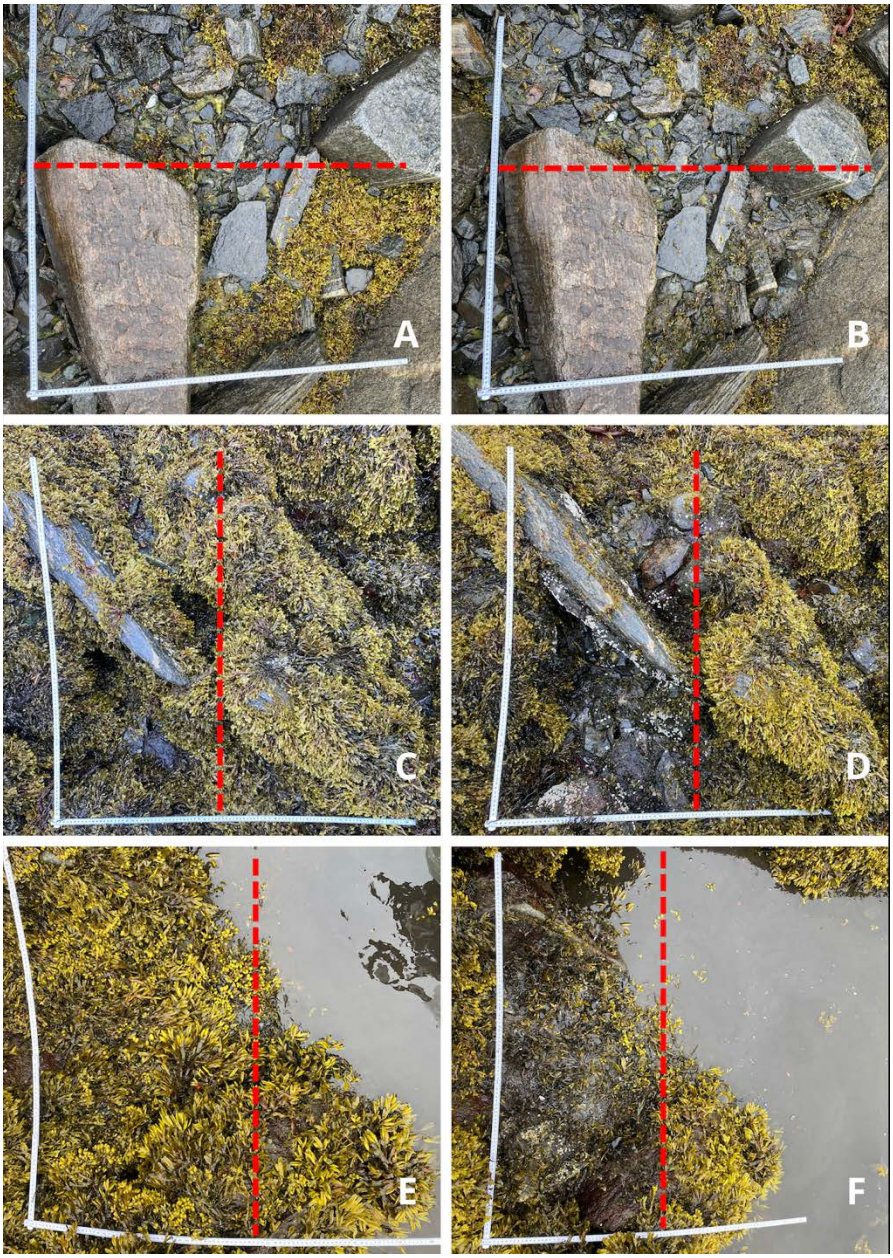

Figure A2. *Non-exposed site for transect 2, plot 1-3, shown before sampling (A, C, D) and after sampling (B, D, F). The top row shows plot 1, the middle row shows plot 2, and the bottom row shows plot 3. Red stripes indicate the area where sampling was conducted in each plot.*

Appendix 3: Non-exposed site, transect 3 plots 1-3

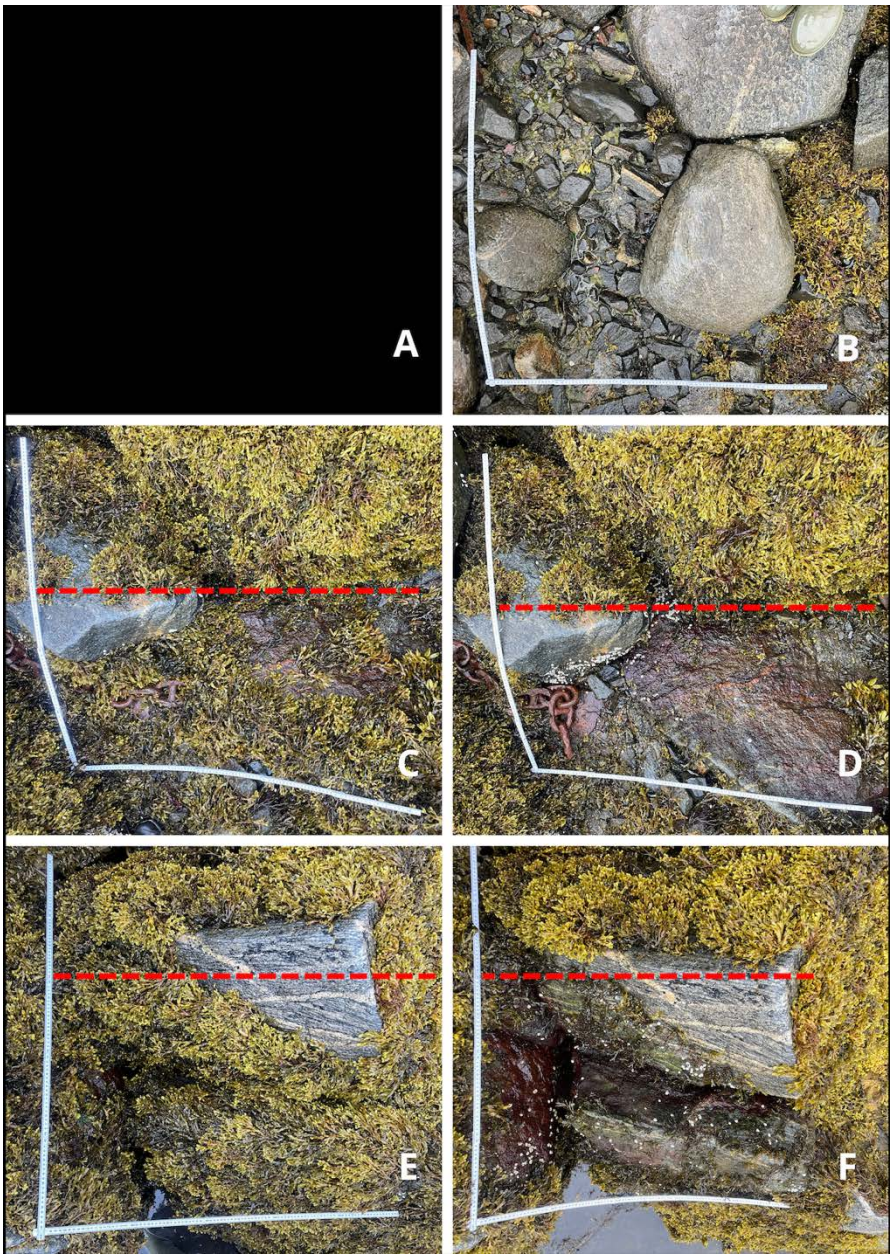

Figure A3. *Non-exposed site for transect 3, plot 1-3, shown before sampling (A, C, D) and after sampling (B, D, F). The top row shows plot 1, the middle row shows plot 2, and the bottom row shows plot 3. Plot 1 is missing the before sampling image, so only the after picture is shown. Red stripes indicate the area where sampling was conducted in each plot.*

Appendix 4: Exposed site, transect 4 plots 1-3

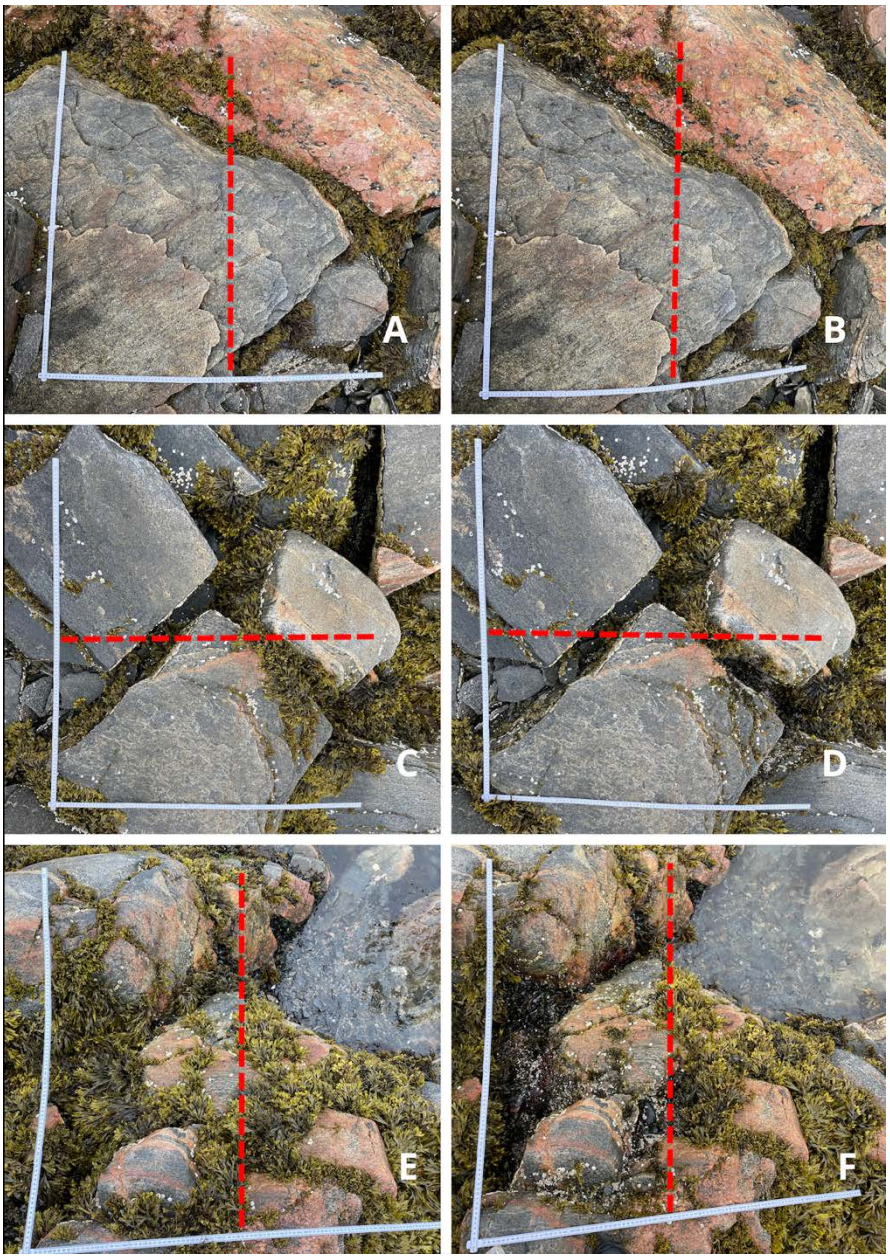

Fig. A4. Exposed site for transect 4, plot 1-3, shown before sampling (A, C, D) and after sampling (B, D, F). The top row shows plot 1, the middle row shows plot 2, and the bottom row shows plot 3. Red stripes indicate the area where sampling was conducted in each plot.

Appendix 5: Exposed site, transect 5 plots 1-3

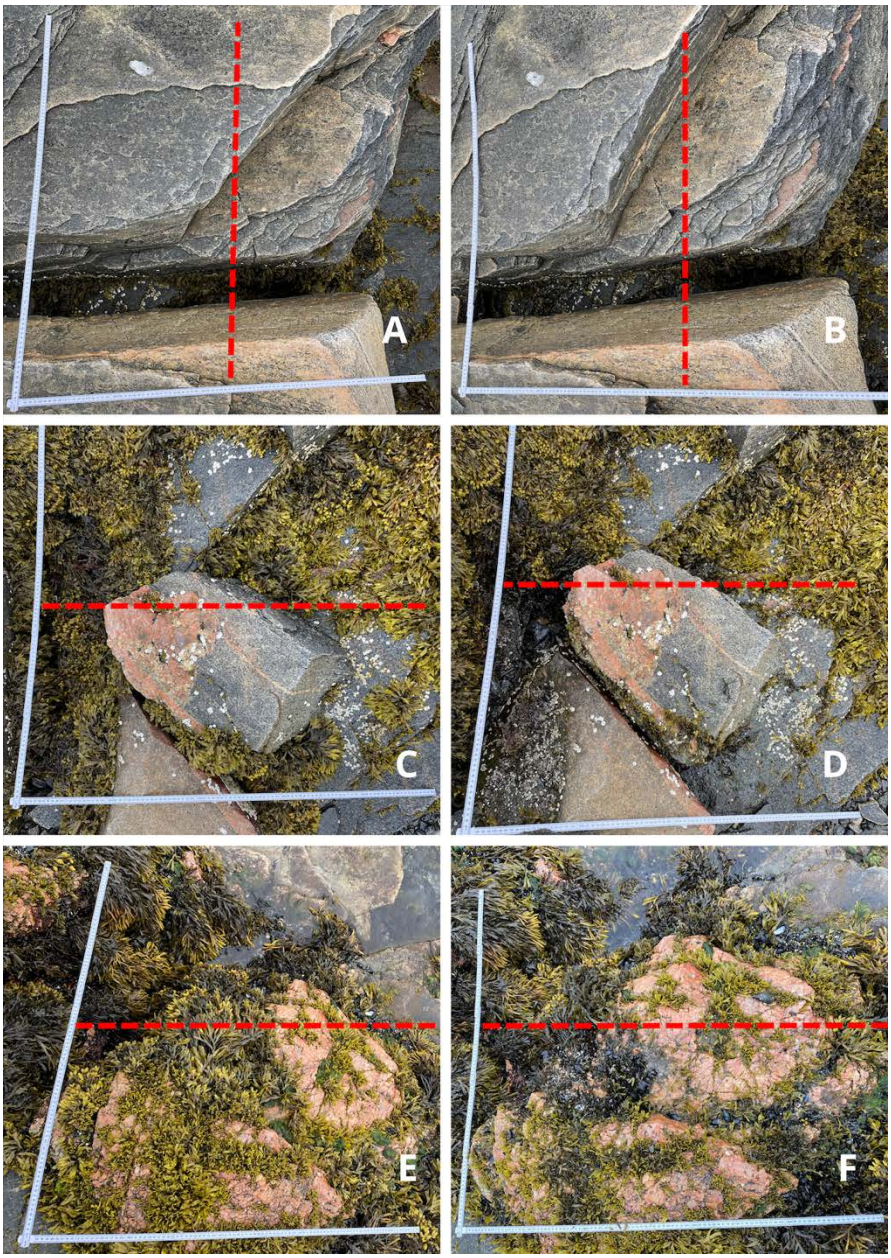

***Fig. A5**. Exposed site for transect 5, plot 1-3, shown before sampling (A, C, D) and after sampling (B, D, F). The top row shows plot 1, the middle row shows plot 2, and the bottom row shows plot 3. Red stripes indicate the area where sampling was conducted in each plot.*

Appendix 6: Exposed site, transect 6 plots 1-3

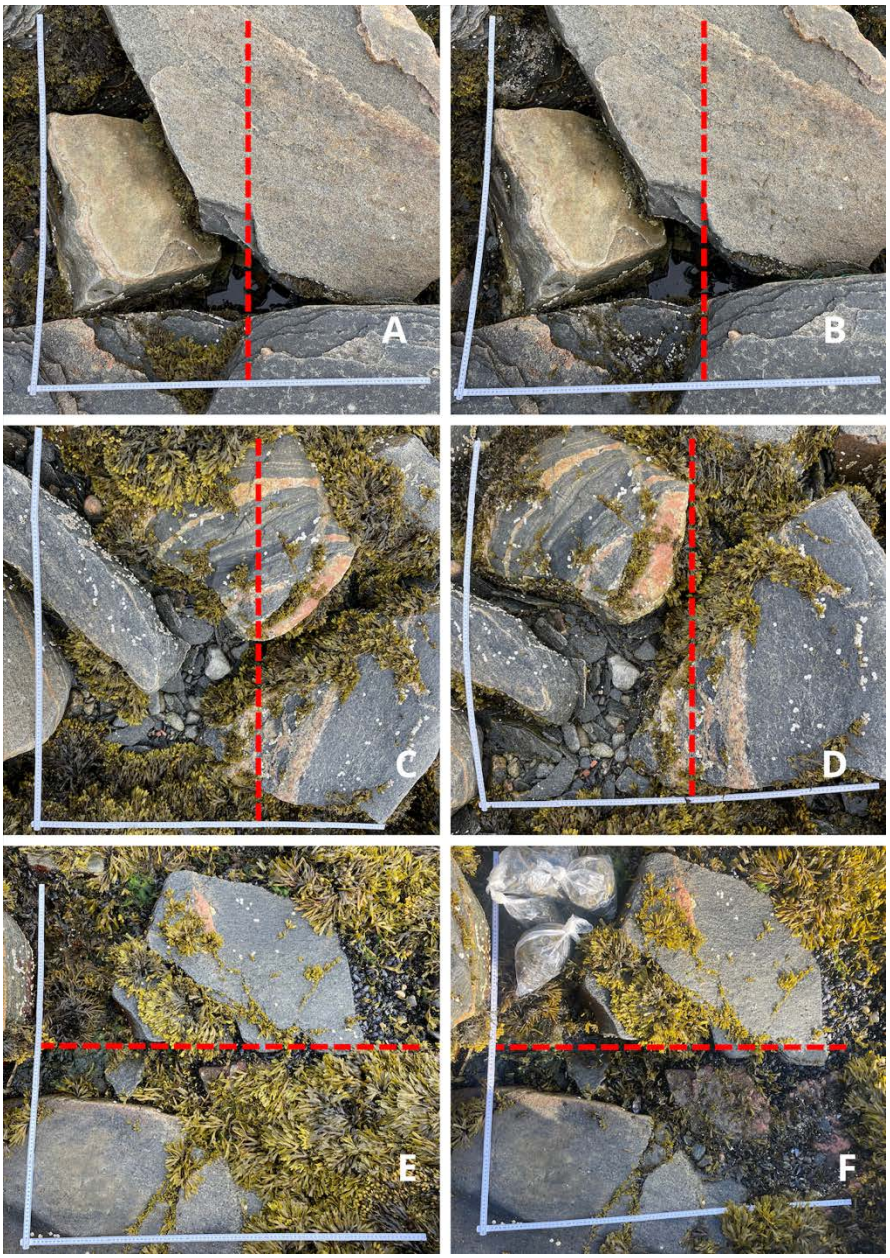

Fig. A6. Exposed site for transect 6, plot 1-3, shown before sampling (A, C, D) and after sampling (B, D, F). The top row shows plot 1, the middle row shows plot 2, and the bottom row shows plot 3. Red stripes indicate the area where sampling was conducted in each plot.

Appendix 7: Plot 4 for non-exposed and exposed site

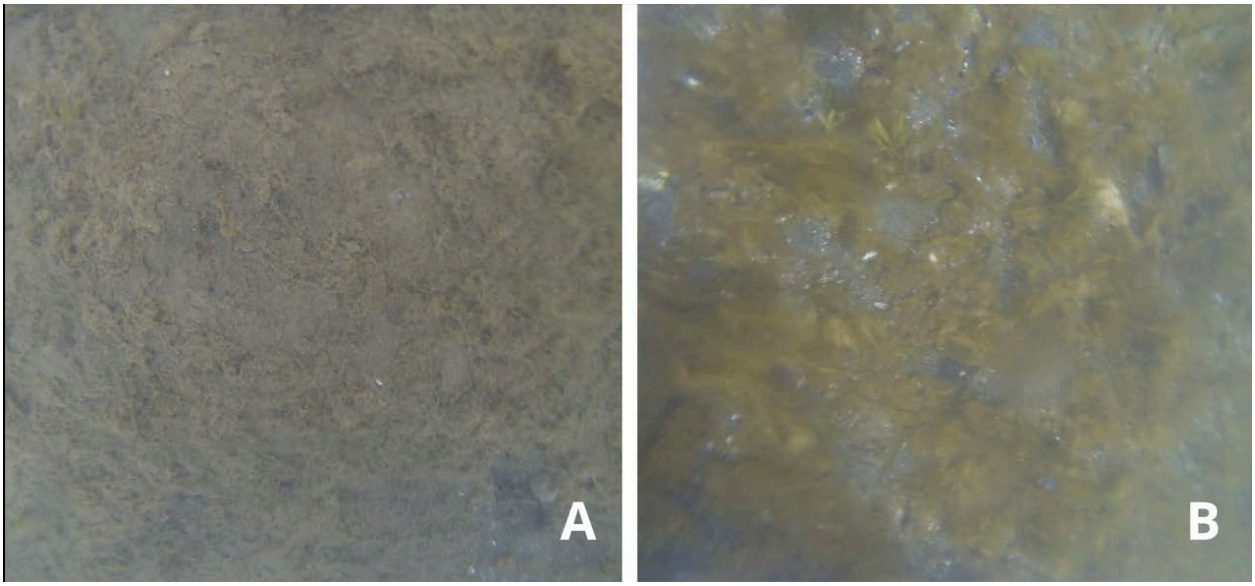

Fig. A7. Bottom of the sublittoral zone in plot 4 for non-exposed site (A) and exposed site (B). The non-exposed site (A) has a muddy and sandy bottom, while the exposed site (B) is rockier, providing better attachment opportunities for algae.

Appendix 8. Subset of calculated biomass for species

The table below shows a subset of the calculated biomass for all species, organized by site (non-exposed and exposed), transect, zone and plot.

Table 1. Subset of calculated biomass for all species across sites, transects, zones and plots.

site	transect	zone	plot	species	biomass
non-exposed	1	littoral	1	f_vesiculosus	4.2223896
non-exposed	1	littoral	2	f_vesiculosus	183.97384
non-exposed	1	littoral	3	f_vesiculosus	160.16706
non-exposed	1	sublittoral	4	f_vesiculosus	0.5385744
non-exposed	2	littoral	1	f_vesiculosus	24.649747
non-exposed	2	littoral	2	f_vesiculosus	248.79919
non-exposed	2	littoral	3	f_vesiculosus	151.3088
non-exposed	2	sublittoral	4	f_vesiculosus	0
non-exposed	3	littoral	1	f_vesiculosus	2.2852908
non-exposed	3	littoral	2	f_vesiculosus	171.59225
non-exposed	3	littoral	3	f_vesiculosus	431.65138
non-exposed	3	sublittoral	4	f_vesiculosus	27.985651
exposed	4	littoral	1	f_vesiculosus	4.9410972
exposed	4	littoral	2	f_vesiculosus	60.257012
exposed	4	littoral	3	f_vesiculosus	148.73428
exposed	4	sublittoral	4	f_vesiculosus	0
exposed	5	littoral	1	f_vesiculosus	2.168478
exposed	5	littoral	2	f_vesiculosus	119.39686
exposed	5	littoral	3	f_vesiculosus	45.395813
exposed	5	sublittoral	4	f_vesiculosus	1.4256216
exposed	6	littoral	1	f_vesiculosus	31.353988
exposed	6	littoral	2	f_vesiculosus	81.342706
exposed	6	littoral	3	f_vesiculosus	0
exposed	6	sublittoral	4	f_vesiculosus	0
non-exposed	1	littoral	1	f_evanescens	0
non-exposed	1	littoral	2	f_evanescens	127.85484
non-exposed	1	littoral	3	f_evanescens	440.92002
non-exposed	1	sublittoral	4	f_evanescens	5.3413776
non-exposed	2	littoral	1	f_evanescens	0
non-exposed	2	littoral	2	f_evanescens	25.739111
non-exposed	2	littoral	3	f_evanescens	75.035657
non-exposed	2	sublittoral	4	f_evanescens	14.694826
non-exposed	3	littoral	1	f_evanescens	0
non-exposed	3	littoral	2	f_evanescens	28.415135
non-exposed	3	littoral	3	f_evanescens	12.906972
non-exposed	3	sublittoral	4	f_evanescens	1.3371696
exposed	4	littoral	1	f_evanescens	0
exposed	4	littoral	2	f_evanescens	0
exposed	4	littoral	3	f_evanescens	13.730839
exposed	4	sublittoral	4	f_evanescens	0
exposed	5	littoral	1	f_evanescens	0
exposed	5	littoral	2	f_evanescens	16.365024

Appendix 9. Mean biomass of Fucus species

Mean biomass (g C m^{-2}) and standard deviation (SD) per plot for *F. vesiculosus, F. evanescens* and non-fertile *Fucus* at the non-exposed site (Table 1) and exposed site (Table 2).

Table 1. Mean biomass (g C m^{-2}) and standard deviation (SD) per plot for F. vesiculosus, F. evanescens and non-fertile Fucus at the non-exposed site.

	Plot 1	Plot 2	Plot 3	Plot 4
	Mean biomass (g C m^{-2}) ± SD			
F. *vesiculosus*	10.4 ± 7.15	201 ± 23.9	248 ± 92.0	9.51 ± 9.24
F. *evanescens*	0 ± 0	60.7 ± 33.6	176 ± 134	7.12 ± 3.96
Non-fertile *Fucus*	13.3 ±7.52	70.1 ± 20.5	28.6 ± 7.41	2.21 ± 1.25

Table 2. Mean biomass (g C m^{-2}) and standard deviation (SD) per plot for F. vesiculosus, F. evanescens and non-fertile Fucus at the exposed site.

	Plot 1	Plot 2	Plot 3	Plot 4
	Mean biomass (g C m^{-2}) ± SD			
F. *vesiculosus*	12.8 ± 9.30	87.0 ± 17.3	64.7 ± 44.0	0.48 ± 0.48
F. *evanescens*	0 ± 0	5.46 ± 5.46	24.9 ± 10.7	0.58 ± 0.58
Non-fertile *Fucus*	21.9 ± 5.61	46.8 ± 10.2	83.3 ± 17.8	2.31 ± 1.18

Report 4

Emma Østergaard Buch, Marie Neel Jørgensen & Nanna Meilholm Christiansen (2025). How low can you go: examining the effect of ocean acidification on Arctic macroalgae.

How Low Can You Go: Examining the Effect of Ocean Acidification on Arctic Macroalgae

By: Emma Østergaard Buch (crm133), Marie Neel Jørgensen (xtn326), and Nanna Meilholm Christiansen (xtq215)

Supervisors: Per Juel Hansen and Niels Daugbjerg
Submitted on: 15/08-2025

Abstract

Arctic coastal ecosystems are facing rapid environmental changes with ocean acidification, increasing temperatures and reducing sea ice cover, posing significant challenges to the organisms and habitats they support. Within these ecosystems, macroalgal communities potentially play a key role as local pH modulators, therefore providing a refuge for sensitive calcifying organisms against the impacts of ocean acidification. The aim of this study was to investigate how controlled pH levels (simulating present-day, projected scenario as well as extreme conditions) may affect the Maximum Quantum Yield (Fv/Fm) for two chosen genera, *Fucus* and *Saccharina*, sampled at two sites (one sheltered and one exposed) in Disko Bay, Western Greenland. Furthermore, we wanted to investigate the natural pH variability *in situ* to understand the capability of macroalgae to modulate their environment in respect to pH. An experiment was set up to measure Fv/Fm of macroalgae exposed to the three chosen pH levels over a duration of three days. We report on no clear significant trends on the effects of pH levels, genera, or site on Fv/Fm. Temporal trends within each pH level all showed increasing Fv/Fm-values ranging from 0.00574-0.0108 day^{-1} across both genera, suggesting that the experimental period had instead effectively served as an acclimatization period. *In situ* measurements over two days revealed a diel pattern of pH, following the light conditions. This was most prominent in the exposed site, contrary to initial assumptions. Altogether, these findings indicate that the genera included in the present study had some short-term resilience towards lowered pH levels and thus potentially resilient in the face of lowered pH due to ocean acidification. Caution must however be applied when extrapolating these results to broader ecosystem responses, as these results are based on limited data, thus highlighting the need for further research on this topic.

1.0. Introduction

1.1. Atmospheric CO_2 and ocean acidification

The ocean plays a crucial role in acting as a buffer against increasing atmospheric CO_2 levels, as approximately 30% of anthropogenically produced CO_2 has currently been taken up by the ocean (IPCC, 2018). Anthropogenic emissions of CO_2 have caused an increase in atmospheric CO_2 particularly since the 1950s (Friedlingstein *et al*., 2025), with atmospheric concentrations going from pre-industrial levels around 278 parts per million (ppm) in 1780 (Gulev *et al*., 2021) to 423 ppm in 2025 (Lan *et al*., 2025). As a result, increasing atmospheric CO_2 concentrations will result in higher levels of CO_2 absorbed in the ocean, thus lowering pH levels and ultimately leading to ocean acidification (Haugan and Drange, 1996; Hernández *et al*. 2018). Since pre-industrial times, the mean ocean surface pH level has decreased by approximately 0.1 and has been projected to decrease by another 0.3-0.5 by the end of this century (IPCC, 2007; Hernández *et al*. 2018).

1.2. Arctic-specific vulnerabilities and ecological importance

The Arctic Ocean is considered one of the most vulnerable regions to ocean acidification, largely due to its unique physical and chemical characteristics, especially as colder temperatures increase the solubility of CO_2 in the water, enhancing the oceanic uptake of atmospheric CO_2. In the future, a reduction of sea ice cover will likely enhance the absorption of atmospheric CO_2 in the Arctic Ocean, as less sea ice cover will enhance the air to sea fluxes (Bates *et al.*, 2006). These processes, combined with changes in stratification and freshwater input from melting sea ice, results in acidification in the Arctic progressing more rapidly than in many other regions. The pH in the Arctic Ocean is simulated to decrease by 0.45 over the 21st century (Steinacher et al., 2009), having potential consequences for both pelagic and benthic marine ecosystems (Qi *et al.*, 2017; Feely *et al.*, 2009).

1.3. Macroalgal ecosystems in the Arctic

Marine macroalgal communities dominate rocky shore habitats and are globally widespread, covering an area of seven million km^2. They are therefore comparable both in area and net primary production to the Amazon forest (Duarte *et al.* 2022). Given that approximately 35% of the world's coastlines are found in the Arctic, macroalgal communities represent ecologically significant ecosystems in the Arctic. Moreover, Greenland's coastline is characterized by rocky reefs that support rich and diverse communities of marine life

(Krause-Jensen and Duarte, 2014). These reefs are densely colonized by fucoids, various filamentous algae (e.g. *Cladophora* sp.), and calcifying organisms such as *Mytilus edulis*, *Balanus* sp., gastropods and encrusting coralline algae, which contribute to the structural complexity and ecological productivity of these coastal habitats (Duarte and Krause-Jensen, 2018). Additionally, these ecosystems host a variety of macroalgal species, among which are *Fucus distichus, Saccharina latissima and Saccharina longicruris* (Pedersen, 2022*).* Macroalgae not only stabilize the reef structure but also enhance local biodiversity by providing shelter and food for invertebrates, including calcifying organisms (Duarte and Krause-Jensen, 2018).

1.4. Local pH modulation and biological sensitivity

Macroalgal communities serve as biological habitats and occupy large stretches of the Arctic coastline where they play a critical role in modifying local water chemistry. Macroalgae influence seawater pH through their photosynthesis, during which CO_2 is consumed, and oxygen is released. Decreasing levels of CO_2 leads to an increase in local pH levels, especially in dense or sheltered communities (Middelboe and Hansen, 2007; Krause-Jensen *et al*., 2015). These effects can vary seasonally and diurnally with the highest pH values typically observed during periods of intense light and limited water exchange (Middelboe and Hansen, 2007; Krause-Jensen *et al*., 2015; Duarte *et al*., 2018). In sheltered tidal pools and areas with high macroalgal coverage, pH levels can rise well above surrounding values (Middelboe and Hansen, 2007). This pH modulating effect is less prominent in wave-exposed areas, where the increased water exchange reduces the potential for sustained photosynthetic upregulation of pH (Krause-Jensen *et al.*, 2016). Thus, the distinction between sheltered and exposed habitats becomes essential for understanding the spatial heterogeneity of ocean acidification resilience.

The local pH modulation makes macroalgal beds crucial refugia for calcifying organisms that are otherwise particularly vulnerable to the impacts of ocean acidification (Orr *et al.*, 2005; Fabry *et al*., 2009; Krause-Jensen *et al*., 2016). Lower pH reduces the concentration of CO_3^{2-} and thus reduces the calcium carbonate saturation state, hindering the formation of biogenic $CaCO_3$ in marine calcifying organisms (Orr *et al.,* 2005). Intense macroalgal photosynthetic activity - especially during the long daylight periods of Arctic summers - can help counteract the negative impacts of ocean acidification. During these periods, macroalgae can significantly raise the pH of the surrounding waters. This creates microhabitats with reduced

CO_2 concentrations and an elevated saturation state for carbonate minerals (Duarte and Krause-Jensen, 2018). Natural pH fluctuations in macroalgal habitats have been observed to exceed one full pH unit, especially in shallow, low-flow environments such as tidal pools and sheltered reefs (Middelboe and Hansen, 2007; Duarte and Krause-Jensen, 2018). The ecological importance of local pH modulation is especially crucial for calcifying organisms during their early developmental stages. Many species, such as mussels and barnacles, are highly vulnerable to elevated CO_2 levels, as larvae and juveniles show reduced survival, developmental abnormalities, and impaired calcification under acidified conditions (Kurihara, 2008). As many of these organisms spread via their juvenile stage, they may be constrained in their ability to disperse in a more acidified ocean (Bashevkin *et al.,* 2020). This impacts not only the benthic biodiversity but also ecosystem functioning by impacting food webs, nutrient cycling and habitat formation. For instance, mussel beds stabilize sediments, support rich epifaunal communities, and serve as prey for higher trophic levels, including fish, sea birds, and marine mammals (Thoisen *et al.*, 2015; Duarte and Krause-Jensen, 2018).

1.5. Macroalgal communities in the Arctic in the face of climate change

In the future Arctic Ocean with lower baseline pH, reduced salinity, and increased temperature, the macroalgae themselves may be affected, which may change the ability of macroalgal communities to sustain elevated local pH (Middelboe and Hansen, 2007), in turn affecting the organisms that rely on these habitats, including vulnerable calcifiers (Fabry *et al*., 2009). Understanding the natural range of pH in which Arctic macroalgae communities can thrive is therefore crucial, particularly in the context of ongoing climate change. We hypothesize that natural pH fluctuations will be significantly amplified through the water column towards macroalgal beds with high coverage due to ongoing photosynthetic activity. Additionally, we hypothesize that this modulating effect may differ between exposed and sheltered locations.

Given the projected environmental changes, it is important to characterize the pH regimes in Arctic macroalgal communities to assess their potential role in modulating ocean acidification impacts. Our aim was to 1) investigate the capacity of macroalgae to influence their surrounding chemical environment focusing on pH, and 2) evaluate how exposure to *in situ* pH values as well as decreased pH values may affect the growth and photosynthetic efficiency of macroalgal species from two different sites - one being sheltered and the other exposed.

Specifically, the objectives of this study were to:

1) Quantify natural pH variability *in situ* at Arctic coastal sites by comparing sheltered and wave-exposed areas in Disko Bay during the period of continuous daylight in July 2025.
2) Assess the physiological response of two dominant macroalgal genera in Disko Bay - *Fucus* and *Saccharina* - to experimental incubations under controlled pH conditions (7.0, 7.5, and 8.2), simulating both present-day, projected scenario as well as extreme conditions (IPCC, 2007; Hernández *et al*. 2018).

2.0. Materials and methods

2.1. Experimental design

We tested our hypotheses by the examination of *in situ* pH fluctuations at two sites in the harbour of Qeqertarsuaq located in the western part of Greenland (Fig. 1) during a 24-hour period of daylight in mid-July 2025. Furthermore, two genera of macroalgae, *Fucus* and *Saccharina*, were collected at the two chosen sites to investigate the impact of varying pH levels (pH of 8.2, 7.5 and 7.0) on the photosynthetic efficiency of the macroalgae expressed as Fv/Fm. A preliminary experiment was set up to determine the final biomass of each genus of macroalgae, followed by an experiment on macroalgae response to varying pH levels over the course of three days.

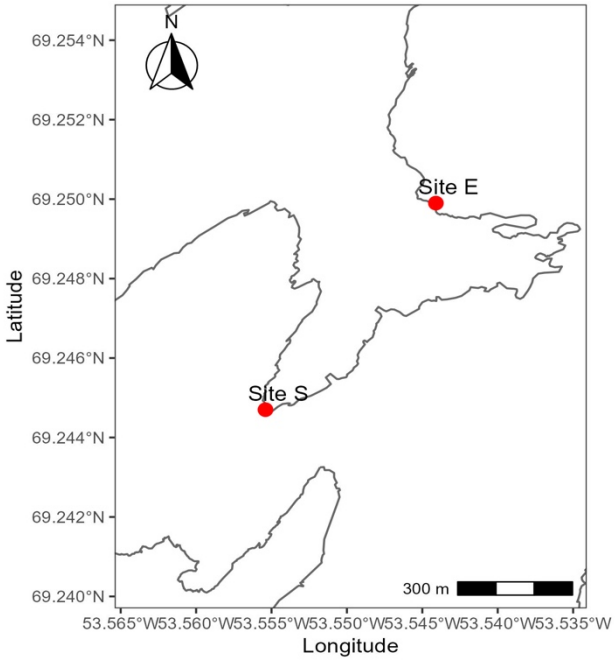

Fig. 1. *Location of sampling sites in the harbour of Qeqertarsuaq, Disko Bay, Western Greenland. The two chosen sites are marked according to their characteristics, as Site S marks the sheltered site, while Site E marks the exposed site.* In situ *measurements were conducted at the same locations.*

2.2. Study area

The two study sites chosen for this study are located along the southern coast of Disko Island, Western Greenland (Fig. 1). The two sites were chosen as one was sheltered (hereafter Site S, 69.2447° N, 53.5554° W), and the other one was exposed (hereafter Site E, 69.2499° N, 53.5441° W). Tidal variability was large for the two chosen sites, ranging from 0.52 - 2.55 m at the sites during the study period. The water temperature ranged from 4.3-8.7°C for Site S and 4.5-6.0°C for Site E during the 13th and 14th July 2025.

The two genera of macroalgae, *Fucus* and *Saccharina*, were collected at the coastal sites by freediving. Individuals of *Fucus distichus* were collected from both sites, while *Saccharina longicruris* was collected only from Site S and *Saccharina latissima* was collected only from Site E. Following collection of the macroalgae, they were transported to the laboratory, located approximately 2 km from the sites, and kept outside in plastic bags with a small amount of water to avoid desiccation. Both sites were characterized by macroalgal communities clearly dominated by *Fucus* species, particularly *Fucus distichus*. Site S had a slightly higher presence of *Fucus vesiculosus* compared to Site E, and fine filamentous algae were additionally more abundant here. In contrast, Site E featured a more continuous algal cover, while Site S exhibited barer substrate between patches. Individuals of *Saccharina longicruris* and *Saccharina latissima* appeared in small, clustered groups at both sites, with few individuals growing close together.

2.3 Laboratory setup

2.3.1 Preliminary pH drift experiment

A preliminary experiment was conducted to determine the appropriate wet weight (WW) biomass of each macroalgal genus that would restrict pH fluctuations within +0.2 units between measurements. This step was necessary to minimize the influence of the macroalgae's photosynthetic activity on the surrounding water during incubations. Establishing the appropriate WW for each genera ensured that observed changes could be attributed to the experimental pH conditions and that these remained relatively stable. This preliminary experiment was conducted over 12 h, corresponding to half the duration between daily seawater changes in the main experiment.

2.3.2 Experimental setup

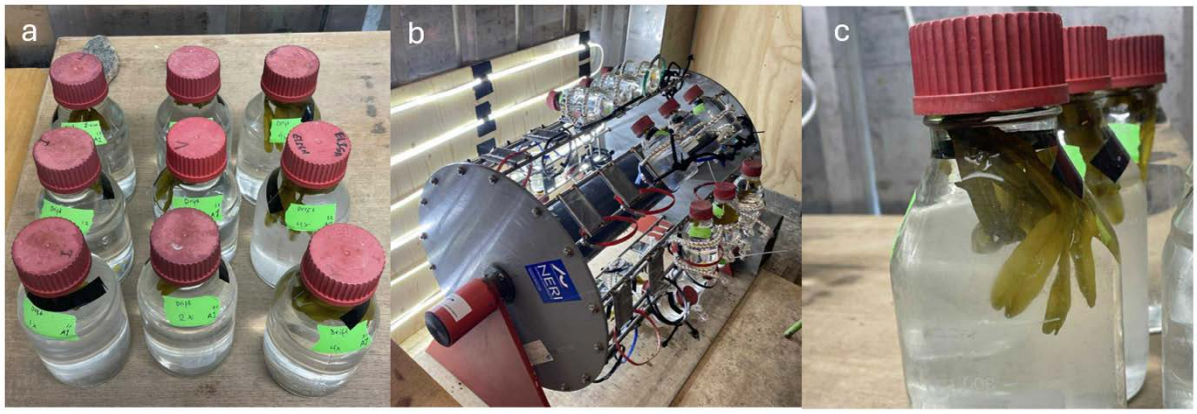

Fig. 2. *Representation of the experimental setup. a) Nine 500 mL bottles for one genera (*Fucus/Saccharina*), one site (Site S/Site E) and three pH levels (7.0, 7.5, and 8.2) with triplicates, resulting in 9 x 4 bottles for the entire experiment. b) Motorized plankton wheel turning at the speed of 1 revolution per minute. The light source was on the posterior part of the plankton wheel, providing the samples with sufficient light during incubation. c) A macroalgal sample fastened by a small piece of fishing line to the lid of the bottle, ensuring equal exposure to the seawater in the bottle and avoiding a thick boundary layer forming during incubation.*

The laboratory setup consisted of 36 bottles of 500 mL placed in a motorized plankton wheel revolving at 1 revolution per minute (Fig. 2a-b). The experiment was conducted in a temperature-controlled climate room with a temperature of approximately 6°C over the course of three days. The bottles were exposed to a light intensity ranging between 10 and 91 µmol photons m^{-2} s^{-1} depending on the bottle's position on the wheel, resulting in a mean light intensity of 41 µmol photons m^{-2} s^{-1}.

The seawater used in the experiment had been heated to 60°C for 2 minutes the day prior to the experiment. This was to ensure the elimination of any microalgae present in the incubation water, as the photosynthetic activity of these could potentially affect the pH levels in the bottles, therefore potentially skewing the observed results. The seawater was kept in three separate bottles and was adjusted to three different pH levels (7.0, 7.5 and *in situ*, measured as 8.2) using small amounts of NaOH and HCL (Axelsson *et al*., 2000; Cornwall *et al.*, 2012; Yu *et al.*, 2022). The seawater with adjusted pH was then added to the experimental bottles together with the samples of macroalgae. The seawater in the experimental bottles was changed daily to maintain stable pH levels. Each replicate of *Fucus distichus* and *Saccharina* spp. weighed in the range of 0.22-0.27 and 0.46-0.56 grams of wet weight (WW),

respectively, at the onset of the experiment. Furthermore, to ensure equal exposure to seawater as well as minimize the formation of a thick boundary layer around the algae during incubations, the samples were suspended in the center of the bottles by attaching it to a small piece of fishing line fixed to the lid (Fig. 2c).

2.4 Measurements

The experiment ran from July 12th to 15th 2025 (hereafter day 0 to 3). Daily measurements of pH were obtained using WTW™ ProfiLine™ pH 3210 Portable pH Meter. The pH-meters were calibrated with a two-point calibration, using buffers of pH 7.0 and 10.0. In addition, biomass (WW in grams), length, width, and Maximum Quantum Yield (Fv/Fm) were determined daily for each sample. Fv/Fm was measured using pulse-amplitude modulated (PAM) chlorophyll fluorescence with the WALZ Diving-PAM II (Heinz Walz GmbH, 2023). The damp and gain settings were set to 3 and 1, respectively, to ensure Ft-values between 300-600, as recommended by the manufacturer. Before each measurement, the samples of macroalgae were dark acclimated for 20 minutes using dark leaf clips, also ensuring a distance between the optical fibre of the device and the sample at approximately 5 mm (Heinz Walz GmbH, 2023). A saturation pulse was then applied to obtain the Fv/Fm measurement.

To give an estimate of *in situ* pH variability, vertical profiles of pH and light intensity, measured in µmol photons m^{-2} s^{-1}, were measured (at the surface, 20 cm and 40 cm below surface) at three intervals daily from July 13th to 14th, 2025 at Site E and S, respectively. Light intensity was furthermore measured in air at each sampling time point using Walz ULM-500 Universal Meter equipped with a 4π light sensor. The measurements in water were positioned above 100% macroalgal cover on the seafloor at both sites.

2.5 Data analysis

The statistical analyses conducted for this study included both one-way and three-way analyses of variance (ANOVA) to assess the effects of pH, genera of macroalgae, sampling site characteristics as well as these factors' interactions on the measured response variable, i.e. the photosynthetic efficiency (Fv/Fm) of the macroalgae. After the ANOVAs, Tukey's Honest Significant Difference (HSD) post-hoc tests were employed to identify any significant pairwise differences. Additionally, linear models were fitted to the data to explore potential temporal trends for Fv/Fm within genus and pH. All data was tested for normality prior to the statistical analyses to ensure no violations of statistical assumptions. Significant differences

were indicated by p-values < 0.05. The statistical analyses were conducted in R (ver. 4.2.2) using RStudio (ver. 2024.09.1 Build 394).

3.0. Results

3.1. Experiment on macroalgae response to pH

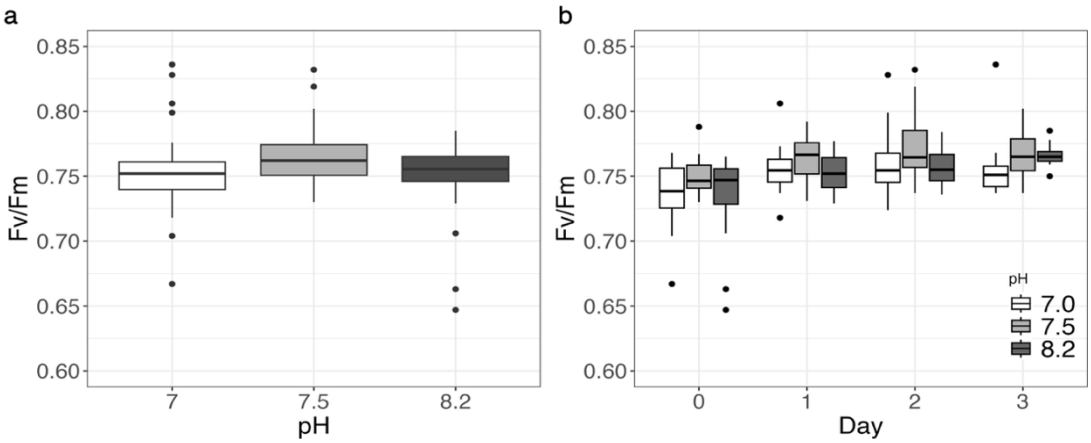

Fig. 3. a) The photosynthetic efficiency (Fv/Fm) represented by boxplots for the three chosen pH levels: 7.0, 7.5, and 8.2, across all included genera of macroalgae, sites and dates of the experiment. b) Fv/Fm values represented by boxplots for each date and pH level. Outliers are marked as black dots, and the boxes represent the interquartile range, depicting the spread of the middle 50% of the data. The experiment began on day 0 (12th July 2025) and concluded on day 3 (15th July 2025).

Fv/Fm was recorded daily over the duration of the experiment (Fig. 3a) and ranged from 0.647 observed at pH 8.2 to 0.836 observed at pH 7, both observations of Fv/Fm recorded for *Saccharina longicruris.* A one-way ANOVA was employed with pH as a factor and revealed a significant effect on Fv/Fm (p-value = 0.0313) when pooling data from all days. However, Tukey's HSD post-hoc analysis (Table S1) showed no significant pairwise differences among the respective pH levels (Fig. 3a). Trends (p-value < 0.10) of significant differences were observed between pH levels 7.0 and 7.5 as well as 7.5 and 8.2 (Table S1), but not between 7.0 and 8.2. When investigating differences within each day of the experiment, there was no significant difference between Fv/Fm at different pH levels when all levels of genera and site were pooled (Fig 3b, Table S2).

Further investigating the effect of pH between the two genera was determined via a one-way ANOVA with genera as a factor for each of the three pH levels: 7.0, 7.5, and 8.2. No

significant differences between the two genera were found for any of the pH levels (Fig. 4, Table S3) in regard to Fv/Fm.

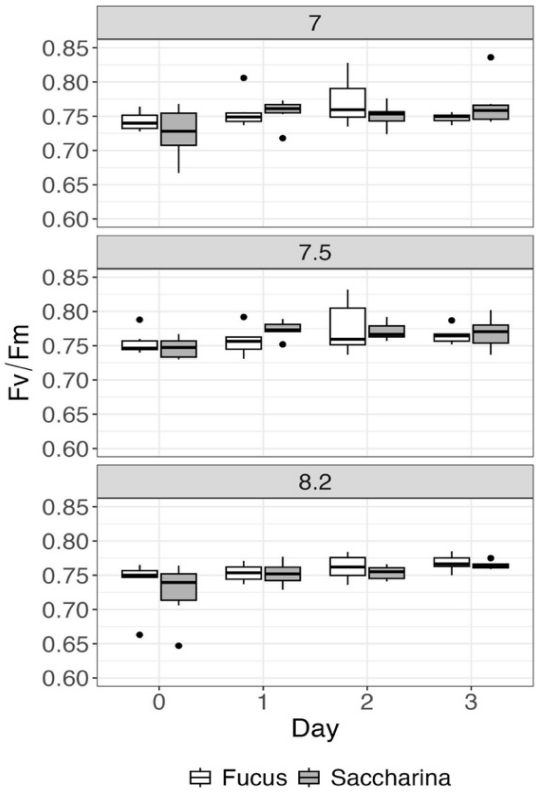

Fig. 4. Fv/Fm values at each pH level: 7.0, 7.5, and 8.2 for Fucus and Saccharina, represented via boxplots. Outliers are marked as black dots, and the boxes represent the interquartile range, depicting the spread of the middle 50% of the data. The experiment began on day 0 (12th July 2025) and concluded on day 3 (15th July 2025).

Table 1. *Results of three-way analysis of variance (ANOVA) on the effect of the factors pH, genera and site on the photosynthetic efficiency (Fv/Fm). The experiment began on day 0 (12th July 2025) and concluded on day 3 (15th July 2025). Significant p-values (p < 0.05) are marked in bold and with a *, while trends (p < 0.10) are marked with '..'.*

Time point	*Factor*	*df*	*F-value*	*p-value*
Day 0	pH	2	1.490	0.2455
	Genera (*Saccharina/Fucus*)	1	1.766	0.1963
	Site (Sheltered/Exposed)	1	1.490	0.2455
	pH x genera	2	0.088	0.9156
	pH x site	2	3.565	**0.0441** *
	Genera x site	1	0.228	0.6370
	pH x genera x site	2	1.015	0.3773
Day 1	pH	2	1.264	0.301
	Genera (*Saccharina/Fucus*)	1	0.565	0.460
	Site (Sheltered/Exposed)	1	0.016	0.900
	pH x genera	2	0.772	0.473
	pH x site	2	0.133	0.876
	Genera x site	1	0.026	0.874
	pH x genera x site	2	1.318	0.286
Day 2	pH	2	1.973	0.1610
	Genera (*Saccharina/Fucus*)	1	2.615	0.1190
	Site (Sheltered/Exposed)	1	7.583	**0.0111** *
	pH x genera	2	0.479	0.6255
	pH x site	1	2.785	0.0817 ..
	Genera x site	1	2.217	0.1495
	pH x genera x site	2	1.837	0.1810
Day 3	pH	2	1.112	0.3452
	Genera (*Saccharina/Fucus*)	1	1.393	0.2495
	Site (Sheltered/Exposed)	1	2.913	0.1008
	pH x genera	2	1.450	0.2543
	pH x site	2	2.155	0.1378
	Genera x site	1	4.562	**0.0431** *
	pH x genera x site	2	0.586	0.5644

Lastly, a three-way ANOVA was performed to test the effect of pH, genera and site on Fv/Fm for each factor separately as well as for potential interactions. Fv/Fm was not significantly influenced by pH or genera, nor interactions between pH and genera as well as between pH, genera, and site for any of the days (Table 1). The interaction between pH and site did have a significant impact on the Fv/Fm ($p = 0.0441$) for day 0. No significant interactions were

found for day 1. A significant effect of sites on Fv/Fm was only detected on day 2 (p = 0.0111), and a trend was observed for the interaction between pH and site (p-value = 0.0817). Finally, the interaction between genera and site on day 3 was significantly impacting the Fv/Fm values observed (p-value = 0.0431, Table 1).

A general linear model (LM) was fitted to the Fv/Fm observations within each of the three pH levels to investigate the temporal trends of the observations (Fig. 5). The slopes of the linear models were positive for all three pH levels when pooling both genera, i.e. increasing Fv/Fm values observed over time (Fig. 5a). The steepest rate of increase of Fv/Fm was observed for the macroalgae incubated at pH 8.2 with an increase of 0.0108 day^{-1}, while the smallest increase was observed at pH 7.5 with an increase of 0.00574 day^{-1}. At pH 7, the rate of increase was 0.00747 day^{-1} (Fig. 5a). When investigating the temporal trends for each genera separately, the steepest increase was observed for *Saccharina* (Fig. 5b) as the rate of increase ranged from 0.00632 - 0.0120 day^{-1}, while *Fucus* (Fig. 5c) had a range of 0.00295 - 0.00957

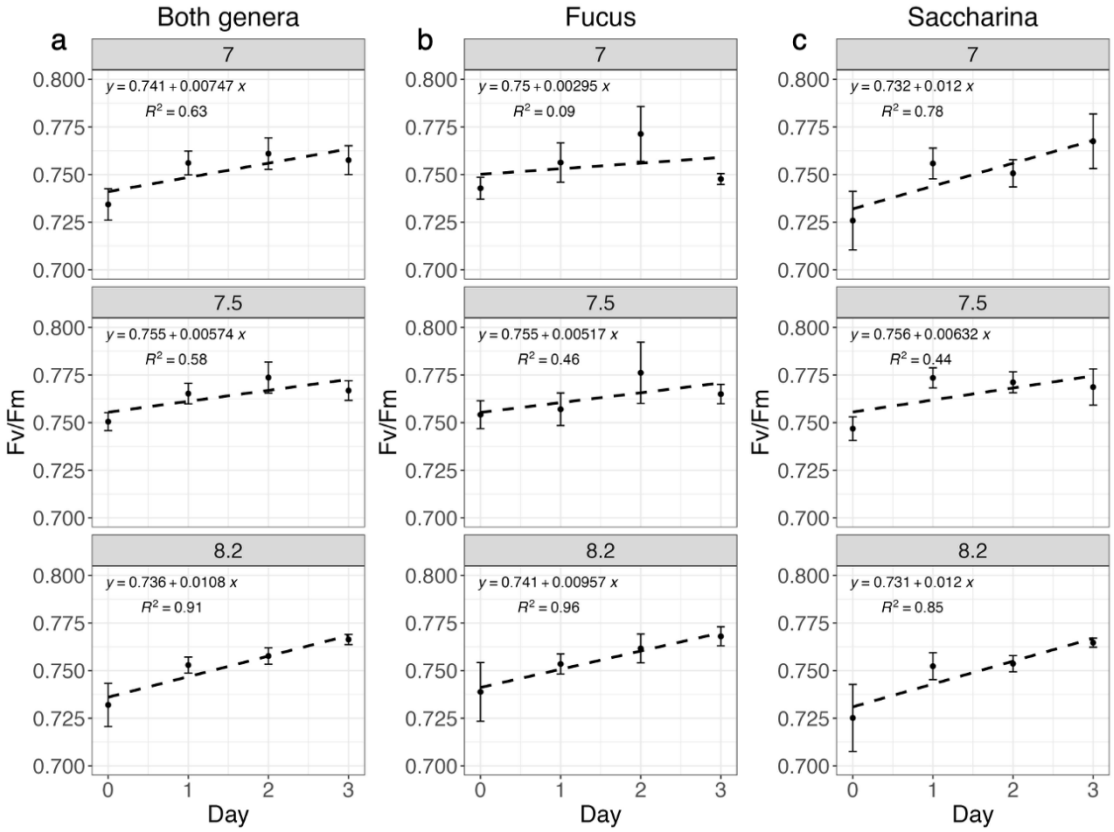

Fig. 5. *Temporal trends of Fv/Fm observations across sites at the three different pH levels: 7.0, 7.5, and 8.2. a) Data pooled for both genera (*Saccharina *and* Fucus*) b) for* Fucus *and c) for* Saccharina*. The dashed lines depict linear models, while the dots mark the mean Fv/Fm for the respective date and error bars indicate ± standard deviation. The experiment began on day 0 (July 12th, 2025) and concluded on day 3 (July 15th, 2025).*

day^{-1}. Notably, at the onset of the experiment, all mean Fv/Fm values were higher for *Fucus* compared to *Saccharina* at the same pH levels (Fig. 5b-c).

The wet weight differences of the macroalgae from the onset of the experiment to the end were not significantly different among the three pH levels (data not shown), i.e. no difference could be determined in the rate of biomass synthesis depending on which pH the macroalgae had been incubated in.

3.2. In situ experiment

In situ pH showed a daily fluctuation with an increase throughout the day followed by a decline until the following morning for all three depth levels at both Site E and S (Fig 6a-b). On the July 13th, a day with high cloud cover, the maximum pH observed at Site S and E were 8.33 and 8.44 at 40 cm depth, respectively, as opposed to the minimum observations of 8.08 and 8.29 at 40 cm depth. Altogether, this results in a daily difference of pH of 0.25 and 0.15 for Site S and E, respectively. The 14th of July had much less cloud cover and increased sun compared to the day before, and showed daily differences of pH of 0.17 and 0.31, for Site S and E, respectively. The maximum values of pH at 40 cm depth on the 14th of July were 8.46 and 8.49, while the minimum values observed were 8.29 and 8.18 for Site S and Site E, respectively. In summary, the daily modulating pH of the macroalgae for Site S ranged between 0.17-0.25, while Site E had differences in pH ranging from 0.15-0.31. The light conditions in water showed a clear declining pattern further away from the surface the measurements were taken (Fig 6c-d). A daily pattern of light conditions was observed at Site S, as a peak was observed during midday, however, this pattern was less prominent for Site E, only visible for the 14th of July, which was in conjunction with sunny conditions (Fig 6c-d). The PAR measured above water (Fig. 6e-f) showed a similar daily pattern for Site S (Fig. 6f) of peak PAR mid-day, which was not as obvious for Site E (Fig. 6e).

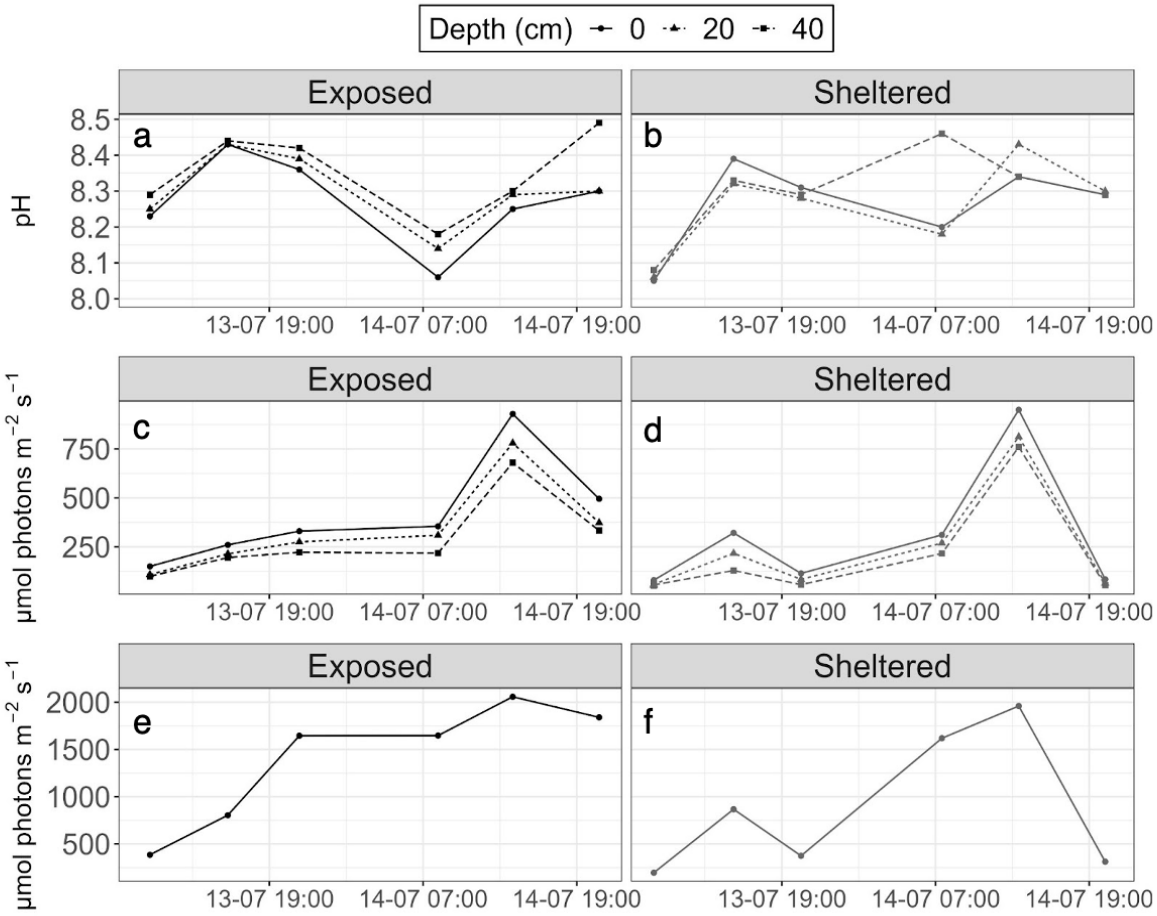

Fig. 6. In situ *measurements through the water column at three different depths from the surface (0, 20 and 40 cm) over a period of approximately 48 hours in mid July 2025 at both sites (Site E and S). Measurements include a) and b): pH-measurements c) and d): photosynthetically active radiation (PAR) in water, e) and f) PAR above the surface in air.*

4. Discussion

Overall, our results indicated that pH had a significant impact on Fv/Fm when pooling data across sites and genera. However, a subsequent Tukey's HSD test did not identify any significant pairwise difference between the selected pH levels. This suggests some variation exists in the response across treatments, but the specific differences remain unclear. Further examination using a three-way ANOVA showed that main effects of pH, site, and genus as well as most interactive relationships between these factors did not have a statistically significant effect on Fv/Fm on any of the experimental days. Temporal trends through the experiment revealed increasing Fv/Fm values for both genera and lastly. Large diel fluctuations in pH were observed *in situ* in macroalgal meadows dominated by *Fucus*, corresponding well to the concurrent light conditions.

4.1. Differences in photosynthetic efficiency between treatments, genera, and sites

The results of the three-way ANOVA were predominantly insignificant, however, there were indications that site had a significant impact on Fv/Fm, albeit this tendency was not apparent through all days of the experiment. Interestingly, site was the only factor that revealed a significant impact on Fv/Fm as a main effect at day 2 and was furthermore included in all observed significant interactive relationships. This suggests that the environmental conditions and characteristics of Site S and E may have had a modulating effect on the Fv/Fm, but nonetheless, the overall results across the entire experiment reveal no clear trends of impacts of the factors. Notably, we observed a significant interactive relationship between pH and site on the very onset of the experiment (day 0) prior to incubations, which appears counterintuitive or even random, as we do not expect the effect of pH to have occurred before exposure to lower pH levels. Additionally, this is the only significant occurrence of this combination of factors through all experimental days and must therefore be regarded with caution.

4.2. Temporal trends of Fv/Fm through the experiment

The temporal trends of Fv/Fm observed for the macroalgae revealed positive trends for all three levels of pH during the experiment. This pattern may indicate that the macroalgae were relatively resilient to being incubated at lower pH compared to *in situ* levels, or alternatively, that the length of the experiment was too short to detect any underlying differences among treatments. The duration of the experiment was shortened considerably due to delays in travel, thus leaving no time for acclimatization of the macroalgae prior to the incubations. Consequently, it was likely that the duration of the experiment, instead effectively served as an acclimatization period rather than testing the ability of the macroalgae to grow under different pH regimes. This argument is supported by the fact that the temporal trends of Fv/Fm did not level off for any of the genera. Both genera exhibited the highest rate of increase in Fv/Fm at pH 8.2 through all experimental days, which is not surprising considering this being the pH they are exposed to in their natural habitat and thus adapted to. Conversely, the overall minimum Fv/Fm observation was observed at pH 8.2 for *Saccharina longicruris*, while the overall maximum Fv/Fm observation was for the same species at pH 7.0, however, this was only for a single measurement and not the overall trend observed.

The required biomass for incubations were determined via the preliminary pH drift experiment, and by extension, the relative productivity between the two genera. Consequently, the final biomass of *Fucus* samples was 50% less than that of *Saccharina*. It was clear that the productivity of *Fucus* was already high at the beginning of the experiment, and relatively less so for *Saccharina*. This relative difference in productivity could potentially have impacted the trajectory of the Fv/Fm of the two genera, as *Fucus* exhibited a higher starting point than that of *Saccharina,* and conversely, a less steep slope in regard to the temporal trends. This may be a result of *Fucus* being sampled in the intertidal zone, while *Saccharina* species were sampled in the subtidal zone at both sites. Intertidal macroalgae such as *Fucus* are regularly exposed to large fluctuations in temperature, light, and salinity and have physiological adaptations that allow them to tolerate such variability (Umanzor *et al*., 2023). In contrast, *Saccharina* is typically found in more stable subtidal environments, where it exhibits some sensitivity to stressors such as reduced salinity, increased temperature and high irradiance (Spurkland and Iken, 2011; Sæther *et al.*, 2024). These ecological and physiological differences could explain why *Fucus* maintained a relatively high Fv/Fm at the start of the experiment, while *Saccharina* began at a lower value and showed a steeper increase over time. This suggests that *Fucus* might therefore be more resilient towards changes in the environment, and consequently better withstand the stress of handling prior to the experiment start. Therefore, the steeper increase of *Saccharina* could indicate that it was more stressed during handling relative to *Fucus*, furthermore pointing to the conclusion that the experiment served as an acclimatization period.

4.3. In situ measurements of pH above macroalgal meadows

The natural pH fluctuations were measured to investigate if they were amplified through the water column towards macroalgal beds with high coverage. For the case of Site E, this was exactly the observed pattern, as higher pH values were observed as measurements were taken towards the sea floor in macroalgal meadows (dominated by *Fucus* for both sites). However, this pattern was less prominent for Site S, as the pH was fluctuating between depths, not showing a clear increase in pH towards the sea floor. This was contradictory to our assumptions, i.e. that sheltered sites would have a clearer pattern throughout the water column due to lower rates of water exchange in the area, compared to more exposed sites. Furthermore, the observed pH was steadily increasing throughout the day, corresponding well to the light conditions that peaked during midday, indeed indicating that macroalgal communities have the capacity of modulating the natural pH via their photosynthetic activity

throughout the day at sites with high macroalgal cover. Contrary to our expectations, the highest diel difference in pH was at Site E, i.e. a potentially higher modulating effect of the macroalgal beds compared to Site S, the opposite dynamic to what previously has been reported on in Denmark (Middelboe & Hansen, 2007). On the day prior to the commencement of our *in situ* measurements, large amounts of macroalgae had been harvested at Site S, and this removal of biomass can potentially have had an impact on the resulting pH modulating effect for this site.

The diel range of minimum to maximum pH above macroalgal meadows was larger than reported in previous studies in Greenland. Krause-Jensen *et al.* (2015) reported on diel variability in pH approximately 50 cm above the seafloor in macroalgal meadows dominated by *Saccharina longicruris* of 0.098 ± 0.061 in a fjord in southwest Greenland during late summer, as opposed to the minimum and maximum diel variation in the present study that was found to be 0.15 and 0.31 respectively. The *in situ* macroalgal communities in Site E and S were predominantly made up by *Fucus* sp., which could have had an influence in the resulting higher diel variation, as the relatively more productive *Fucus* species may have a larger modulating effect on pH.

A potential source of error for the present study comes from the fact that measurements were conducted manually, and while attempts were made to locate the exact same position at each site, the influence of tide occasionally affected these efforts, potentially introducing some bias to the data. Moreover, it is important to emphasize that the foundation of data on *in situ* pH was scarce for this present study and therefore must be regarded with some caution. Furthermore, a previous study found the pH to continuously increase over the duration of 10 days in an Arctic kelp forest exposed to 24 h of daylight, however with daily oscillations driven by tides and variable light conditions (Krause-Jensen *et al*., 2015). Additional research that expands on the duration of the present study is therefore needed to assess if this phenomenon also occurs in a coastal macroalgae community. Furthermore, measurements throughout the entire day are needed, e.g. via the deployment of loggers over multiple days, to enhance the robustness, resolution and overall reliability of the data.

4.4. Ecological implications

This present study investigated the response to varying pH levels of two genera of macroalgae during periods of midnight sun in the summer in the Arctic. This marks the period with peak macroalgal activity which coincides with important life history events for

many calcifying organisms in the Arctic. This is the case for organisms like mussels and barnacles, whose dispersal relies heavily on pelagic larval stages, which are often released during this period and rely on favorable carbonate chemistry for successful development and settlement (Kurihara, 2008). During this period, elevated photosynthetic activity in macroalgal beds can locally raise seawater pH and carbonate saturation as shown in the present study, potentially providing temporary refugia for vulnerable early life stages such as larvae (Duarte and Krause-Jensen, 2018). The spatial and temporal overlap between macroalgal buffering and calcifier vulnerability is therefore an important ecological link that could influence future benthic community dynamics (Lebrun *et al.*, 2022) in the Arctic. However, in the face of climate change, the magnitude and timing of this interaction is likely to be altered. Ocean acidification, rising temperatures, and changing sea ice cover may alter macroalgal species composition, as some species may be able to better withstand future conditions than others (Krause-Jensen and Duarte, 2014). For example, coralline red algae are proven more sensitive to low pH due to their calcareous deposits in their thallus. Declines in these species could reduce habitat complexity, as they are important foundation species in the Arctic (Lebrun *et al.*, 2022). In contrast, brown macroalgae genera such as *Fucus* and *Saccharina* - the focus of this study - may be more tolerant to pH reductions as indicated in the present study as they showed no clear response to exposure to lower pH levels. However, these findings should be interpreted with caution due to the limited duration of the experiment and limited number of replicas. Nevertheless, they suggest that some macroalgal species may tolerate reduced pH levels to some degree and could potentially persist or even expand under future conditions, altering the structure and ecological functions of Arctic coastal ecosystems. Moreover, these species have the potential to locally elevate seawater pH through photosynthetic activity, partially counteracting the effects of ocean acidification and creating temporary refugia for sensitive calcifiers, with downstream effects on benthic biodiversity and food webs (Porzio *et al.*, 2011; Krause-Jensen and Duarte, 2014). A previous study showed that *Saccharina* sp. is sensitive to low salinity and high irradiance (Spurkland and Iken, 2011), and therefore, other environmental factors such as temperature, irradiance, and salinity, may also exert a stronger influence on their physiology and productivity than pH alone. This effectively means that future changes in Arctic coastal ecosystems could not only be driven by acidification but also by warming (Iñiguez *et al*., 2016).

It must be considered that our results represent effects observed in a limited number of species and under a restricted set of experimental parameters. Naturally, caution is required in

extrapolating these findings to the entire ecosystem. Further research is therefore needed to determine how different macroalgal functional groups will respond to ocean acidification and whether these changes will impact their pH modulating capabilities, as well as influence their role as ecosystem engineers. Understanding these dynamics will be paramount in predicting the resilience of Arctic coastal ecosystems under future climate scenarios.

5. Conclusion

In conclusion, the present study reported no clear significant response in Fv/Fm when the two genera of macroalgae, *Fucus* and *Saccharina*, were exposed to three levels of pH: 7.0, 7.5 and 8.2 (*in situ*) over the course of three days. However, temporal trends within the varying levels of pH all resulted in increasing rates of Fv/Fm, thus arguing that the experiment had effectively served as an acclimatization period, as mean Fv/Fm did not level off or even decrease for either genera. Altogether, these results indicate that both genera included in the present study had some resilience towards lowered pH. *In situ* measurements revealed that pH levels were following the light condition patterns, indicating that macroalgae at both an exposed and sheltered site had a pH modulating effect on their environment. Altogether, this confirms that macroalgae may constitute a refugia for calcifying organisms in the face of ocean acidification. Studies on this topic in the Arctic are still scarce, highlighting the importance and novelty of this study. Therefore, further research is needed to understand how the interplay between ocean acidification and other derivative effects of climate change may impact Arctic macroalgae and their role in Arctic coastal ecosystems.

6. References

Axelsson, L., Mercado, J., & Figueroa, F. (2000). Utilization of HCO_3^- at high pH by the brown macroalgae *Laminaria saccharina*. *European Journal of Phycology, 35*(1), 53–59. https://doi.org/10.1080/09670260010001735621

Bashevkin, S. M., Dibble, C. D., Dunn, R. P., Hollarsmith, J. A., Ng, G., Satterthwaite, E. V., & Morgan, S. G. (2020). Larval dispersal in a changing ocean with an emphasis on upwelling regions. *Ecosphere, 11*(1), e03015. https://doi.org/10.1002/ecs2.3015

Bates, N. R., Moran, S. B., Hansell, D. A., & Mathis, J. T. (2006). An increasing CO_2 sink in the Arctic Ocean due to sea-ice loss. *Geophysical Research Letters, 33*(23). https://doi.org/10.1029/2006GL027028

Cornwall, C. E., Hepburn, C. D., Pritchard, D., Currie, K. I., McGraw, C. M., Hunter, K. A., & Hurd, C. L. (2012). Carbon-use strategies in macroalgae: Differential responses to lowered pH and implications for ocean acidification. *Journal of Phycology, 48*(1), 137–144. https://doi.org/10.1111/j.1529-8817.2011.01085.x

Duarte, C. M., & Krause-Jensen, D. (2018). Greenland tidal pools as hot spots for ecosystem metabolism and calcification. *Estuaries and Coasts, 41*(5), 1314–1321. https://doi.org/10.1007/s12237-018-0368-9

Duarte, C. M., Gattuso, J. P., Hancke, K., Gundersen, H., Filbee-Dexter, K., Pedersen, M. F., Middelburg, J. J., Burrows, M. T., Krumhansl, K. A., Wernberg, T., Moore, P., Pessarrodona, A., Ørberg, S. B., Pinto, I. S., Assis, J., Queirós, A. M., Smale, D. A., Bekkby, T., Serrão, E. A., & Krause-Jensen, D. (2022). Global estimates of the extent and production of macroalgal forests. *Global Ecology and Biogeography, 31*(7), 1422–1439. https://doi.org/10.1111/geb.13515

Fabry, V. J., McClintock, J. B., Mathis, J. T., & Grebmeier, J. M. (2009). Ocean acidification at high latitudes: The bellwether. *Oceanography, 22*(4), 160–171. https://doi.org/10.5670/oceanog.2009.105

Feely, R. A., Doney, S. C., & Cooley, S. R. (2009). Ocean acidification: Present conditions and future changes in a high-CO_2 world. *Oceanography, 22*(4), 36–47. https://doi.org/10.5670/oceanog.2009.95

Friedlingstein, P., O'Sullivan, M., Jones, M. W., Andrew, R. M., Hauck, J., Landschützer, P., Le Quéré, C., Li, H., Luijkx, I. T., Olsen, A., Peters, G. P., Peters, W., Pongratz, J., Schwingshackl, C., Sitch, S., Canadell, J. G., Ciais, P., Jackson, R. B., Alin, S. R., Arneth, A., … Zeng, J. (2025). Global carbon budget 2024. *Earth System Science Data, 17*(2), 965–1039. https://doi.org/10.5194/essd-17-965-2025

Gulev, S. K., Thorne, P. W., Ahn, J., Dentener, F. J., Domingues, C. M., Gerland, S., Gong, D., Kaufman, D. S., Nnamchi, H. C., Quaas, J., Rivera, J. A., Sathyendranath, S., Smith, S. L., Trewin, B., von Schuckmann, K., & Vose, R. S. (2021). Changing state of the climate system. In *Climate change 2021: The physical science basis*. Cambridge University Press. https://doi.org/10.1017/9781009157896.004

Haugan, P. M., & Drange, H. (1996). Effects of CO2 on the ocean environment. *Energy Conversion and Management*, *37*(6–8), 1019–1022.

Heinz Walz GmbH. (2023). *DIVING-PAM-II: Underwater chlorophyll fluorometer – Manual*. https://www.walz.com/files/downloads/manuals/diving-pam-II/DIVING_PAM_II_08.pdf

Hernández, A. C., Sangil, C., Fanai, A., & Hernández, J. C. (2018). Macroalgal response to a warmer ocean with higher CO_2 concentration. *Marine Environmental Research, 136*, 99–105. https://doi.org/10.1016/j.marenvres.2018.01.010

Iñiguez, C., Carmona, R., Lorenzo, M. R., Niell, F. X., Wiencke, C., & Gordillo, F. J. L. (2016). Increased temperature, rather than elevated CO_2, modulates the carbon assimilation of the Arctic kelps *Saccharina latissima* and *Laminaria solidungula*. *Marine Biology, 163*(12), 248. https://doi.org/10.1007/s00227-016-3024-6

IPCC. (2007). *Climate change 2007: The physical science basis*. Cambridge University Press. https://www.ipcc.ch/report/ar4/wg1/

IPCC. (2018). *Global warming of 1.5°C*. https://www.ipcc.ch/sr15/

Krause-Jensen, D., & Duarte, C. M. (2014). Expansion of vegetated coastal ecosystems in the future Arctic. *Frontiers in Marine Science, 1*, 77. https://doi.org/10.3389/fmars.2014.00077

Krause-Jensen, D., Duarte, C. M., Hendriks, I. E., Meire, L., Blicher, M. E., Marbà, N., & Sejr, M. K. (2015). Macroalgae contribute to nested mosaics of pH variability in a subarctic fjord. *Biogeosciences, 12*(16), 4895–4911. https://doi.org/10.5194/bg-12-4895-2015

Krause-Jensen, D., Marbà, N., Sanz-Martin, M., Hendriks, I. E., Thyrring, J., Carstensen, J., Sejr, M. K., & Duarte, C. M. (2016). Long photoperiods sustain high pH in Arctic kelp forests. *Science Advances, 2*(12), e1501938. https://doi.org/10.1126/sciadv.1501938

Kurihara, H. (2008). Effects of CO_2-driven ocean acidification on the early developmental stages of invertebrates. *Marine Ecology Progress Series, 373*, 275–284. https://doi.org/10.3354/meps07802

Lan, X., Tans, P., & Thoning, K. W. (2025). Trends in globally averaged CO_2 determined from NOAA Global Monitoring Laboratory measurements. https://doi.org/10.15138/9N0H-ZH07

Lebrun, A., Comeau, S., Gazeau, F., & Gattuso, J. P. (2022). Impact of climate change on Arctic macroalgal communities. Global and Planetary Change, 219, 103980. https://doi.org/10.1016/j.gloplacha.2022.103980

Middelboe, A. L., & Hansen, P. J. (2007). Direct effects of pH and inorganic carbon on macroalgal photosynthesis and growth. Marine Biology Research, 3(3), 134–144. https://doi.org/10.1080/17451000701320556

Orr, J. C., Fabry, V. J., Aumont, O., Bopp, L., Doney, S. C., Feely, R. A., Gnanadesikan, A., Gruber, N., Ishida, A., Joos, F., Key, R. M., Lindsay, K., Maier-Reimer, E., Matear, R., Monfray, P., Mouchet, A., Najjar, R. G., Plattner, G. K., Rodgers, K. B., … Yool, A. (2005). Anthropogenic ocean acidification over the twenty-first century and its impact on calcifying organisms. Nature, 437(7059), 681–686. https://doi.org/10.1038/nature04095

Pedersen, P. M. (2022). Marine algae of Greenland (1st ed.). Forlaget Epsilon.

Porzio, L., Buia, M. C., & Hall-Spencer, J. M. (2011). Effects of ocean acidification on macroalgal communities. Journal of Experimental Marine Biology and Ecology, 400(1–2), 278–287. https://doi.org/10.1016/j.jembe.2011.02.011

Qi, D., Chen, L., Chen, B., Gao, Z., Zhong, W., Feely, R. A., Anderson, L. G., Sun, H., Chen, J., Chen, M., Zhan, L., Zhang, Y., & Cai, W. J. (2017). Increase in acidifying water in the

western Arctic Ocean. Nature Climate Change, 7(3), 195–199. https://doi.org/10.1038/nclimate3228

Spurkland, T., & Iken, K. (2011). Salinity and irradiance effects on growth and maximum photosynthetic quantum yield in subarctic Saccharina latissima (Laminariales, Laminariaceae). Botanica Marina, 54(4), 355–365. https://doi.org/10.1515/BOT.2011.042

Steinacher, M., Joos, F., Frölicher, T. L., Plattner, G.-K., & Doney, S. C. (2009). Imminent ocean acidification in the Arctic projected with the NCAR global coupled carbon cycle–climate model. Biogeosciences, 6(3), 515–533. https://doi.org/10.5194/bg-6-515-2009

Sæther, M., Diehl, N., Monteiro, C., Li, H., Niedzwiedz, S., Burgunter-Delamare, B., Scheschonk, L., Bischof, K., & Forbord, S. (2024). The sugar kelp Saccharina latissima II: Recent advances in farming and applications. Journal of Applied Phycology, 36(4), 1953–1985. https://doi.org/10.1007/s10811-024-03213-1

Thoisen, C., Riisgaard, K., Lundholm, N., Nielsen, T. G., & Hansen, P. J. (2015). Effect of acidification on an Arctic phytoplankton community from Disko Bay, West Greenland. Marine Ecology Progress Series, 520, 21–34. https://doi.org/10.3354/meps11123

Umanzor, S., Sandoval-Gil, J. M., & Conitz, J. (2023). Ecophysiological responses of the intertidal seaweed Fucus distichus to temperature changes and reduced light driven by tides and glacial input. Estuaries and Coasts, 46(5), 1269–1279. https://doi.org/10.1007/s12237-023-01207-9

Yu, H., Kim, J., Rhee, C., Shin, J., Shin, S. G., & Lee, C. (2022). Effects of different pH control strategies on microalgae cultivation and nutrient removal from anaerobic digestion effluent. Microorganisms, 10(2), 312. https://doi.org/10.3390/microorganisms10020357

Supplementary material

Table S1. Results of Tukey's HSD post-hoc analysis for the factor pH on the Fv/Fm, comparing the three pH levels included in this study: 7.0, 7.5 and 8.2.

Groups	*p-value*
7.0 *vs* 7.5	0.0583
7.0 *vs* 8.2	1.000
7.5 *vs* 8.2	0.0577

Table S2. Results of one-way analysis of variance (ANOVA) on the effect of pH levels on the photosynthetic efficiency (Fv/Fm) when all levels of genera and site were pooled.

Time point	*Factor*	*df*	*F-value*	*p-value*
Day 0	pH	2	1.392	0.263
Day 1	pH	2	1.435	0.252
Day 2	pH	2	1.396	0.262
Day 3	pH	2	0.890	0.420

Table S3. Results of one-way analysis of variance (ANOVA) on the effect of species on the photosynthetic efficiency (Fv/Fm) at different pH levels.

Time point	*pH*	*Factor*	*df*	*F-value*	*p-value*
Day 0	7.0	Species	1	1.071	0.325
	7.5	Species	1	0.585	0.462
	8.2	Species	1	0.341	0.572
Day 1	7.0	Species	1	0.001	0.970
	7.5	Species	1	2.705	0.131
	8.2	Species	1	0.0180	0.897
Day 2	7.0	Species	1	1.652	0.228
	7.5	Species	1	0.0870	0.774
	8.2	Species	1	0.854	0.377
Day 3	7.0	Species	1	1.844	0.204
	7.5	Species	1	0.116	0.740
	8.2	Species	1	0.361	0.561